# INVESTIGATION OF HEAT TRANSFER ENHANCEMENT AND FLOW PHENOMENA OF GAS TURBINE BLADE INTERNAL COOLING PASSAGE

by

Farah Nazifa Nourin

A Dissertation Submitted in

Partial Fulfillment of the

Requirements for the Degree of

Doctor of Philosophy

in Engineering

at

University of Wisconsin-Milwaukee

August 2022

# ABSTRACT

INVESTIGATION OF HEAT TRANSFER ENHANCEMENT AND FLOW PHENOMENA OF GAS TURBINE BLADE INTERNAL COOLING PASSAGE

by

Farah Nazifa Nourin

The University of Wisconsin-Milwaukee, 2022
Under the Supervision of Professor Ryoichi S. Amano

The turbomachinery industry is constantly struggling to improve gas turbine efficiency. The efficiency of a gas turbine depends on the turbine inlet temperature. Currently, the turbine inlet temperature can be as high as 1600°C. The turbine blade material is not able to withstand high temperatures. Efficient cooling can increase the durability and performance of the blade. Over the years, researchers have investigated different cooling methods such as rib turbulated cooling, dimple cooling, pin fin cooling, and jet impingement cooling. Rib cooling is applicable for the serpentine mid-section of the blade cooling channel. It was used for a long time as it shows better heat transfer enhancement compared to a smooth surface. The drawback of using a ribbed surface is excessive pressure drop which affects the thermal performance negatively. Dimple and pin-fin cooling are used for trailing edge cooling. The leading edge of the blade is cooled using the jet impingement method, where the rotor blade experiences the highest heat. Intense air-jet strikes at the target surface to heat transfer. This study investigated the heat transfer and airflow behavior of dimpled, rib-turbulated, pin-finned cooling channels and the application of guide vane with the dimpled cooling passages both experimentally and numerically.

The investigation was conducted with a baseline case of a smooth surface cooling channel. The dimpled surface cooling channel was studied for partial spherical dimples. Three different dimple depths to diameter ratios i.e., 0.10, 0.25, and 0.50 were considered with one column of dimple in each leg. Later, the study moved to 2 column dimples with a 0.50 dimple depth to diameter ratio to obtain the maximum thermal efficiency. A newly designed dimple–leaf dimple was introduced in this investigation. The investigation showed that leaf dimples are more efficient compared to conventional partial spherical dimples. The research was also conducted to find out the best rib design. The ribbed surface was studied based on two different rib designs i.e., 30° ribs and 45° ribs. In addition, the current study investigated the effect of pin-fin on the cooling surface with two different designs of pin-fins i.e., partial spherical pin–fins and dome- shaped pin-fins. The study has been conducted both computationally and experimentally for stationary and rotational cases. The dome-shaped pin-finned channel exhibits better thermal performance based on the heat transfer and pressure drop effect. U and curve guide vanes were inserted at the bend region of the partial spherical dimpled cooling channel using different orientations i.e., depression and protrusion.

© Copyright by Farah Nazifa Nourin, 2022
All Rights Reserved

# Table of Contents

LIST OF FIGURES

LIST OF TABLES

NOMENCLATURES

A Heater surface area, $(m^2)$

$D_h$ Hydraulic diameter, $(m)$

f Friction factor, $(f = \frac{\Delta P}{(L/D_h)(\rho u^2/2)})$

$f_0$ Smooth surface friction factor, $(f_o = 0.316Re^{-0.25})$

h Convective heat transfer coefficient, $(W/m^2.K)$

k Thermal conductivity of air, $(W/m.K)$

Nu Nusselt number $(Nu = \frac{hD_h}{k})$

$Nu_o$ Theoretical Nusselt number $(Nu_o = 0.023Re^{0.8}Pr^{0.4})$

Pr Prandtl number

$Q^{"}$ Convective heat flux $(W/m^2)$

Re Reynolds number $(Re = \frac{\rho u D_h}{\mu})$

$R_o$ Rotation number, $(R_0 = \frac{\Omega D_h}{u})$

$T_s$ Surface temperature, (K)

$T_0$ Local air temperature, (K)

u Velocity of air, $(m/s)$

## LIST OF ABBREVIATIONS

| | |
|---|---|
| LES | Large Eddy Simulation |
| RANS | Reynolds Averaged Navier-Stokes |
| VFD | Variable Frequency Drive |

## GREEK SYMBOLS

| | |
|---|---|
| $\rho$ | Density of air, $(kg/m^3)$ |
| $\mu$ | Dynamic viscosity of air, $(kg/m.s)$ |
| $\Omega$ | Rotational speed (RPM) |
| η | Thermal Efficiency, (%) |

# ACKNOWLEDGMENTS

I would like to express my appreciation and thanks to my advisor Dr. Ryoichi Amano, for his continuous support and encouraging my research, and for allowing me to grow as an independent researcher. His supervision has been precious. He provided me a platform to exercise analytical thinking and develop research and leadership skills. I would like to sincerely thank my thesis committee, Dr. Deyang Qu, Dr. John Reisel, Dr. Istvan Lauko, and Dr. Wilkistar Otieno.

My acknowledgment extends to my colleagues and peers, and I wish them all the best in their future endeavors. Finally, thanks to my family and friends for their continuous support, encouragement, and inspiration.

***I could have started this journey because I have amazing parents and completed it as I do have a super supportive husband!!!***

***I dedicate this work to my parents, siblings, and my better half Arif Hossain.***

# 1. Introduction

The gas turbine is one of the most widely used power generation equipment in today's world. It was first used back in 1939 for power generation. With time, the demand for power increases and the necessity of a more efficient turbine increases. There are five ways to improve the gas turbine efficiency such as increase in turbine inlet temperature, use of regeneration, reheating, and intercooling, improvement in turbine metals. Among the possible opportunities to increase efficiency, increasing the turbine inlet temperature is the most promising as it offers considerable improvement in thermal efficiency. The higher inlet temperature demands a metal surface which can withstand it. Nowadays, there are several composite materials such as nickel-based alloy which can withstand high-temperature. But it is not good enough to withstand at 1600°C surface temperature of gas turbine blade. So, effective gas turbine internal cooling is mandatory. There are several cooling methods to cool the internal blade surface such as smooth surface cooling, dimple cooling, rib turbulator cooling, pin-fin cooling, and jet impingement cooling.

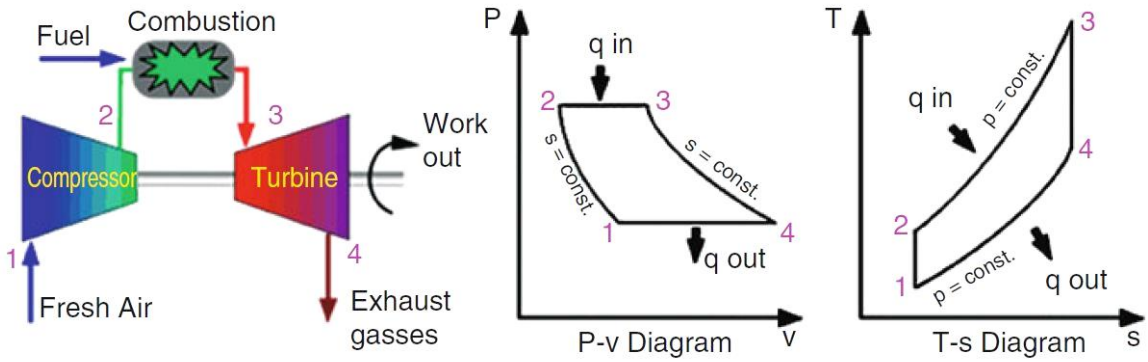


Figure 1-1: Brayton cycle [1]

The gas turbine runs on Brayton cycle. Figure 1-1 represents an open gas turbine cycle. A compressor takes ambient air (stage 1) and compresses it to a high-temperature and pressure (stage 2). Fuel and high pressurized air are sent to the combustion chamber (stage 3). In the combustion

chamber, fuel is burned at constant pressure. The resulting high-temperature gases are sent to a turbine. The high-temperature gases expand to the ambient pressure (stage 4) in the turbine and generate power. The exhaust gases leave the turbine to ambient.

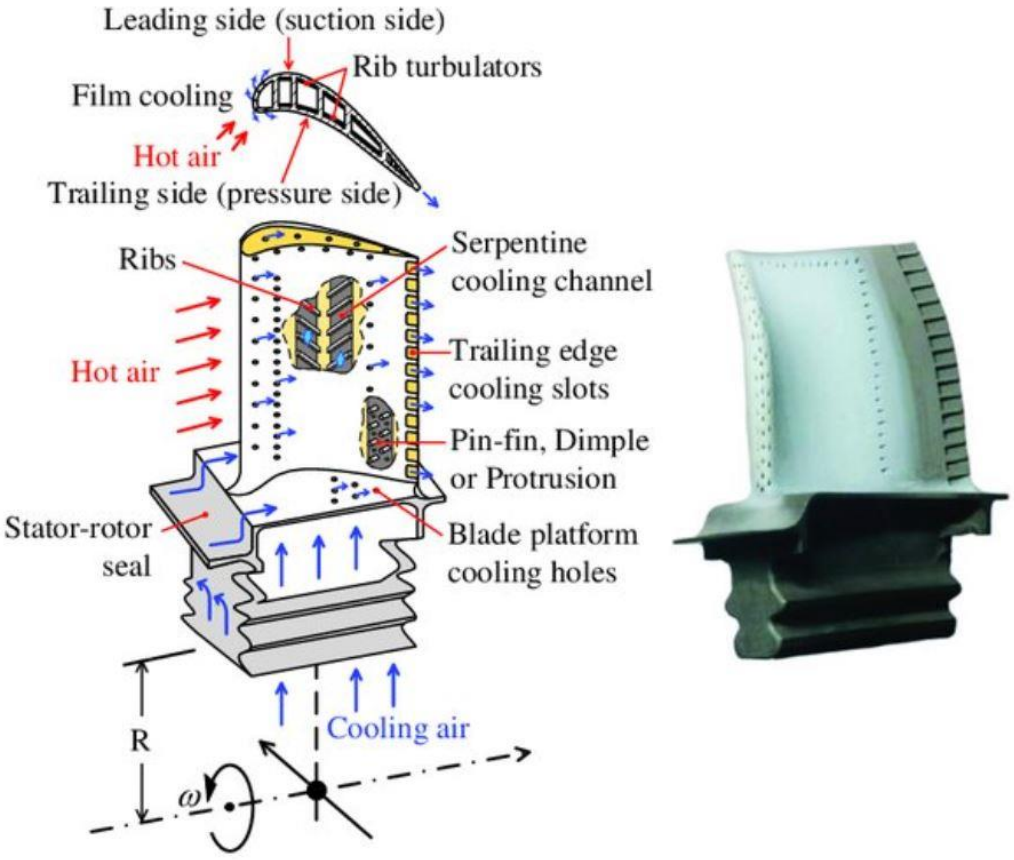


Figure 1-2: Gas turbine blade internal cooling [2]

Figure 1-2 represents gas turbine internal cooling. Complex flow pattern around the blade and vanes makes it difficult to predict the metal surface temperature. On the leading edge, the flow transits from laminar to turbulent which increases the heat transfer coefficient. Similar changes occur in the trailing edge. Combustor high turbulence, laminar to turbulent transition, film cooling, secondary flow, surface roughness, rotational effect, centrifugal forces, buoyancy forces, Coriolis forces etc. affect the gas turbine internal blade cooling. Internal convective cooling is the method of directing coolant to the regions of the components requiring cooling and in turn increasing the

heat transfer coefficient. It is performed using three different methods. They are jet impingement cooling, rib turbulator cooling, pin-fin/dimple cooling.

Jet impingement cooling is highly efficient for the first stage vanes of the turbine blade. The cooling method is only used in leading edge of the rotor blade as the structure constraints on the rotor blade under rotation and centrifugal loads. It is effective as the cooling air is delivered to impinge on the hot region. Jet impingement cooling performance depends on the geometry of the target plate, stand-off distance, arrangement of the nozzle holes, etc. To enhance the heat transfer of serpentine passage of turbine blades, rib turbulators are mounted on the internal cooling passages. Ribs contribute to the flow separation at the top of the rib and again reattaches to the flow between the ribs. The turbulence of the flow increases due to presence of it. Pin-fin/ dimple cooling is used in the trailing edge of the gas turbine blade. Pin-fin arrays are used to promote the flow turbulence in the trailing edge. Additionally, it increases the surface area which contributes positively to the heat transfer distribution. The alternative to pin-fin cooling is dimple cooling. Dimple cooling represents a promising heat transfer distribution along the trailing edge as it shows less pressure drop compared to pin-fin cooling.

In this study, dimple cooling, rib turbulator cooling, pin fin cooling and the effect of guide vanes in the cooling channel were studied both experimentally and computationally. Large Eddy Simulation (LES) was used for the computational study using a commercial package of Star CCM+ 2021 software. The purpose of this study is to provide an insight on overall gas turbine blade internal cooling. The study provides a detailed heat transfer distribution along the channel, pressure drop effects. The performance was investigated based on Nusselt (Nu) number, Reynolds (Re) numbers, friction factor and efficiency. The LES study predicts a detailed flow direction and streamlines at different Re numbers and heat transfer distribution.

# 2. Literature Review

## 2.1. Gas Turbine Blade Internal Cooling with Smooth Surface

The internal cooling channel of gas turbine blade surface is treated by dimples, ribs, or pin-fins. But smooth surface wall should investigate to conduct fundamental investigations. Simpler geometry is desirable as a baseline of this study. Hence, the investigation of gas turbine internal cooling channel has started with smooth surface. Several researchers completed a detailed study on stationary and rotational effects, channel orientation, turning effects, Reynolds numbers, wall heating condition etc. The initial stage of this study was a stationary, smooth, and single pass channel. But a single pass channel does not provide the complex behavior of turning effects of multi-pass cooling channel.

Li et al. [3] investigated the heat transfer augmentation for smooth surface both stationary and rotational cases. The inlet Reynolds number and rotation number range from 10,000 to 30,000 and 0 to 2, respectively. The research team normalized the stationary Nusselt number with Nusselt number for smooth, fully developed, stationary round pipe. The higher Re number causes the more chaotic flow along the channel and less wall temperature ratio. Smaller wall temperature ratio shows a positive effect on heat transfer by increasing the local Re number. It gets weaker at high Re numbers. Han et al. [4] described heat transfer in the 180° bend channel. According to them, the turn has positive effect in the turn region and downstream.

The heat transfer in rotational cases depends on several factors. It can be classified in two major classes such as effect of geometrical factors and effect of physical factors. 180° turn, channel orientation, channel aspect ratio, and channel entrance form are considered as geometrical factors. Inlet density ratio, buoyancy number, and rotation number are considered as physical factors [5]. All researchers emphasized the buoyancy and centrifugal forces in a rotating channel [6 - 10].

Buoyancy forces are significant for rotational gas turbine blades because of the high rotational speeds and large blade-wall-to-coolant temperature differences. The effects of buoyancy on heat transfer without complicating effects of Coriolis generates secondary flow. The buoyancy force is the factor of density ratio, rotation number, and a geometric configuration. The Nu number ratio increases with the Buoyancy number on the passage suction side in the radially outward flow [11]. Another crucial factor is Coriolis forces and inlet density ratio. The combination of Coriolis and centrifugal forces derive the rotation effect on heat transfer. Inlet density ratio had a larger effect on the pressure side compared to the suction side and reduced its influence in the second passage [12].

## 2.2. Gas Turbine Blade Internal Cooling with Dimples

Dimples are depressions or cavities on the cooling channel surface. It was formerly known from golf ball aerodynamics. It was used on golf balls to decrease the flow resistance. In the last few decades, dimples got popular because of the low-pressure loss penalty compared with the rib-turbulators cooling channel with considerable heat transfer augmentation. Dimples generate strong vortices which drive higher turbulence around the dimples, and thus, heat transfer increases. Dimples do not protrude in to flow to produce a minimal level of drag. Thus, less pressure drop is expected in a dimpled channel.

Researchers mostly studied spherical dimples for the cooling channel [13 - 17]. The local heat transfer mechanism is shown in Figure 2-1. The flow gets separated at the entrance of dimples and recirculation forms in the upstream half of the dimples where the heat transfer is exceptionally low. The flow is reattached a little before exiting the dimples. The air experiences flow circulation in the wide section of it. Upwash flow is generated after the incoming advection mixed impingement. It gets mixed and forms a mixed flow passing to the next dimples [18]. The flow

mechanism is more or less same for different dimple shapes. The minor change in flow pattern affects the heat transfer depending on the dimple shapes. Figure 2-1 represents that large velocity vectors are generated around the downstream of the dimple and a high heat transfer occurs. The main factors for the improvement of the heat transfer are flow separation, reattachment, impingement, and vortex roll generation [19].

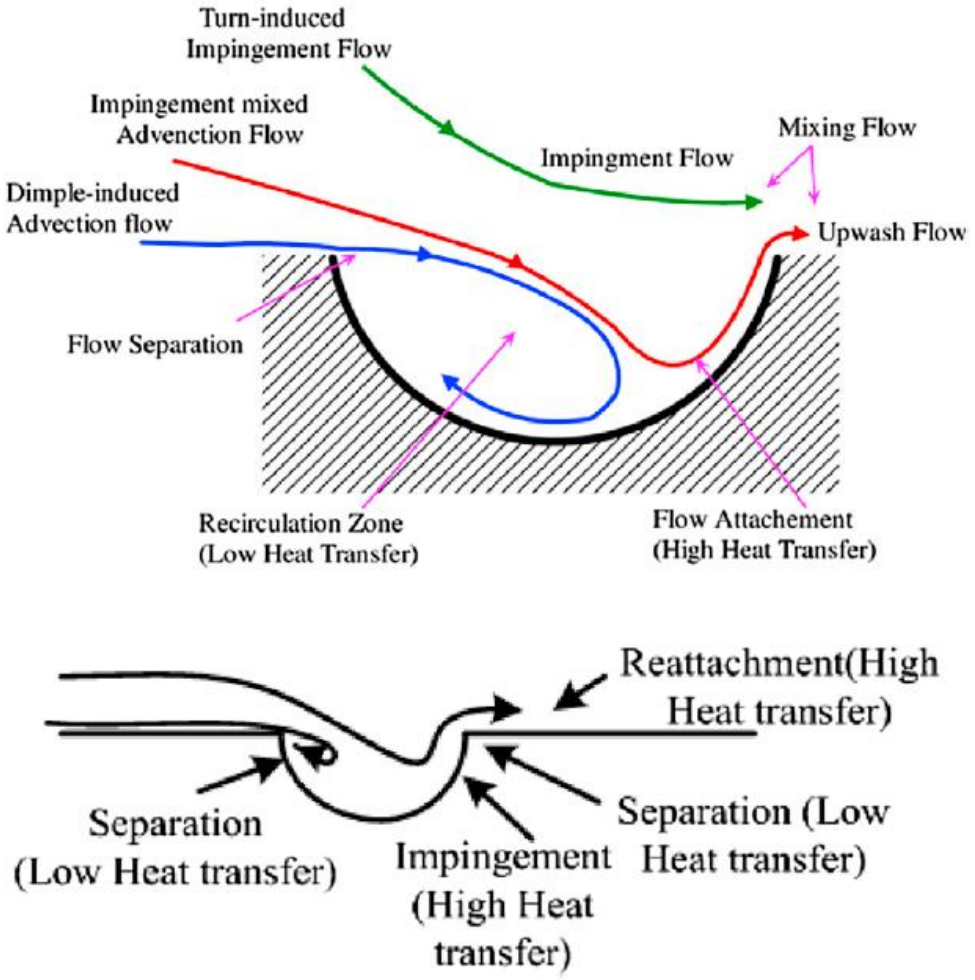


Figure 2-1: Potential flow mechanisms responsible for heat transfer improvement by dimples [19]

Afanasyev et al. [20] investigated the heat transfer and friction behavior of the spherical cavities for turbulent flow of spherical dimples in a staggered arrangement. The dimple depth to diameter ratio was considered 0.067. They concluded that by inserting dimples in a cooling

channel surface, heat transfer can be increased by 30-40% without any appreciable effect on the pressure loss. Chyu et al. [21] researched the heat transfer on a staggered hemispherical and teardrop dimpled cooling channel. They found that heat transfer ratios are higher for dimpled surfaces than the smooth walls for the Reynolds number between 10,000 and 50,000. The heat transfer enhancement is more than 2.5 for the downstream area of the dimples. Moon et al. [22] examined the heat transfer and friction of a turbulent flow of a dimpled channel with the depth to diameter ratio 0.19. The comparison between smooth surface and dimpled surface channel revealed that the dimpled cooling channel remained almost constant of about 2.1 times for different Reynolds number in terms of heat transfer augmentation. The reason of heat transfer enhancement in a dimpled cooling channel was described by Mahmood et al. [23]. The study showed that the action of vortex flow shedding from the dimples causes convective heat transfer augmentation. Xie and Sunden [24] presented a numerical study on hemispherical dimpled cooling channel. The numerical results showed that the heat transfer enhancement of dimpled-tip passage is up to 2 times higher than of the smooth passage. Additionally, the dimpled channel has a low-pressure loss penalty. However, a low dimple depth shows a low heat transfer enhancement at high Reynolds number.

Rao et al. [25] investigated the heat transfer in dimples of four different shapes i.e., spherical, elliptical, inclined-elliptical, and teardrop, both numerically and experimentally for a single pass cooling channel. For the numerical investigation, the study employed $k$- $\omega$ SST turbulence model using the software named ANSYS FLUENT 14.5 software. The study determined that the teardrop dimples have about 18% higher heat transfer augmentation compared to spherical ones. Elliptical and inclined -elliptical dimples showed almost similar results. The teardrop dimpled experienced the highest friction factor though the overall thermal performance was high for this case. Nishida

et al. [26] investigated the teardrop dimples with straight and curved slopes and compared them with the hemispherical one. The study showed that the heat transfer deterioration and flow separation at the edge of dimples were prevented by the leading-edge slopes. The straight slope teardrop dimpled channel showed higher heat transfer than the curved one as the flow near the spanwise edge in the upstream section of the dimple. Kim et al. [27] discussed the heat transfer behavior of inclined elliptical dimples numerically. The numerical study concluded that geometrical parameters such as the ratio of the channel height to the dimple diameter, ratio of the dimple depth to diameter and angle of ellipse major axis to flow direction caused a significant impact on the heat transfer boost.

The study of heat transfer augmentation in a rotational dimpled cooling channel is limited in open literature. However, a few researchers investigated rotational cases. Zhou and Acharya [28] investigated the hemispherical depressions with rotation number 0.2 at Reynolds number 21,000. The leading and trailing surfaces were dimpled surface, and the rest of the other surfaces were smooth. The dimpled walls lead to an increase in heat transfer over smooth surfaces both stationary and rotational cases. The results also concluded that the maximum heat/mass transfer rates were obtained at the downstream of the dimples. The minimum rates were found along the row containing the dimples. Griffith et al. [29] revealed the reasons for enhanced heat transfer in rotational motion. The study was conducted for rotational number 0.04 to 0.3 varying the Reynolds number 5,000 to 40,000. The two-channel orientation i.e., 90° and 135° angled with respect to the plane of rotation were considered. In a rotating dimpled channel, Coriolis vortex force affects significantly thermal behavior. The 90° angled channel experienced the heat transfer enhancement at the trailing surfaces almost 100%. However, the leading surface showed little dependence on the rotation number. In case of 135° angled channel, the trailing outer surface showed the increase

of heat transfer more than 100%. The trailing inner and leading outer surfaces experienced approximately equal improvement of heat transfer, increasing by more than 50% from the stationary to the highest rotation number cases. Kim et al. [30] conducted an experimental study in a dimpled rotating test rig and concluded that heat transfer coefficient on the trailing surface is higher than that on the leading surface.

### 2.3. Gas Turbine Blade Internal Cooling with Ribs

Different geometries were used over the years to enhance the turbulence within the channel and hence increase the heat transfer. Modern gas turbine blades carry a serpentine section in the mid portion of the blade to increase the heat transfer. Rib turbulators are mostly used for the mid-section of the serpentine cooling channel to further increase the heat transfer rate. The reattaching and detaching air flows cause the secondary flow in the cooling channel which leads to the increase of heat transfer. Ribs also cause the pressure drop in the channel [31]. Amano et al. [32] investigated the air flow phenomena through a stationary rib roughened channel. The numerical study was conducted using the Reynolds- Stress Model (RSM), k- ε, and k–ω for 45 ° and 90 ° angled ribbed cooling channel and compared with the experimental results of Kyung et al. [33]. By comparing the Nusselt number distribution along the channel, they concluded that the RSM and non-linear k–ω models showed a good agreement for the 45°, and 90 ° angled ribbed. However, the k- ε model showed deviation from the experimental results. The air flow started to develop at the inlet which leads to a slight decrease in heat transfer at the entrance. Once the flow is fully developed, a recirculation zone is noticeable around the ribs and the bend section. The bend section undergone a significant increase in turbulence.

Hahn et al. [34] investigated the heat transfer variations experimentally using four different rib geometry. 60° angled rib from its center, 60° angled rib from its center inversely positioned,

60° angled broken ribs, and 60° angled broken ribs inversely positioned in a staggered position. They used a 0.0508 × 0.0508 m plexiglass channel as an internal passage with Reynolds numbers 70,000 and 90,000. For both the Reynolds numbers, 60° angled broken ribs inversely positioned in a staggered position showed the highest heat transfer. Kumar et al. [35] studied V rib turbulators with bleed holes. Different combination of V ribs such as 60° V ribs, 60° inverted V ribs, combination of 60° V rib at the inlet and inverted 60° V ribs at outlet and 60° inverted V rib at the inlet and V rib at outlet were considered with Re numbers 12,500 and 28,500. Turbulence models were used SST k–ω and RSM. Temperature distribution along the channel showed that a distinctive peak in heat transfer around the bleed holes and rib turbulators. The numerical study claimed that the combination of 60° inverted V rib at the inlet and V rib at outlet with bleed holes provided better heat treatment. The authors suggested that the use of rib turbulator with bleed holes suitable for augmenting blade cooling to obtain an optimal balance between thermal and mechanical design requirements. Several studies showed that skewing the ribs contributes the heat transfer enhancement. Ribs angled into mainstream flow increase the heat transfer enhancement due to turbulence of the air. Taslim and Spring [36] investigated the effect of blockage in a cooling channel. The blockage can increase the heat transfer, but it comes with the friction loss penalty. The optimum rib turbulator design should be implemented which has maximum heat transfer enhancement with minimum pressure loss penalty.

A number of ribs studies have been conducted for rotational gas turbine blade internal cooling channel. Buoyancy, centrifugal forces, and Coriolis forces have an important effect on the heat transfer coefficient. Mochizuki et al. [37] examined the effects of these forces in a ribbed surface cooling channel. The Buoyancy, centrifugal forces, and Coriolis forces produce secondary flow and force the heavier fluid to flow away from the center of rotation.

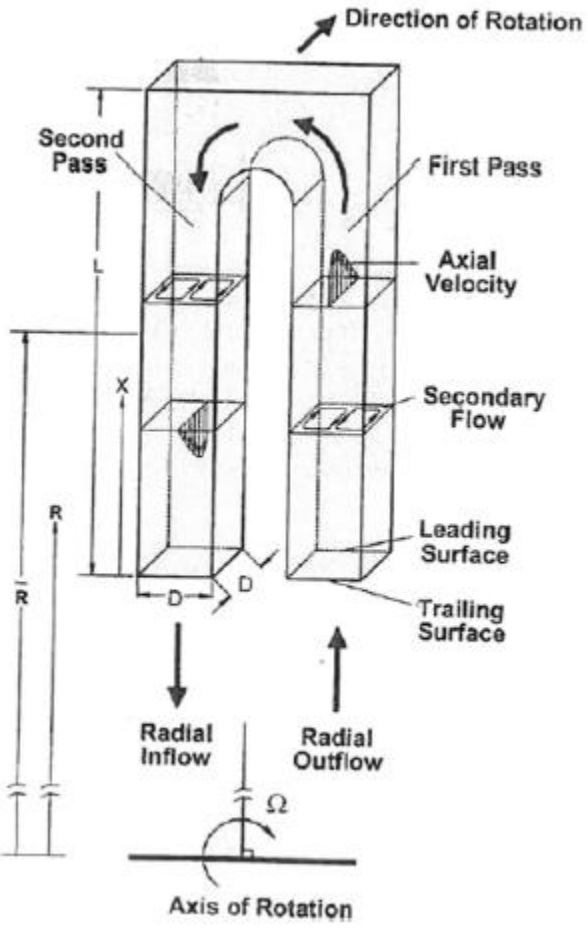


Figure 2-2: Coolant flow through a two-pass rotating passage [38]

Figure 2-2 represented the coolant flow through a two-pass rotating passage. It is described by Han and Chen [38]. Rotation in the cooling passage stimulated centrifugal and Coriolis forces which causes cross-stream secondary flow in the passage. That is why the heat transfer behavior is quite different in a rotating frame than a stationary frame. The result of their study shows that rotation increases heat transfer on one side of the channel even though it reduces on the opposite side due to secondary flow.

Kiml et al. [39] conducted an experimental study with 45°, 60°, 75°, and 90° ribs in a rectangular channel with an aspect ratio of 2:1. The experimental study confirmed that rib turbulators induces a secondary flow which contributes heat transfer enhancement. The flow along the ribs hit the top wall, turn back, and carry clod air from the passage core region towards the bottom wall. The 60° ribs had the highest heat transfer coefficient because of the strong rotational momentum of the secondary flow.

Wang et al. [40] examined the 60° inclined ribs in a cooling channel. It produces a pair of counter rotating vortices. The vortices lead the air from the center of the passage to the smooth wall adjacent to the leading edge of the ribs. The low cooling region was found at the core of the vortices. The research team concluded that the flow field behind the parallel ribs was considerably affected by the secondary flows as the heat transfer coefficient contours do not run parallel to the ribs. Baggetta et al. [41] explored the gas turbine blade internal cooling based on the 45° inclined ribs. They examined three cases: (a) without intersecting rib, (b) with one intersecting rib, and (c) with two intersecting ribs. Due to the influence of the secondary flows, the vortices move along the ribs and join the mainstream. The moving vortices contain the core air at low temperatures which affects the local heat transfer enhancement.

## 2.4. Gas Turbine Blade Internal Cooling with Pin-fins

Gas turbine blade trailing edge contains limited space. Pin-fin cooling is suitable in this limited space. The distribution of heat transfer is affected by the shape and geometry of the pin-fins. Flow separation and wake drops take place at the downstream due to the arrangement of the pin-fins in the cooling channel. It leads to the enhancement of the heat transfer. Cylindrical shapes of pin-fins with circular cross-section are the most common shapes of pin-fins which was studied

widely. It was used in the cooling passage of gas turbine blade where impingement or multi pass channels with ribs cannot be accommodated because of manufacturing constraints [42]. Metzger et al. [43] performed the experimental study on pin-fins in 1982. The research team investigated the effect of air flow in a wedge-shaped duct. The results indicated that the pin-fins caused significant amount of heat transfer in a cooling section. The study of Hwang and Lui [44], Carcassi et al. [45], and Facchini et al. [46] investigated the pin-fin arrays on a pedestal in a converging duct. They revealed the effect of an accelerating flow both on heat transfer and pressure drop.

Sahiti et al. [47] contributed to the literature by studying different shaped of pin-fins. Six different cross section of pin-fins were studied with inline and staggered arrangement. The configurations were NACA, Dropform, Lancet, Elliptic, Circular and Square. The study was performed numerically using $K$- $\varepsilon$ model. The results showed that the staggered elliptic profile performed better compared to other pin-fins shapes based on the heat transfer enhancement. Siw et al. [48] investigated the triangular and semi-circular shaped pin-fin arrays numerically. The computational study focused on realizable $K$- $\varepsilon$ model. The residuals were less than $10^{-5}$ for velocity, energy, turbulence kinetic energy, dissipation rate, and continuity equation. $K$- $\varepsilon$ model. Horseshoe vortices were reflected semi-circular shaped pins. It contributed to considerable heat transfer enhancement at the leading and adjacent areas of the pin-fins elements. But for triangular pins the heat transfer performance was different. For the triangular shapes, the more streamline profile was found at the leading region and the flow tends to pass through the pins generating minimal turbulence effects and flow mixing. As a result, the heat transfer was lower at that region. Heat transfer increased substantially at the trailing region because of additional wakes generated by the two sharp edges which directed to better mixing and heat transfer enhancement. The wakes generated by the triangular pins were wider compared to the semi-circular pins.

Jin et al. [49] studied five different turbulence models. They are standard *K*- *ε,* realizable *K*- *ε,* RNG *K*- *ε,* standard *K*- *ω,* and SST *K*- *ω.* The numerical results were compared with the experimental results from the literature. Six pin -fin shapes i.e., circular, elliptic, oblong, teardrop, lancet, and NACA were considered to study. The research claimed that Realizable *K*- *ε* model is better at capturing the microstructure of flow field and has higher precision in predicting the averaged Nusselt number. The pin-fins orientation on cooling performance was studied by Effendy et al. [50]. The computational study was performed with five different arrangements – circular staggered, elliptic streamwise staggered, elliptic spanwise, elliptic inline staggered (45°), elliptic counter rotating staggered (45°). The 45° angled configuration was the feasible solution to enhance the heat transfer coefficient of pin-fins and end walls while keeping the friction loss at a minimum level. Another numerical study of Ricklick and Carpenter [51] compared different turbulence models. They are realizable *K*- *ε,* SST *K*- *ω,* the $v^2$-f model, and a quadratic formulation of the realizable *K*- *ε* model. The staggered orientation was considered with 10 rows of pin-fins. The study claimed that the quadratic version of the realizable *k*-*ε* model tends to predict heat transfer levels most accurately.

The Unsteady Reynolds-Averaged Navier–Stokes model was used by Delibra et al. [52]. The study also used large eddy simulation technique. It is one of the rarely studied model in the open literature. At higher Re numbers, the LES model worked better. A few studies have been conducted in rotational pin-fin arrays. Liang and Rao [53] conducted a rotational study on it recently. The computational study was conducted using the rotation number 0 – 0.3 with Re number ranging from 20,000 to 80,000. They used the standard *K*- *ε* model. The rotation effects increased the friction factors and the heat transfer enhancement in the pin-fin arrays and the

detached pin-fin arrays. However, the overall thermal performance factors of the detached pin-fin arrays might be about 18.3% higher compared to those of the pin-fin arrays.

The literature review on pin-fin arrays on gas turbine blade cooling channel shows that the study was mostly conducted numerically. The *K*- $\varepsilon$ turbulence model was highly used for the computational study. The circular, semi-circular and elliptical shapes of pin-fins were used both in inline and staggered arrangements. Most of the studies were conducted with a stationary motion. There is a gap in literature to find out other pin-fin shapes of pin-fin's heat transfer and friction loss behavior in a rotational motion.

## 2.5. Goals and Objectives of the Research

The literature review on gas turbine internal cooling has been completed. It covered the surface roughness of the cooling channel using smooth, dimpled, ribbed, and pin-fin. It also covered the effect of guide vanes on a cooling channel. The study reveals that further research is required in this field. The literature has good research on smooth surface cooling channel and rib roughened channel. Few researchers worked on dimpled channel, but rotational dimpled channel was rarely investigated. The least investigated cooling channel is pin-fin cooling channel. Researchers have completed numerical study using Reynolds-averaged Navier–Stokes model mostly. There is a room to study Large Eddy Simulation methods to get a clear idea on flow direction.

The motivation of this experimental and numerical study is to investigate the dimpled cooling channel with different arrangements of the dimples. It also investigated the comparison of different ribs in a cooling channel. The pin fin cooling channel was investigated thoroughly so that it can add new research to the literature. The effect of guide vanes in a cooling channel investigation has

added to the completeness of this research. For all the cases, the same cooling channel was used as a mold. The main goals of the current study have been mentioned below in a nutshell-

1. The smooth surface was considered as a baseline case for U-bend cooling channel.
2. Different dimple shapes and arrangements were considered.
3. Comparison of various ribbed surfaces was completed.
4. Pin-din cooling channels were investigated.
5. All the cases were investigated both stationary and rotational cases.
6. The effect of guide vanes in cooling channel was investigated.
7. The maximum rotation was considered 900 rpm with Reynolds number 65,000.
8. Experimental results were presented to reveal the complex three-dimensional flows and heat transfer phenomena.
9. Large Eddy Simulation Methods (LES) were applied for computational study.
10. Validation of experimental and numerical study was obtained.

# 3. Study on Gas Turbine Blade Internal Cooling with Dimpled Surface

## 3.1. Introduction

The study presents the investigation on heat transfer distribution along a gas turbine blade internal cooling channel. Six different cases were considered in this study, using the smooth surface channel as a baseline. Three different dimples depth-to-diameter ratios with 0.1, 0.25, and 0.50 were considered. Different combinations of partial spherical and leaf dimples were also studied with the Reynolds numbers of 6,000, 20,000, 30,000, 40,000, and 50,000. Besides, rotational study has been conducted with 300 RPM, 600 RPM and 900 RPM. In addition to the experimental investigation, the numerical study was conducted using Large Eddy Simulation (LES) to validate the data. It was found that the highest depth-to-diameter ratio showed the highest heat transfer rate. However, the deepest dimpled channel shows the highest pressure drop which affects the overall thermal performance of the cooling channel. The results showed that the leaf dimpled surface is the best cooling channel based on the highest Reynolds number's heat transfer enhancement and friction factor. However, at the lowest Reynolds number, partial spherical dimples with a 0.25 depth to diameter ratio showed the highest thermal performance. The rotational study indicates that the rotation effect, dimple arrangement, and design have significant influences on heat transfer. Results indicated that the partial spherical 1-row dimpled surface experienced the highest heat transfer coefficient and pressure drop. In contrast, the leaf-shaped dimpled cooling channel experienced the highest thermal efficiency.

## 3.2. Experimental Procedure and Data Reduction

An experimental setup was built in the gas turbine lab of the University of Wisconsin – Milwaukee to run stationary and rotational cases. Figure 3-1 shows the experimental setup. A-36 steel alloy was used to make the test rig. Figure 3-2 indicates the dimensions of the test rig. Leg 1 is 490 mm, and leg 2 is 460 mm long. The hydraulic diameter of the channel is 40 mm. The set-up can run a maximum of 1000 RPM. The rotation was enabled with a 7.5 HP 3 phase induction motor via a pulley. The same channel was mounted to the system to balance the test rig while rotation. 3D printed dimples were glued in this channel. The bottom wall of this channel experienced a constant heat flux, i.e., 2,000 $W/m^2$. The constant heat flux was delivered using a variable transformer to the channel. The variable transformer was connected to the electrical heaters, which were inserted at the bottom wall. A thin layer of packing foam and a 0.125mm thick layer of a resin based phenolic sheet was set from inside to minimize the heat loss. Dimples were wrapped with copper foil to ensure uniform temperature distribution. A 1.5 hp 3-phase blower was connected to the setup to provide the coolant. A VFD was used to change the air speed. Figure 3-3 represents the block diagram of the experimental setup. An in-line flow meter was attached to record the flow entering the channel. 13 Omega® miniature portable wireless thermocouples were used to record the temperature and the dimpled test rig. Thermocouples probes were taped to the bottom surface of the cooling channel. The signal was sent to the receiver which was kept a little away from the set-up. Table 3-1 shows the thermocouple locations along the channel.

Figure 3-1: Experimental test rig

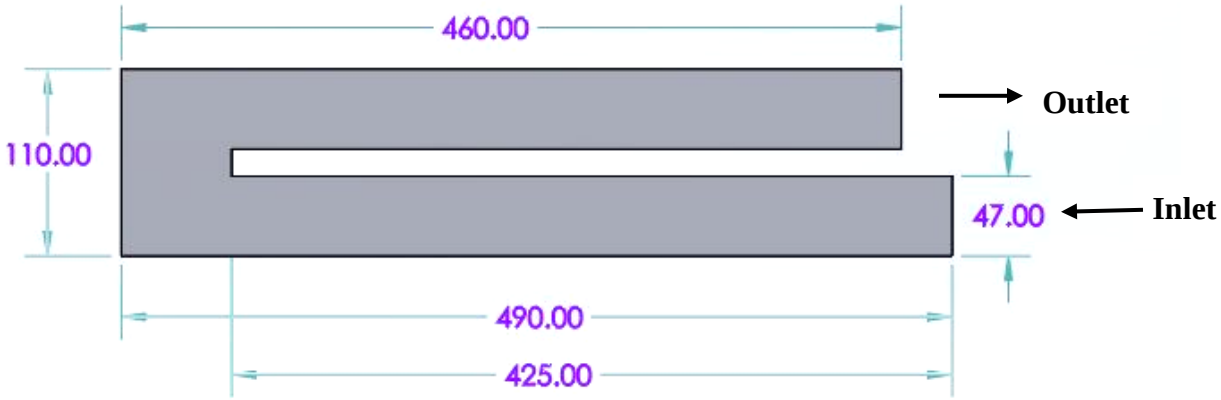


Figure 3-2: Dimensions of the cooling channel (all dimensions are in mm)

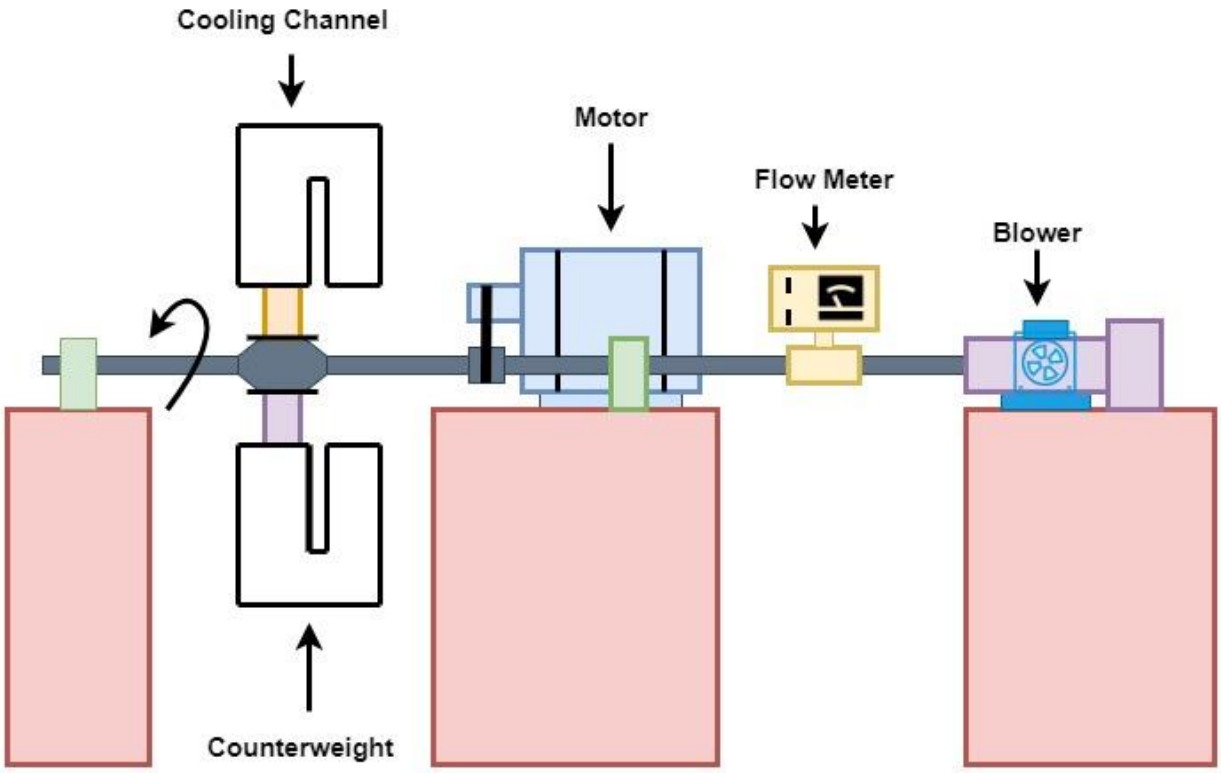


Figure 3-3: Diagram of the experimental setup

Table 3-1: Thermocouple locations along the cooling channel

| Thermocouple Number | Thermocouple Locations |
|---|---|
| 1 | 210 mm from the inlet |
| 2 | 300 mm from the inlet |
| 3 | 360 mm from the inlet |
| 4 | 410 mm from the inlet |
| 5 | 450 mm from the inlet |
| 6 | 480 mm from the inlet |
| 7 | Bend is the location at the center |
| 8 | 350 mm from the outlet |
| 9 | 200 mm from the outlet |
| 10 | 100 mm from the outlet |
| 11 | 70 mm from the outlet |
| 12 | 40 mm from the outlet |
| 13 | 10 mm from the outlet |

Table 3-2 describes the details of the six channels considered in stationary cases study. The study includes a smooth surface channel with different combinations of dimples in both legs. Three different dimple depths-to-diameter ratios with 0.1, 0.25, and 0.50 were considered in this study. Table 3-3 shows the cases considered for rotational cases study and Table 3-4 represents the rotation numbers for the respective RPMs.

Table 3-2: Channel details for Ro = 0

| **Channel Name** | **Surface Type** | **Number of Dimples in Leg 1** | **Number of Dimples in Leg 2** | **Dimple Diameter, (mm)** | **Dimple Depth, (mm)** | **Dimples Depth to Diameter Ratio** | **Percentage of Area Occupied by Dimples (%)** |
|---|---|---|---|---|---|---|---|
| Case A | Smooth | N/A | N/A | N/A | N/A | N/A | N/A |
| Case B | Partial Sphere | 8 × 1 | 7 × 1 | 40 | 20 | 0.50 | 20.65 |
| Case C | Partial Sphere | 8 × 1 | 7 × 1 | 40 | 10 | 0.25 | 20.65 |
| Case D | Partial Sphere | 8 × 1 | 7 × 1 | 40 | 4 | 0.10 | 20.65 |
| Case E | Partial Sphere | 8 × 2 | 7 × 2 | 20 | 10 | 0.50 | 10.30 |
| Case F | Leaf | 8 × 2 | 7 × 2 | 20 | 10 | 0.50 | 10.30 |

Table 3-3: Channel details with rotational cases

| Channel Name | Surface Type | Number of Dimples in Leg 1 | Number of Dimples in Leg 2 | Dimple Diameter, (mm) | Dimple Depth, (mm) | Dimples Depth to Diameter Ratio | Percentage of Area Occupied by Dimples (%) |
|---|---|---|---|---|---|---|---|
| Case A | Smooth | N/A | N/A | N/A | N/A | N/A | N/A |
| Case C | Partial Sphere | 8 × 1 | 7 × 1 | 40 | 10 | 0.25 | 20.65 |
| Case E | Partial Sphere | 8 × 2 | 7 × 2 | 20 | 10 | 0.50 | 10.30 |
| Case F | Leaf | 8 × 2 | 7 × 2 | 20 | 10 | 0.50 | 10.30 |

Table 3-4: Summary of rotational experimental cases

| Cooling Surface | RPM | Rotation Number |
|---|---|---|
| Case A | 300 | 0.36, 0.15, 0.07 |
| | 600 | 0.71, 0.30, 0.13 |
| | 900 | 1.07, 0.45, 0.20 |
| Case C | 300 | 0.36, 0.15, 0.07 |
| | 600 | 0.71, 0.30, 0.13 |
| | 900 | 1.07, 0.45, 0.20 |
| Case E | 300 | 0.36, 0.15, 0.07 |
| | 600 | 0.71, 0.30, 0.13 |
| | 900 | 1.07, 0.45, 0.20 |
| Case F | 300 | 0.36, 0.15, 0.07 |
| | 600 | 0.71, 0.30, 0.13 |
| | 900 | 1.07, 0.45, 0.20 |

The air velocity, $u$, was recorded during the experiment. The standard properties of density, $\rho$, and dynamic viscosity (air), μ was considered. The hydraulic diameter, $D_h$ was used as the characteristic length for the Reynolds number,

(1) $Re = \frac{\rho u D_h}{\mu}$

The heat input into the system was equal to the electrical power input which is defined by the equation (2). The heat flux, $Q''$ can be calculated using power input, $Q$, and the heat transfer area, $A$ which leads equation (3).

(2) $Q = R \times I^2$

(3) $Q'' = \frac{Q}{A}$

The convective heat transfer, h was calculated using the heat flux, $Q''$ and the difference between the surface temperature, $T_s$ and the ambient temperature, $T_\infty$.

(4) $h = \frac{Q''}{T_s - T_\infty}$

The convective heat coefficient, $h$ leads the Nusselt number for the channel.

(5) $Nu = \frac{h \times D_h}{k}$

The theoretical Nusselt Number, $Nu_o$, for the turbulent flow, was calculated using the Dittus-Boelter equation,

(6) $Nu_0 = 0.023 \times Re^{0.8} \times Pr^{0.4}$

The pressure coefficient was calculated using the pressure drop performance of the cooling channel, $\Delta P$ , density of air $\rho$, and inlet velocity $u$.

$$(7)\ C_p = \frac{\Delta P}{0.5\rho u^2}$$

The friction factor, *f*, represents the pressure drop performance of the cooling channels. The Darcy friction factor of the flow across the cooling channel can be shown as follows,

$$(8)\ f = \frac{\Delta P}{(L/D_h)(1/2\rho u^2)}$$

Friction factors for all channels were normalized with the Blasius formula [30]. For Re < $10^5$, the Blasius formula for the friction factor is as follows,

$$(9)\ f_0 = 0.316Re^{-0.25}$$

Calculating the efficiency of the channel is essential. Sometimes, the heat transfer shows a satisfying performance. However, pressure drop plays a vital role in the case of thermal performance. Using a dimpled, ribbed and pin-finned surface, pressure drop acts as a negative influence for an effective heat transfer efficiency. By calculating the efficiency of a channel, the optimum pressure drop can be identified. The efficiency was calculated using the following formula,

$$(10)\ \eta = \frac{Nu/Nu_o}{(f/f_o)^{1/3}}$$

The rotational speed was found from the controller of the rotation speed and leads to the calculation of the rotation number, which is

$$(11)\ R_o = \frac{\Omega D_h}{u}$$

### 3.3. Physical Model and Boundary Conditions

The numerical solutions were set up to understand the flow behavior and heat transfer in smooth surfaces and dimpled surface cooling channels. The same dimensions of the cooling channel conducted in the experiments were used in the numerical study to compare with the experimental research. The LES solution technique was considered. No-slip velocity condition was set to the walls. Turbulent velocity distribution was selected for the inlet, and a pressure outlet was set for the outlet. The inlet boundary condition was set as velocity inlet and segregated flow. To compare with the experimental results, the same heat flux, i.e., 2,000 $W/m^2$ was applied to the bottom surface of the channels, and the rest of the wall was considered adiabatic.

The mesh independent study was conducted for 1.8, 2.5, 4.2, and 10 million cells for Case C. Figure 3-4 shows the surface average Nusselt Number (Nu) for four different cells at Re = 30,000. The 2.5 and 4.2 million cells have the closer Nu number. The LES solution takes a substantial amount of time to complete a solution. Thus, the 2.5 million cells were considered for all the cases. The physical time is 1s with time step 0.0001s. Surface remesher and prism layers were considered. There was a total of 12 prism layers set to capture the near-wall behavior with 1.2 stretching of the cells. Figure 3-5 reveals the meshed scene for Case E at Re = 30,000.

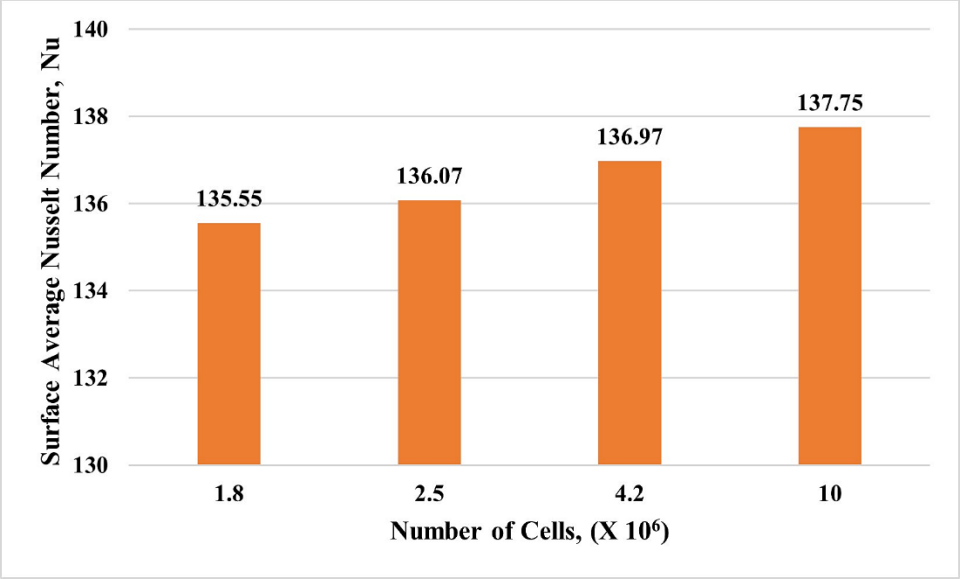


Figure 3-4: Mesh independent study at Re = 30,000 for Case E

Figure 3-5: Mesh scene with 2.5 X $10^6$ number of cells

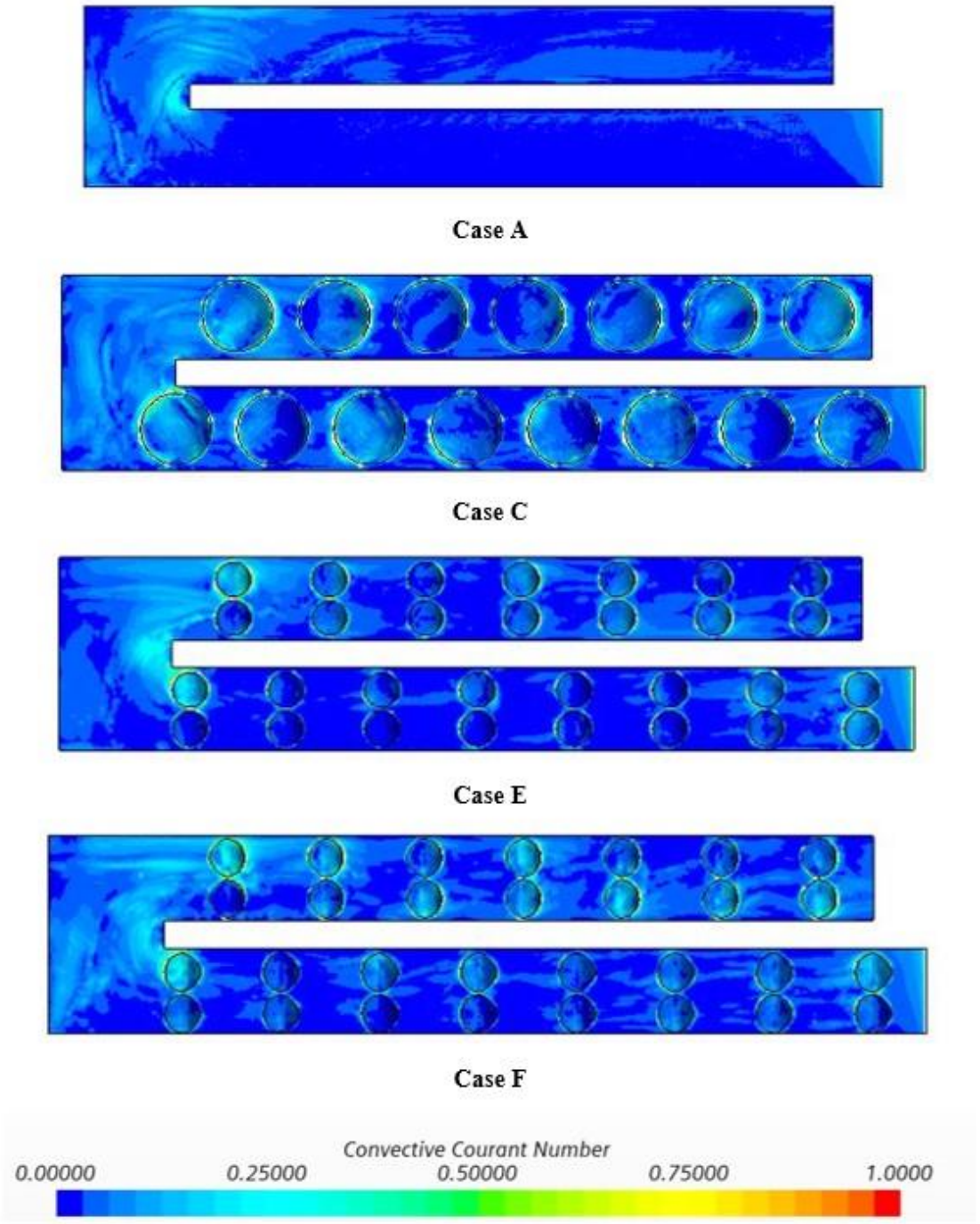


Figure 3-6: Convective courant number at Ro = 0.20

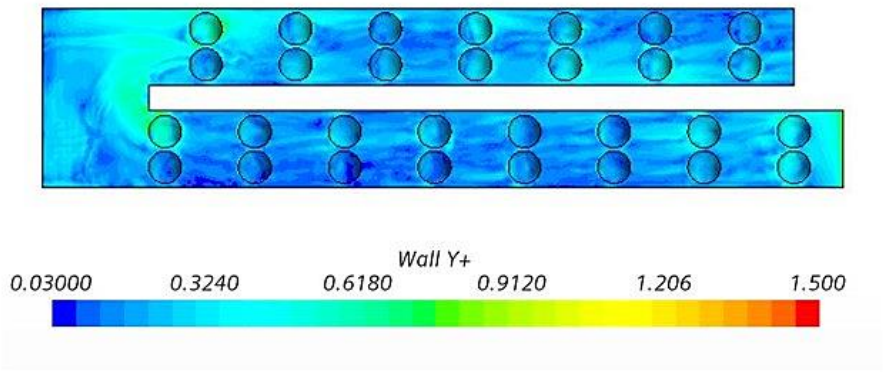


Figure 3-7: Wall Y+ at Ro = 0.20

An implicit unsteady solver was considered in these solutions, which resulted in a maximum Convective Courant Number (CCN) of 0.36 for a smooth surface and 0.54 partial spherical dimpled surface at the maximum Re number = 50,000 at 900RPM (Figure 3-6). Figure 3-7 represents the Wall Y+ behavior of Case C. Wall distance, Y+, indicates the non-dimensional distance from a wall. The maximum value of wall Y+, 0.91, was found in the bend section of the channel. In the bend section, airflow changes its flow direction and becomes more turbulent.

## 3.4. Computational Model Validation and Uncertainty Analysis

The experimental Nusselt number was normalized with the theoretical one. The scatter bars of Figure 3-8 are obtained using a 95% confidence level [54]. Figure 3-9 shows the comparison between the experimental and numerical results. There is a slight difference between experimental and numerical results. The maximum deviation is 12%, and it is found right before the bend section. Before entering the bend, the air becomes more turbulent, which causes an irregular airflow. Figure 3-10 represents the heat transfer along the leaf dimpled cooling channel for rotation number 0.20. The difference between experimental and numerical results is observed as the

environment was not ideal during the experiment, but the ideal condition was considered in the computational study.

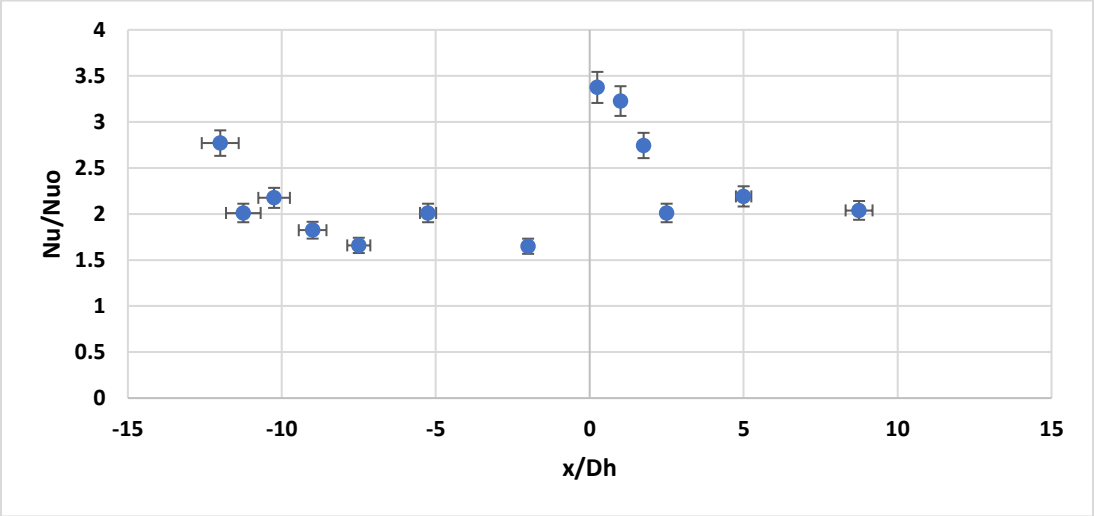


Figure 3-8: Error analysis of experimental data at 95% confidence level (Case E at Re =50,000)

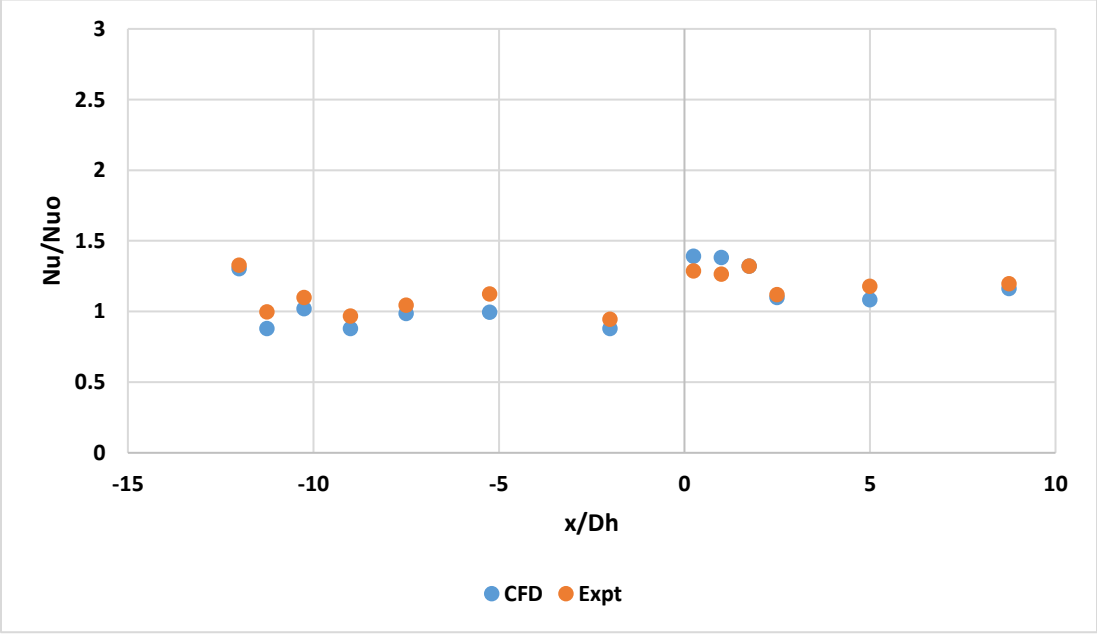


Figure 3-9: Comparison between experimental and numerical data (Case E at Re = 50,000)

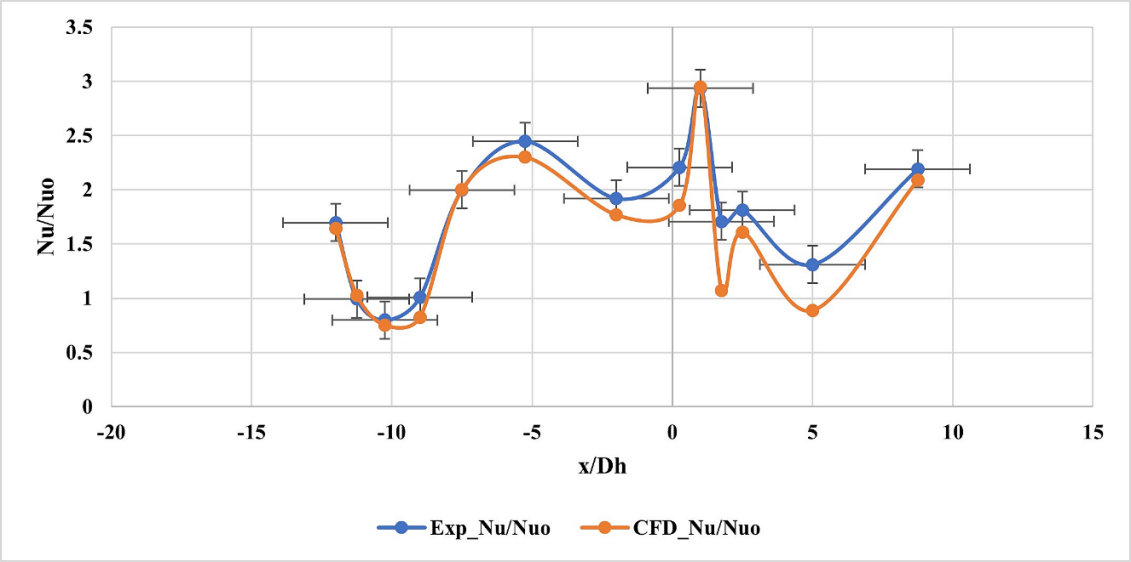


Figure 3-10: Error analysis of experimental data at 95% confidence level (Case F at $R_o$ = 0.20)

## 3.5. Results

### 3.5.1. Velocity distribution along the channel

The heat transfer distribution along the channel can be predicted from the velocity profile. The velocity profile shown in Figure 3-11 is at Re = 50,000 for the first leg. For Case A, the air flows along the channel evenly before reaching the bend section. A vast vortex roll has been seen before the bend. For Case B to Case F, the first vortex roll appears at the first dimple. After the dimple, it became less turbulent. The bend section of the dimpled surface acts the same as the smooth surface channel. Leg 2 shows more turbulent airflow compared to leg 1 (Figure 3-12). The vortex rolls act more irregularly near the bend region, and it continues almost the entire second leg passage. After the bend, the airflow changes the direction of action. All the dimple channels experience flow separation and recirculation upstream of the dimples. It weakens the heat transfer upstream. The flow again attaches and creates vortex rolls downstream, increasing the heat transfer at the dimpled channels.

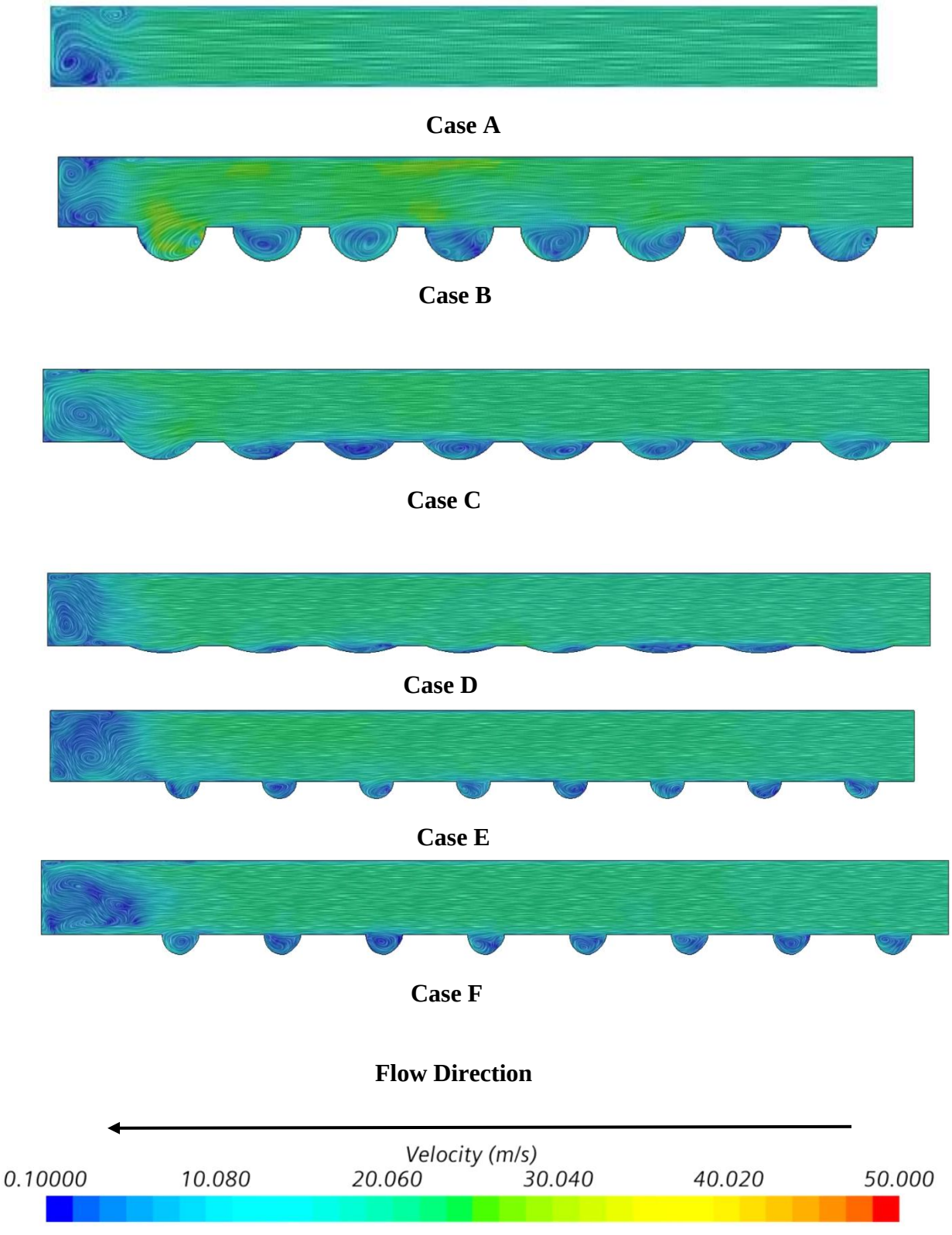


Figure 3-11: Velocity distribution along leg 1 for all cases at Re = 50,000 with $R_o = 0$

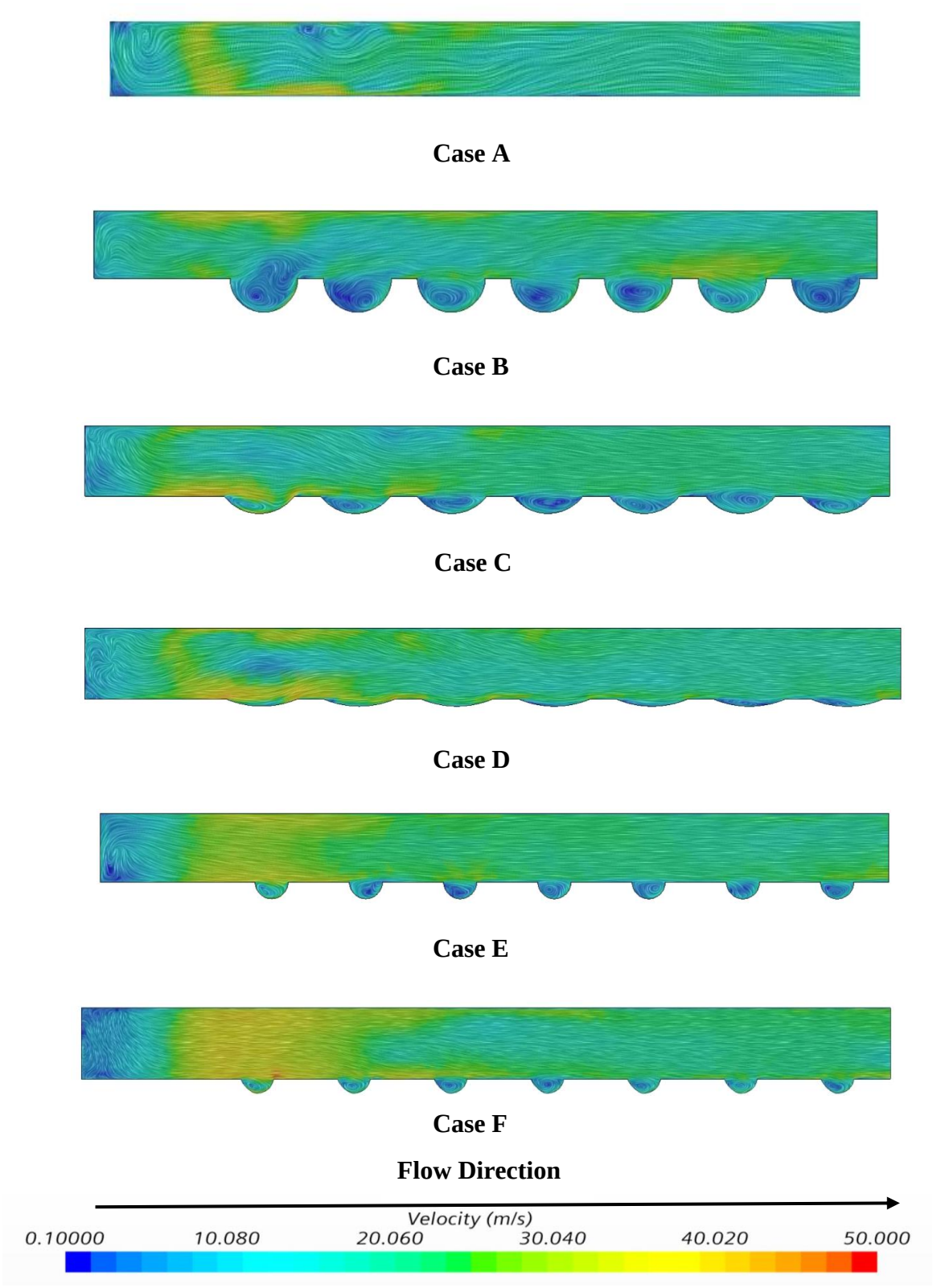


Figure 3-12: Velocity distribution along leg 2 for all cases at Re = 50,000 with $R_o = 0$

Figure 3-13 represents the velocity distribution at leg 1 for Re = 50,000 at 900 RPM. The flow pattern is different in the case of rotational cases. There is a strong effect of Coriolis and buoyancy forces in the rotational motions, which also increases the heat transfer in the case of the rotor and reduces the pressure drop. The entrance through before the bend, the flow pattern is regular. However, near the bend region, flow started getting irregular. The first vortex roll appears near the bend region for Case A. For Case C, Case E and Case F or dimpled cases, the first vortex appears at the first dimple, and near the bend section, the flow pattern is more irregular with huge turbulence. Figure 3-14 represents the velocity pattern of leg 2. In leg 2, the direction of flow changes, and after the bend, it shows higher turbulence which carries around the mid-portion of leg 2. This phenomenon describes the higher heat transfer in the bend region and leg 2.

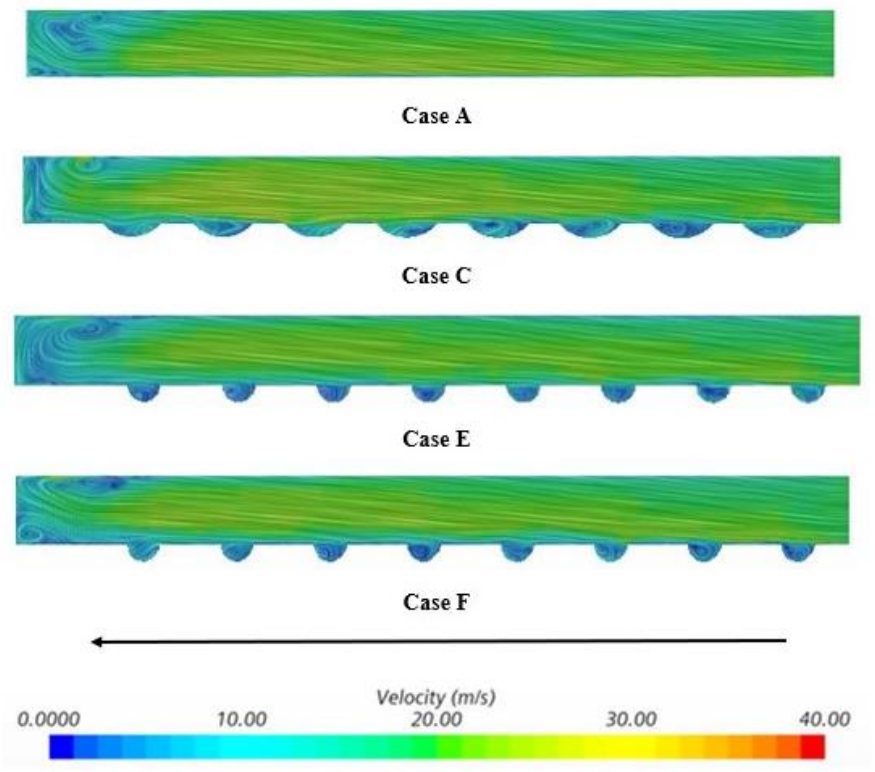


Figure 3-13: Velocity Distribution along Leg 1 for different cases at Re = 50,000, RPM = 900, and Ro = 0.20

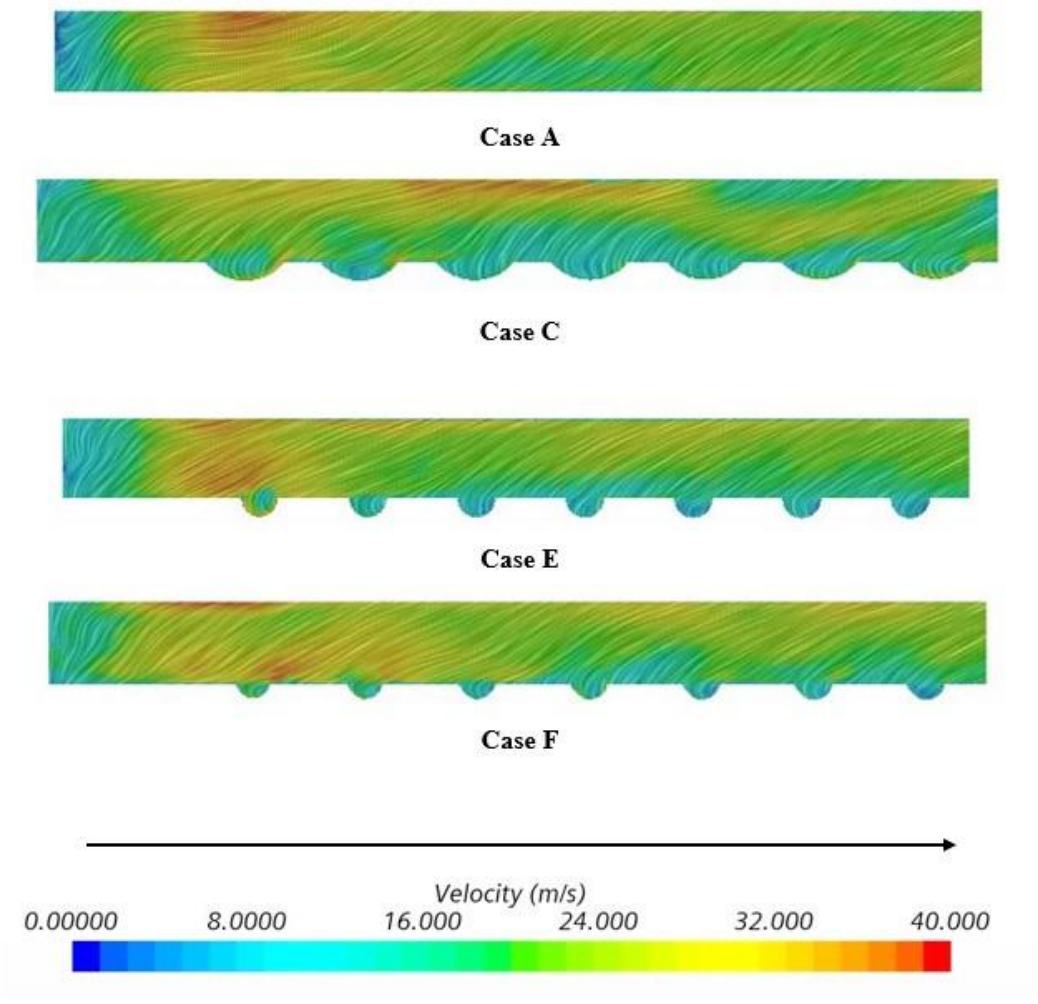


Figure 3-14: Velocity Distribution along Leg 2 for different cases at Re = 50,000, RPM = 900 and Ro = 0.20

### 3.5.2. Temperature distribution along the channel

The temperature distribution at the bottom wall along the cooling channels has shown in Figure 3-15. For a smooth surface channel, the temperature right after the entrance is lower than its mid-section. As the air passes the entrance, the temperature increases and reaches the highest point before entering the bend due to continuous heat extraction from the bottom wall. The bend

section experiences a higher local velocity. As a result, it has a comparatively low temperature. The local air velocity decreases with the increase of distance from the bend section, leading to a higher temperature at the second leg.

The different combinations of dimpled channels showed the lower temperature in the mid-section of the first leg. This observation is because the dimples in the bottom surface ease the temperature distribution along the channel. The bend section and the second leg of the channel showed comparatively low temperature compared to the smooth surface channel due to the contribution of the dimples, which can be more visualized from velocity and heat transfer augmentation results. Case B, Case C, and Case E covered 20% of the total cooling channel area with dimples, while Case E and Case F covered 10%. The temperature distribution profile shows that the higher dimpled covered area channels produce a higher heat transfer than the lower one.

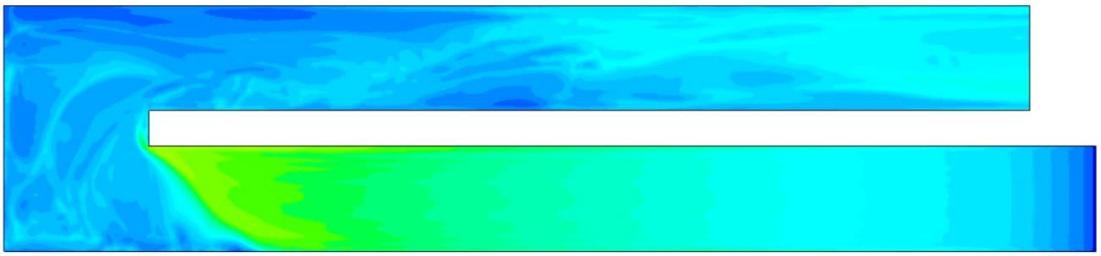

**Case A**

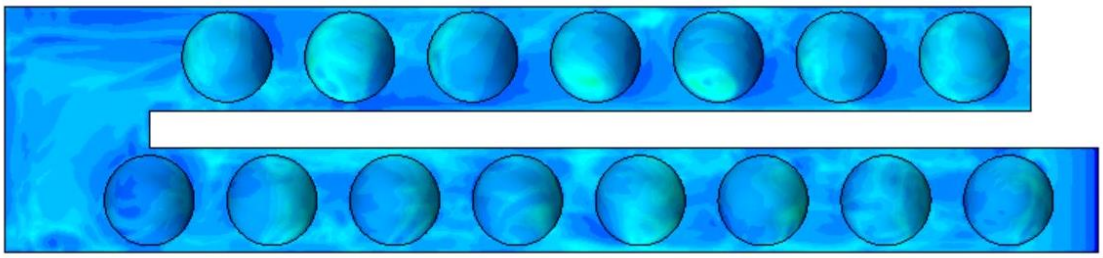

**Case B**

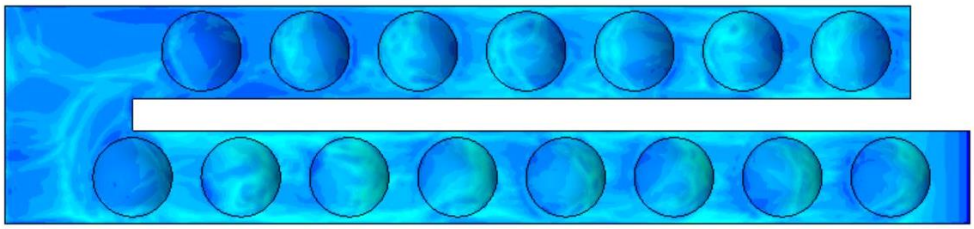

**Case C**

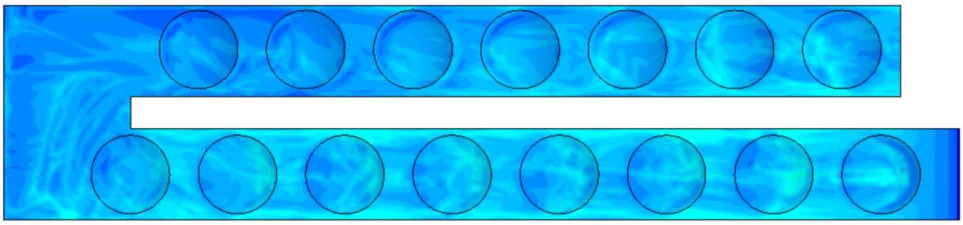

**Case D**

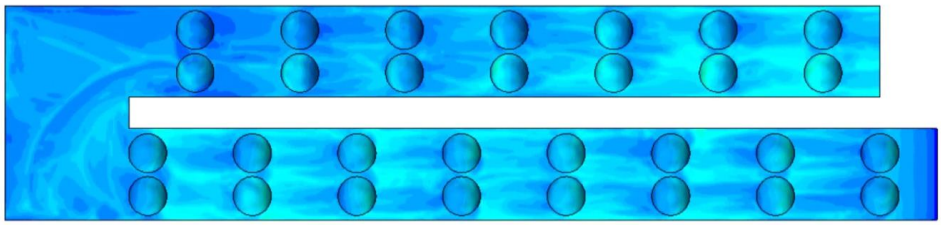

**Case E**

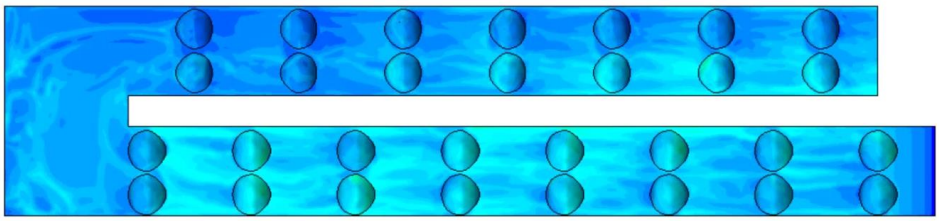

**Case F**

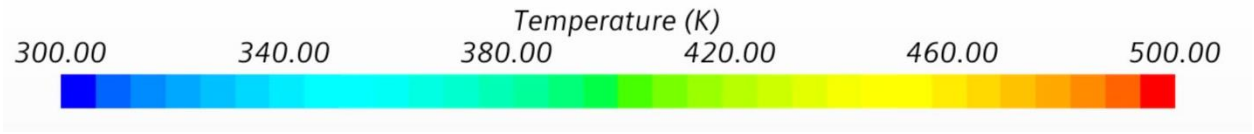


Figure 3-15: Temperature distribution along the channels at Re = 50,000 at Ro = 0

### 3.5.3. Heat transfer augmentation along the channel

The experimental results of heat transfer augmentation along the smooth surface channel are shown in Figure 3-16 At the entrance of the channel, the Nu number reaches the higher values. It decreases in the mid-portion, and at the bend section, it reaches the highest peak and decreases along the second passage. It matches with the temperature distribution shown in Figure 3-15. The highest temperature region had the lowest heat transfer and vice versa. The highest temperature region needs more air to be cooled. As the mass flow rate of air is the same all over the channel, the high-temperature area shows low heat transfer. Figure 3-17, Figure 3-18, and Figure 3-19 represent the dimpled channel heat transfer distribution. Figure 3-17 represents the partial sphere dimpled case with 1-row dimple heat transfer. In this case, the heat transfer is slightly asymmetrical due to the highest dimple depth. In the mid-section of the first leg, there is a sudden decrease in heat transfer. Due to the thermal entrance flow phenomena, the heat transfer showed significantly high values and rapidly decreased after that [55]. Later it increased and showed the highest heat transfer at the bend region.

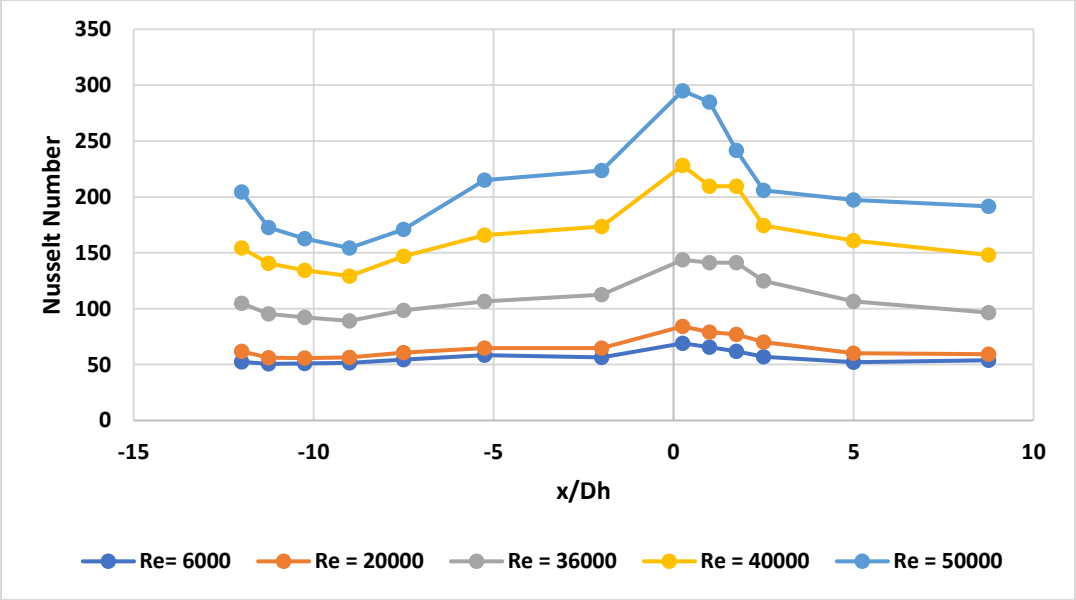


Figure 3-16: Heat transfer augmentation along the channel for Case A at Ro = 0 (experimental)

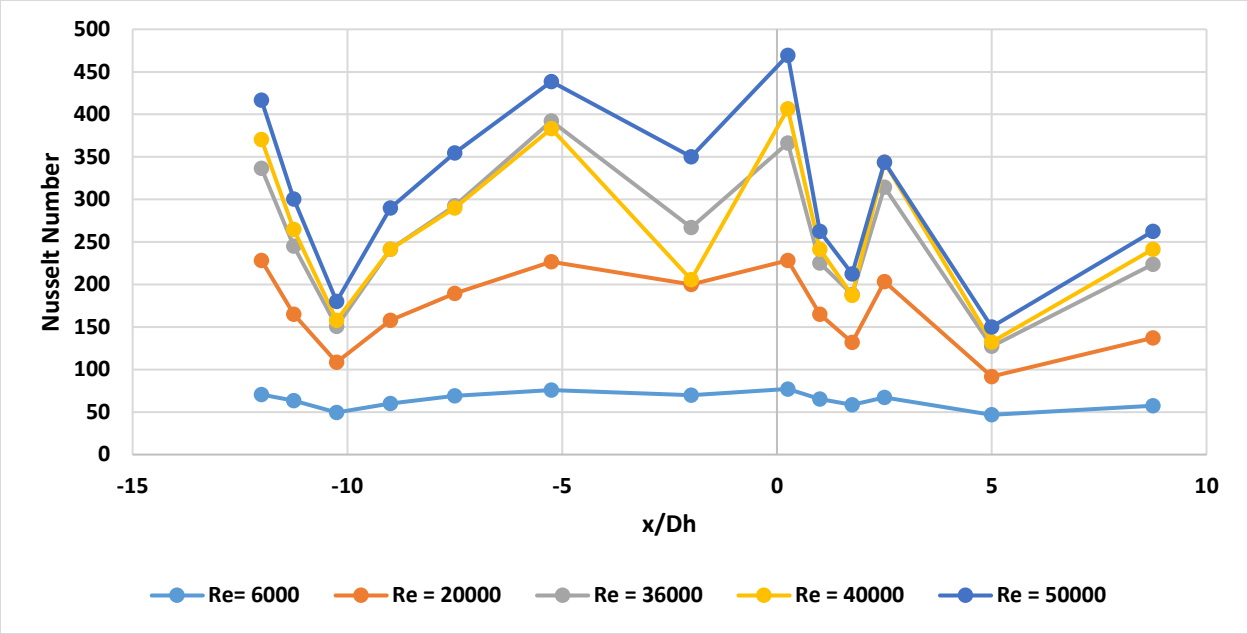


Figure 3-17: Heat transfer augmentation along the channel for Case C at Ro = 0 (experimental)

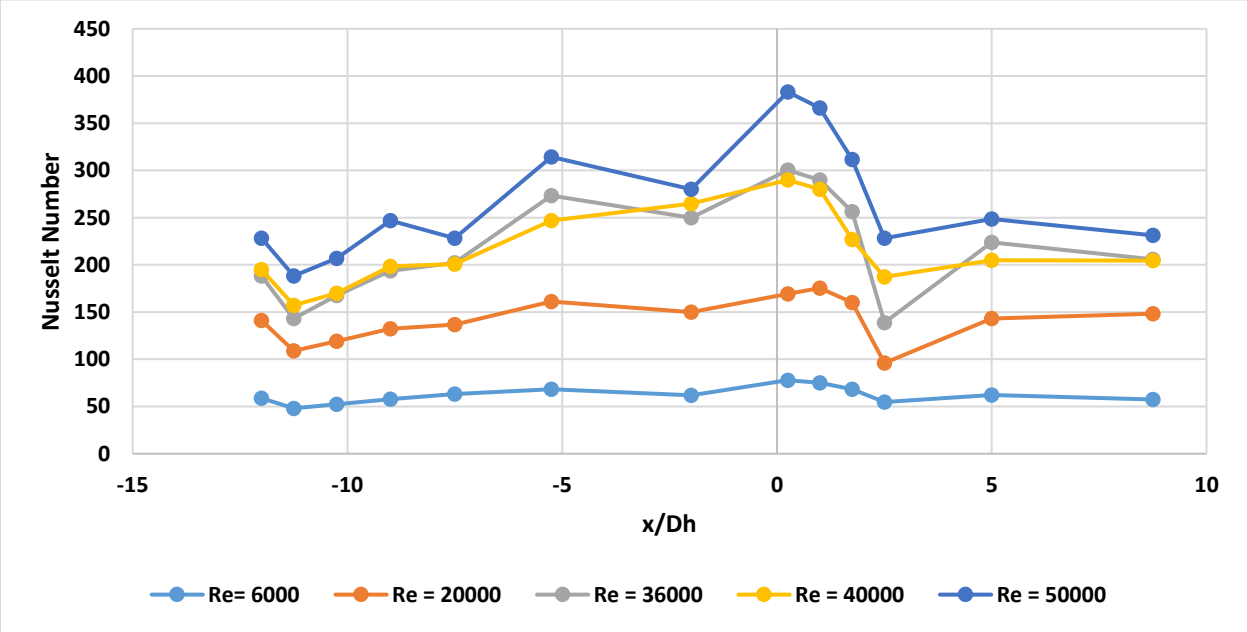


Figure 3-18: Heat transfer augmentation along the channel for Case E at Ro = 0 (experimental)

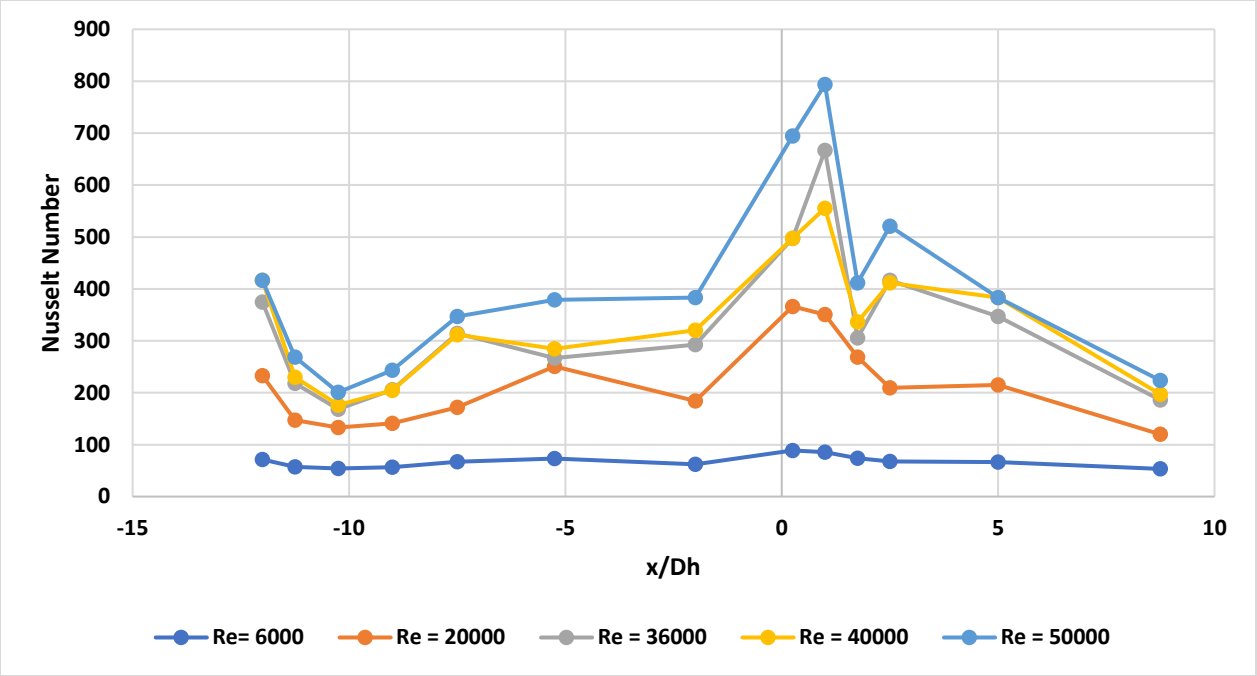


Figure 3-19: Heat transfer augmentation along the channel for Case F at Ro = 0 (experimental)

Figure 3-18 indicates the heat transfer distribution along the channel for Case E. It shows a similar behavior as Case C. The heat transfer distribution along the channel for leaf dimpled cases is found in Figure 3-19. The heat transfer trend is similar to other cases. However, the leaf dimpled case indicates the highest transfer among all the channels due to a slight inward tilted curve.

Due to rotational speeds, Coriolis force generates secondary forces inside the cooling channel. It creates crossflow patterns. Density gradients cause buoyancy forces, making the free convection heat transfer more significant. Figure 3-20, Figure 3-21, and Figure 3-22 represent the heat transfer distribution along the smooth surface channel at the rotational speed of 300 RPM, 600 RPM, and 900 RPM. At the entrance of leg 1, the heat transfer is higher near the inlet, and however, it decreases until the flow reaches the bend region. In the bend region, the U-turn induced secondary flow vortices, increasing the heat transfer in this region.

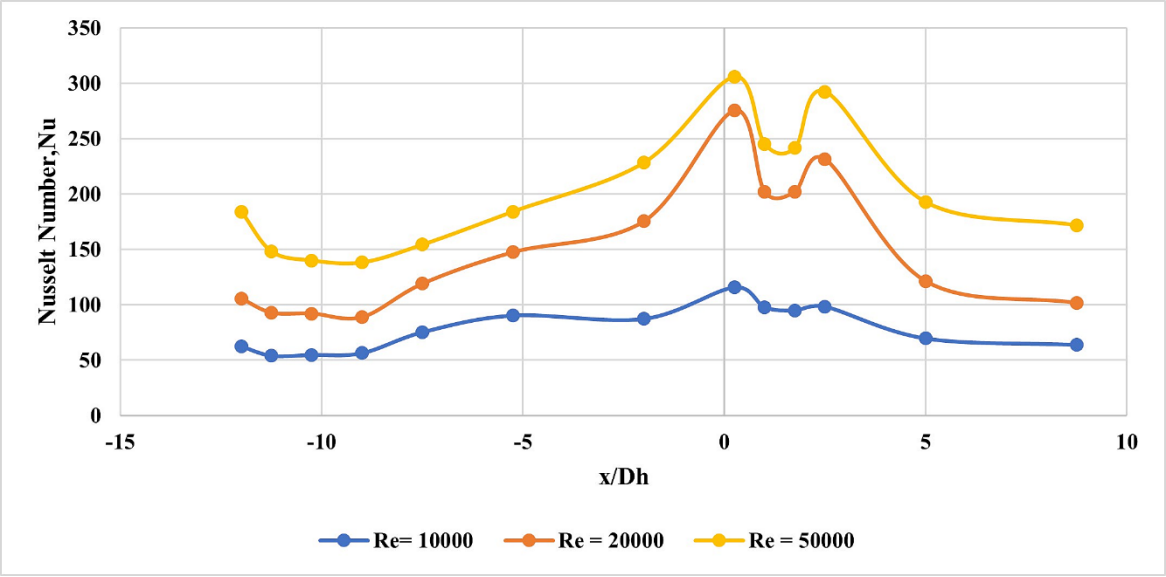


Figure 3-20: Heat transfer distribution along the cooling channel of Case A at Ro = 0.36, 0.15, and 0.07

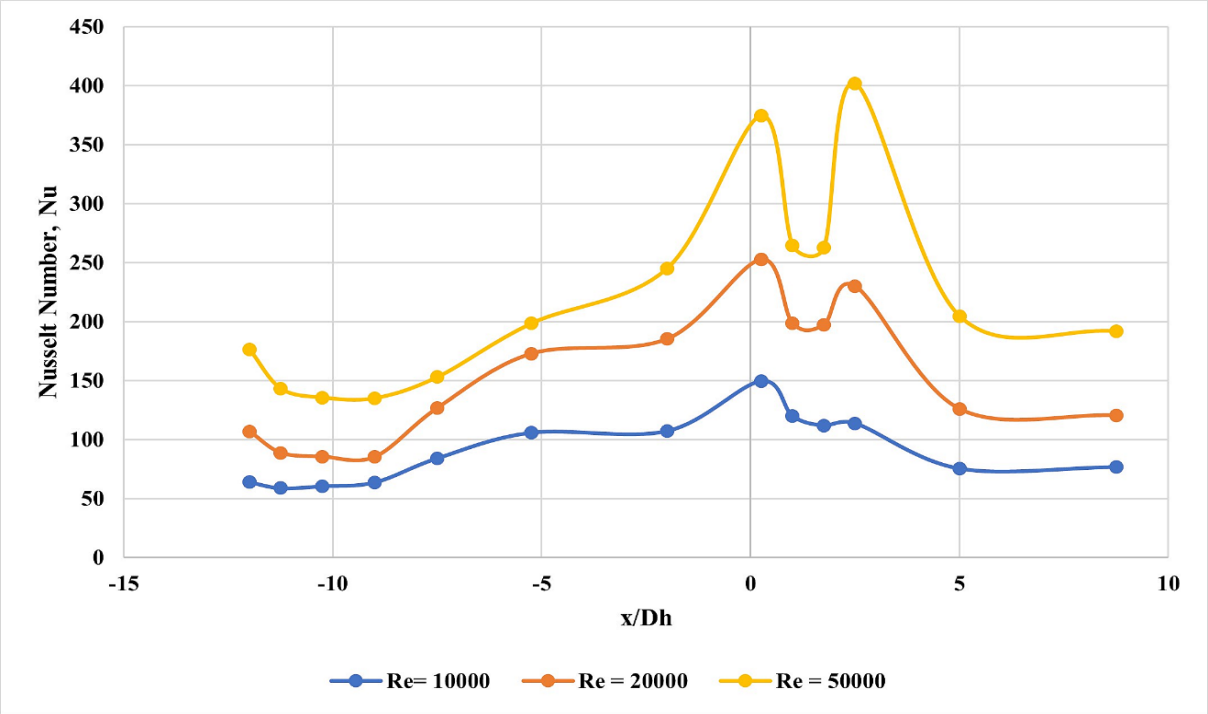


Figure 3-21: Heat transfer distribution along the cooling channel of Case A at Ro = 0.71, 0.30, and 0.13

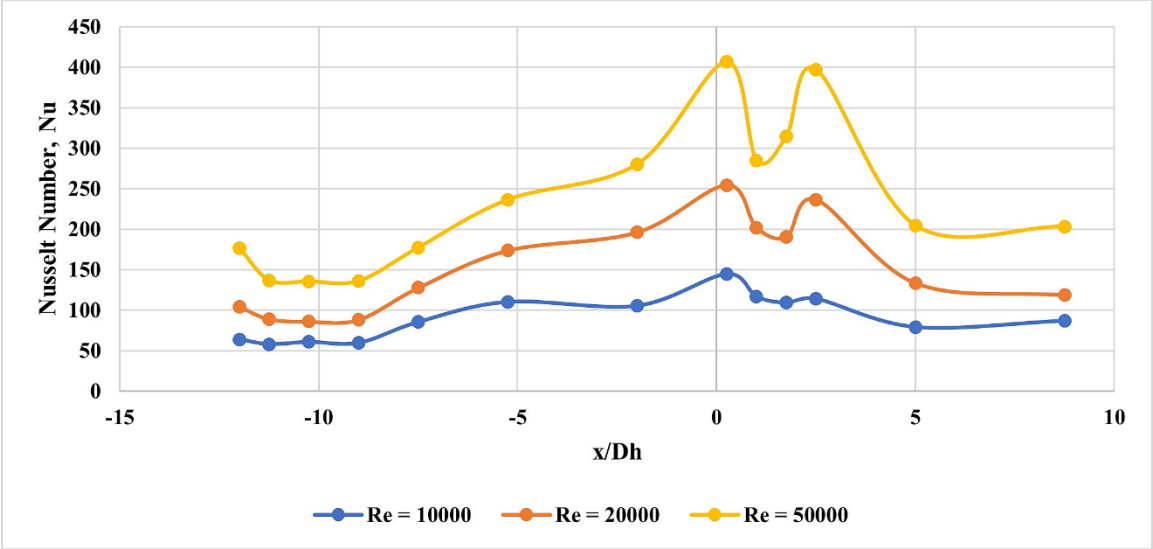


Figure 3-22: Heat transfer distribution along the cooling channel of Case A at Ro = 1.07, 0.45, and 0.20

The heat transfer distribution follows a similar trend along the dimpled surface channel (Figure 3-23 to Figure 3-31). Figure 3-23, Figure 3-24 and Figure 3-25 represent the heat transfer along the dimpled cooling channel with a 1-row partial spherical dimple arrangement. For rotation numbers, $R_o$ = 0.07, 0.13, and 0.20, the heat transfer distribution in the bend region encounters a peak considering the other rotational number as at the highest air velocity, and the Coriolis force affects significantly. A similar trend is observed for Case E (Figure 3-26, Figure 3-27 and Figure 3-28). For Case F (Figure 3-29, Figure 3-30 and Figure 3-31), the heat transfer coefficient showed a higher peak right before and after the bend region as irregular airflow phenomena create more turbulence in this region. Additionally, the Coriolis and buoyancy force strongly affect the heat transfer here.

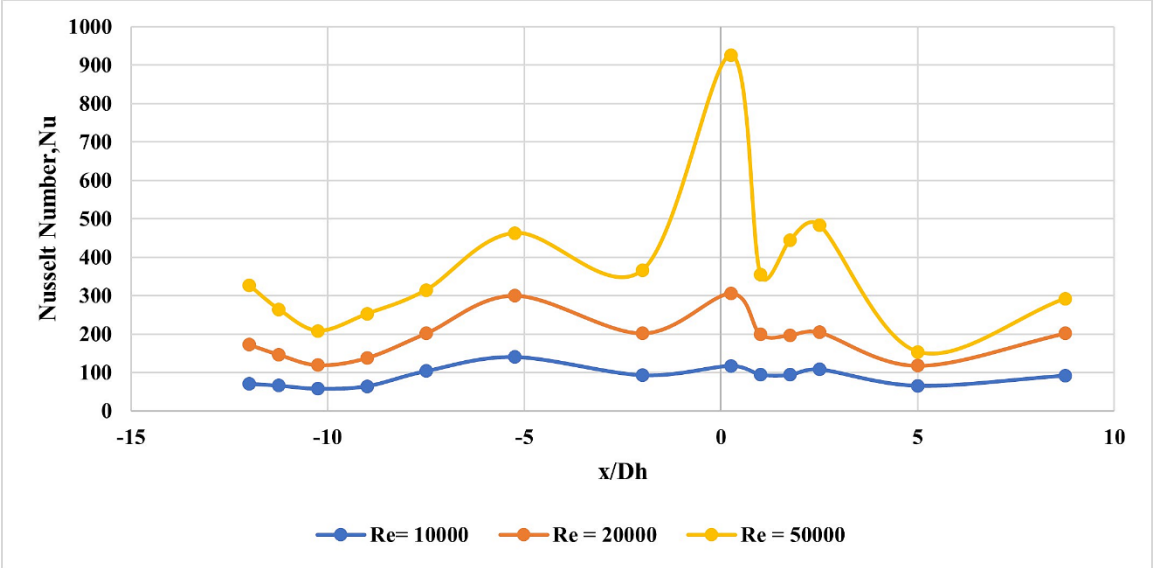


Figure 3-23: Heat transfer distribution along the cooling channel of Case C at Ro = 0.36, 0.15, and 0.07

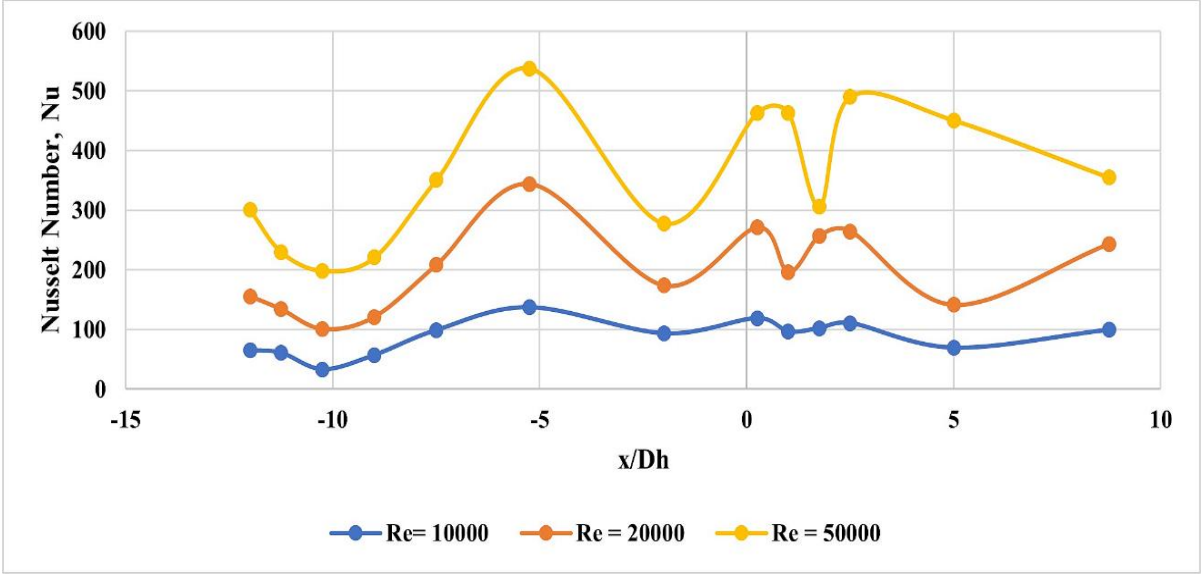


Figure 3-24: Heat transfer distribution along the cooling channel of Case C at Ro = 0.71, 0.30, and 0.13

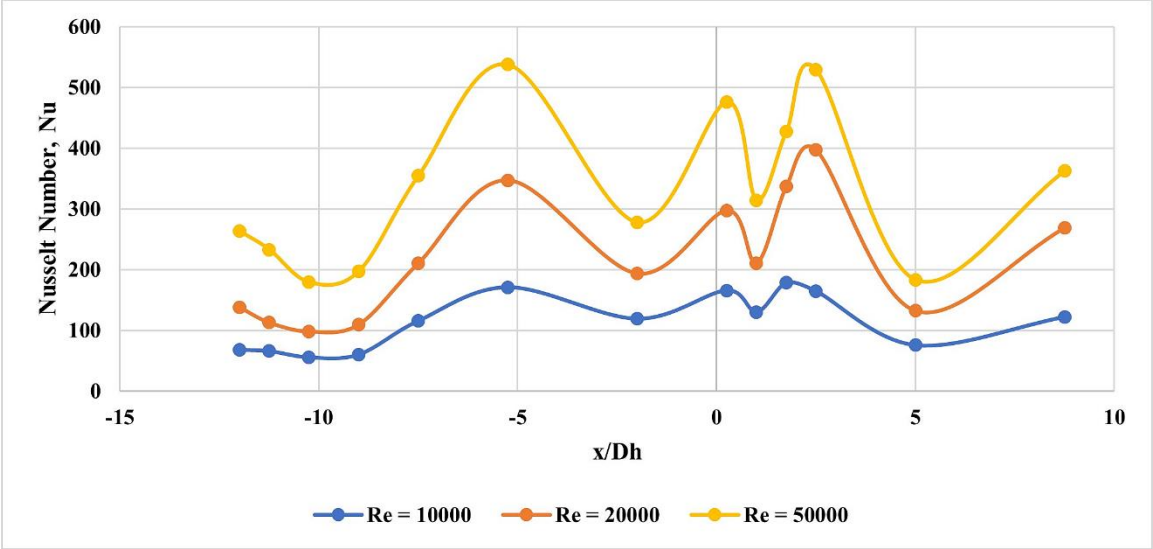


Figure 3-25: Heat transfer distribution along the cooling channel of Case C at Ro = 1.07, 0.45, and 0.20

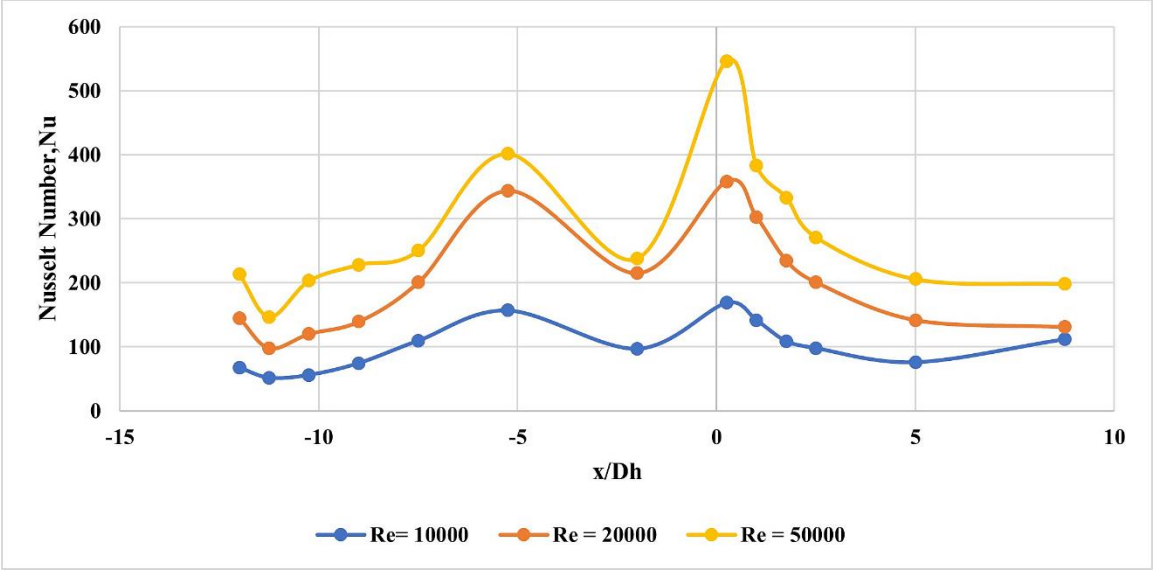


Figure 3-26: Heat transfer distribution along the cooling channel of Case E at Ro = 0.36, 0.15, and 0.07

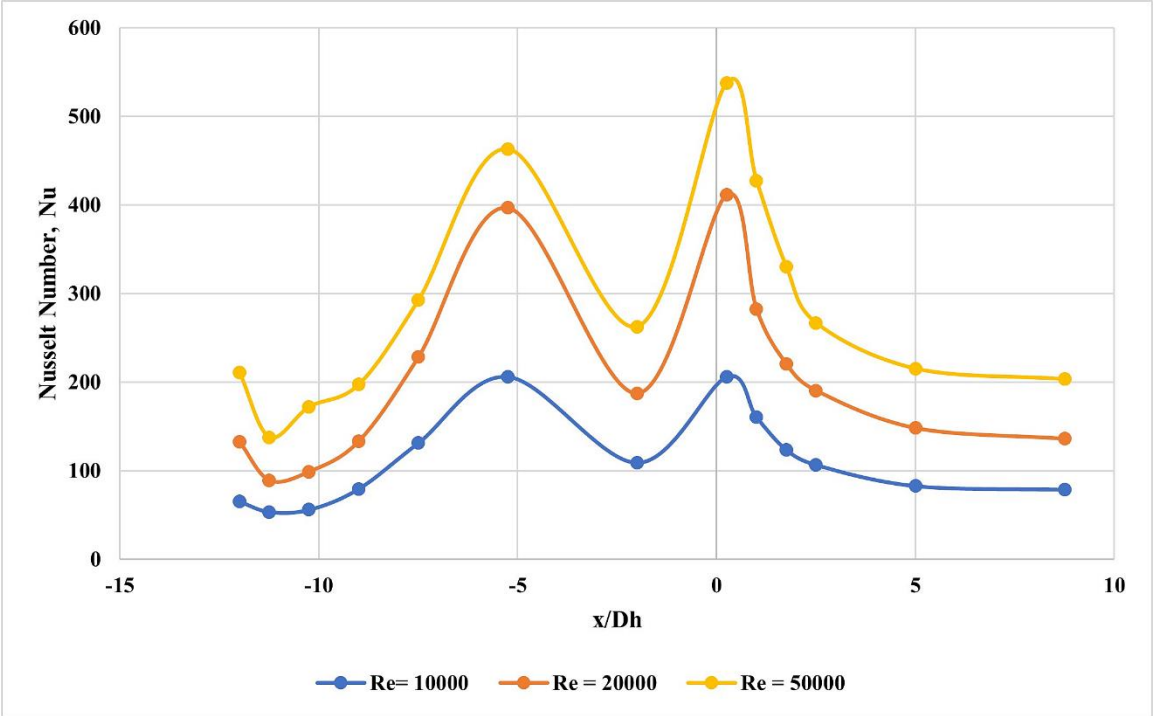


Figure 3-27: Heat transfer distribution along the cooling channel of Case E at Ro = 0.71, 0.30, and 0.13

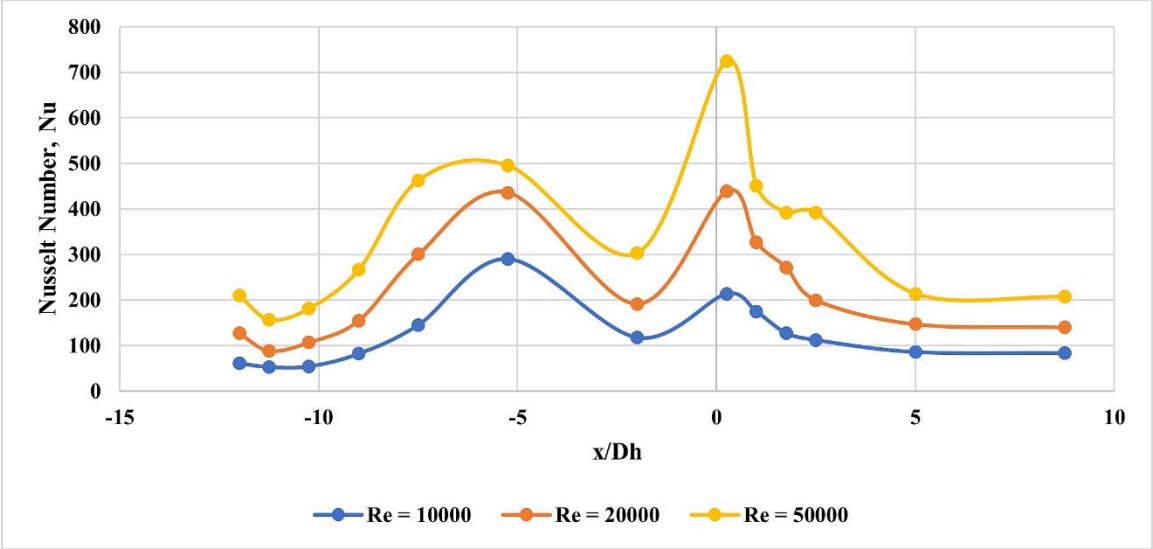


Figure 3-28: Heat transfer distribution along the cooling channel of Case E at Ro = 1.07, 0.45, and 0.20

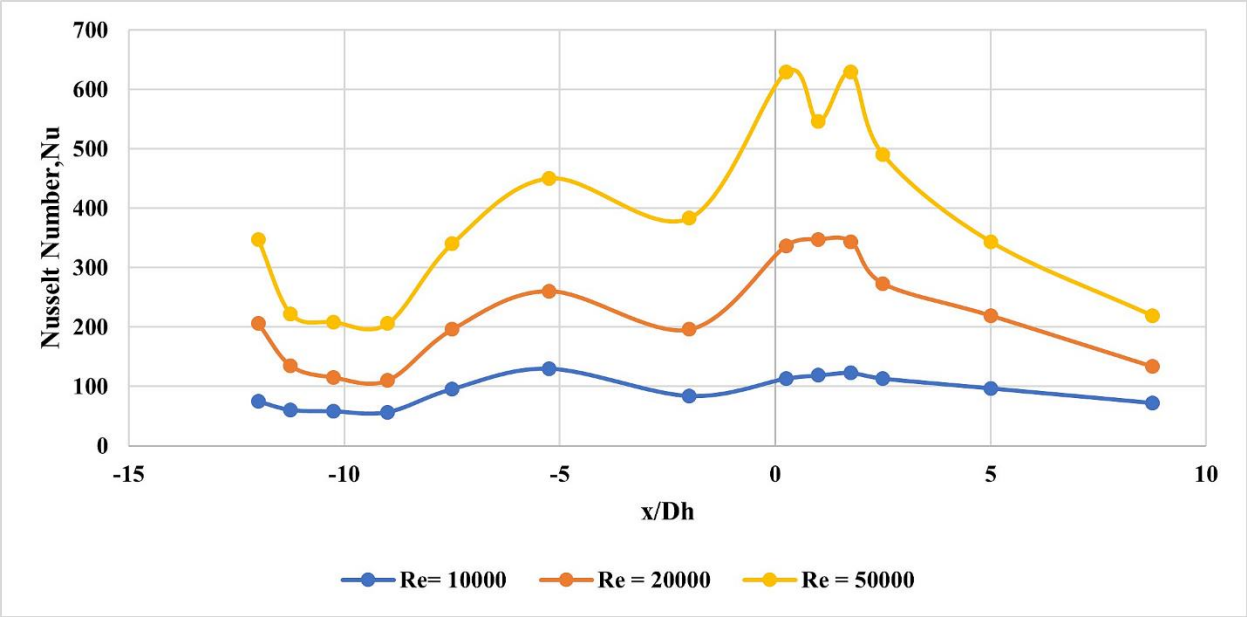


Figure 3-29: Heat transfer distribution along the cooling channel of Case F at Ro = 0.36, 0.15, and 0.07

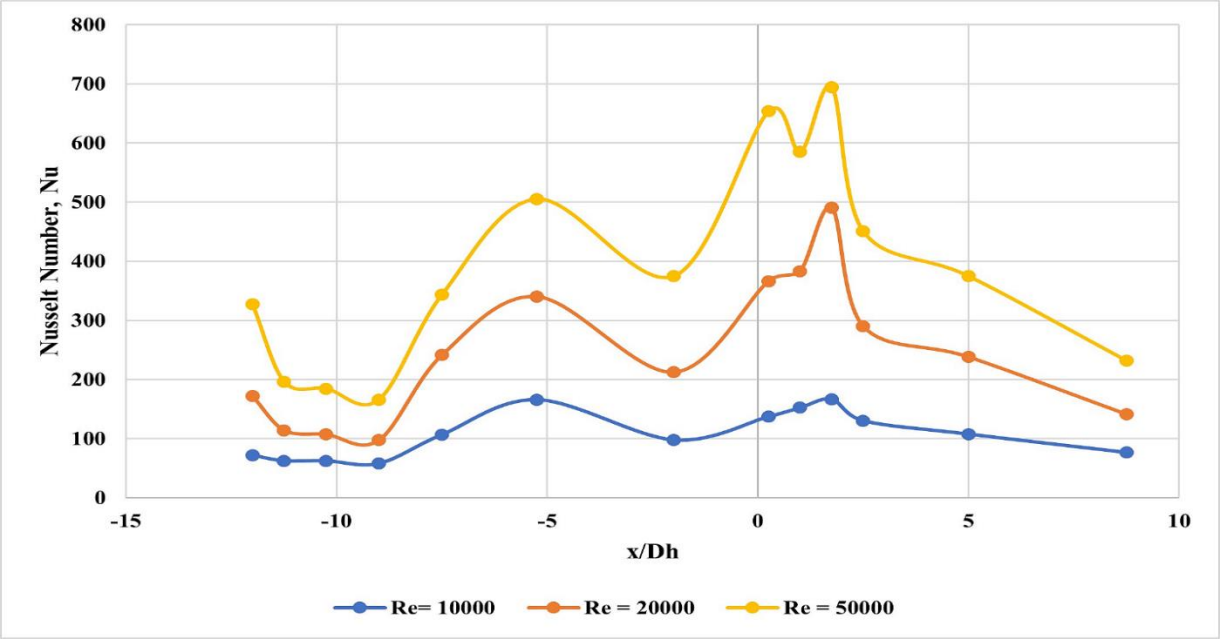


Figure 3-30: Heat transfer distribution along the cooling channel of Case F at Ro = 0.71, 0.30, and 0.13

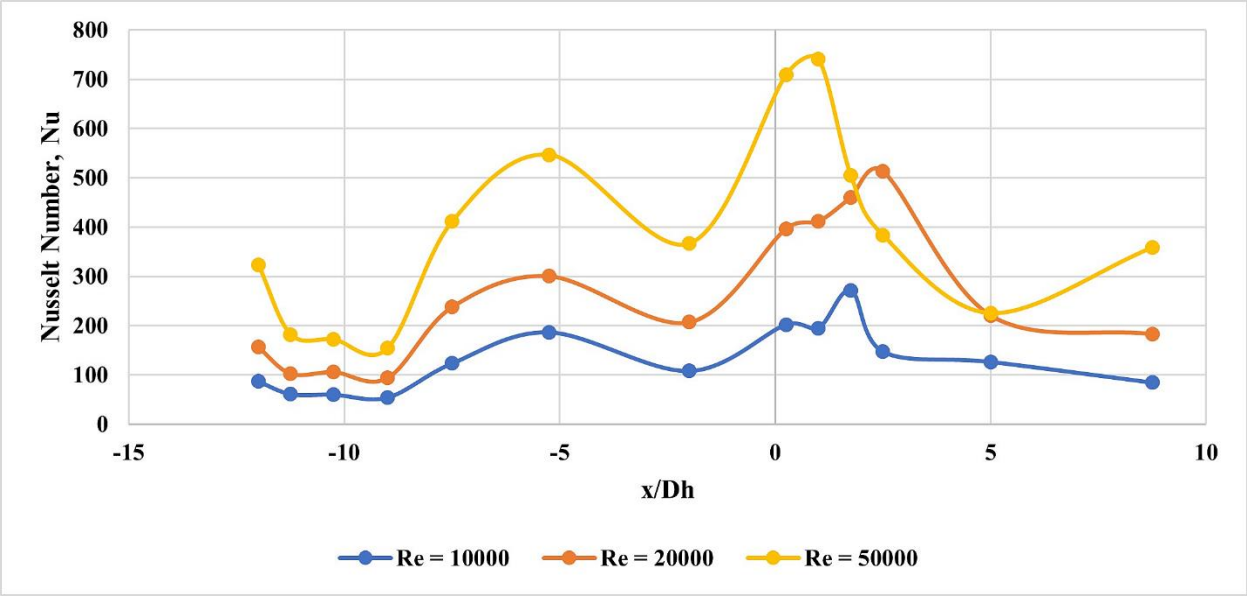


Figure 3-31: Heat transfer distribution along the cooling channel of Case F at Ro = 1.07, 0.45, and 0.20

### 3.5.4. Thermal Performance

Case B showed the highest heat transfer. Also, as was mentioned in the preceding subsection, the penalty of having dimples on the surface is the pressure drop. Pressure drop affects the thermal performance of the cooling channel. The friction factor for different cases is represented in Figure 3-32. The friction factor decreases with the increase of Re numbers for all the cases. The results are consistent with the data of heat transfer distribution; that is, L/Dh is the same for all the cases in this study. Figure 3-33 shows the normalized friction factor for all the channels. At Re = 6,000, the pressure drop is exceptionally low for all the cases. At Re = 6,000, the airflow is at a low speed, which leads to a low-pressure drop. For Case A and Case F, the normalized friction factor decreases with the increase of Reynolds numbers. However, the trend is not similar for Case B, Case C, and Case D. The partial spherical dimples with 20 mm dimple depth, i.e., Case B carries

the highest dimple depth. The airflow creates large vortex rolls inside the dimples and increases the heat transfer, leading to a higher pressure drop. At low air velocity, the pressure drop is low. It results in a low f/fo. Case B, Case C, Case D, and Case E, normalized friction factor increases at Re number =30,000 but decreases at Re number = 50,000. The rise in pressure drop rate is not the same at all the Reynolds numbers for all the cases, which leads to an irregular trend of normalized friction factor. The trend of $f/f_0$ observed in this study is consistent with the results by Rao et al. [25] for Case B through Case E; that is, f/f0 increases as the Reynolds number goes up. However, the $f/f_0$ does not behave similarly for Case A and Case F, which show the opposite trend; as the Reynolds number increases, $f/f_0$ drops. This phenomenon is mainly because Case A and Case F do not cause significant pressure drops due to their insensitivity to small friction effects. Case A is smooth, and Case F is not affected by the roughness phenomenon. With increasing Re numbers, the pressure drop increases, which affects the thermal performance of the channel shown Figure 3-34. At the lowest Re number, i.e., 6,000, all the channels demonstrate the highest thermal performance, decreasing with the Reynolds number. At the lowest Reynolds number, i.e., 6000, Case C indicates the highest thermal performance. At the lowest air velocity, the pressure drop is much less than at the highest air velocity, which leads to higher thermal performance. However, at the higher Re number, i.e., at Re=30,000 and 50,000, Case F represented the highest thermal performance, around 86 and 85%, respectively. At the Re number = 50,000, the closet thermal performance to Case F is shown by Case D, which is 83%. Considering the thermal performance at a higher Reynolds number, Case F is the best solution to consider.

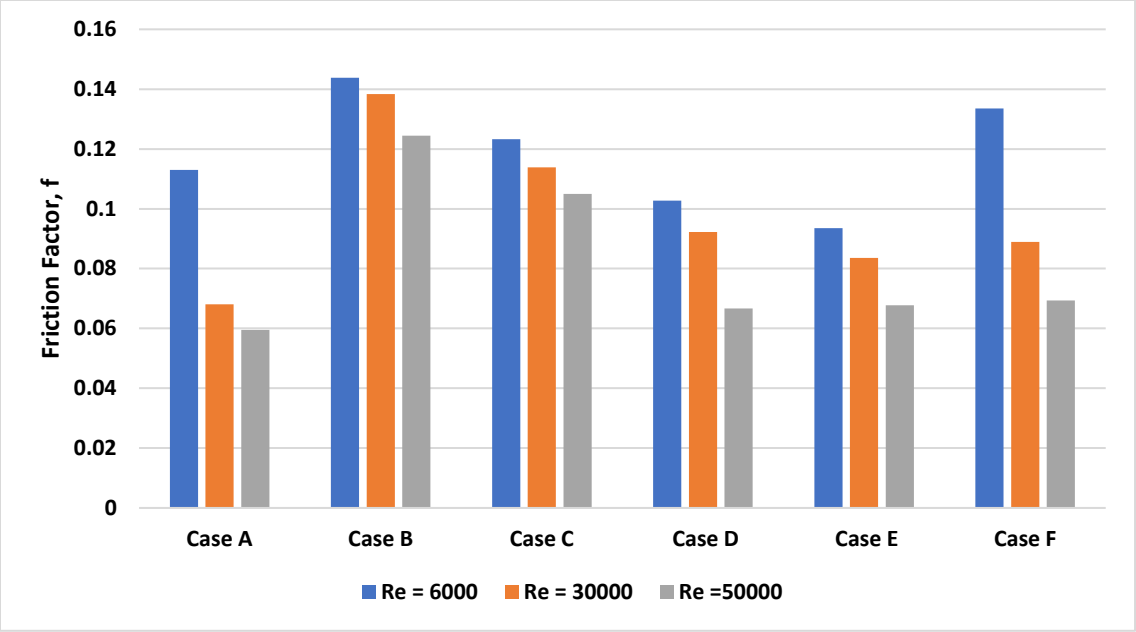


Figure 3-32: Friction factor for all the cases at Ro = 0

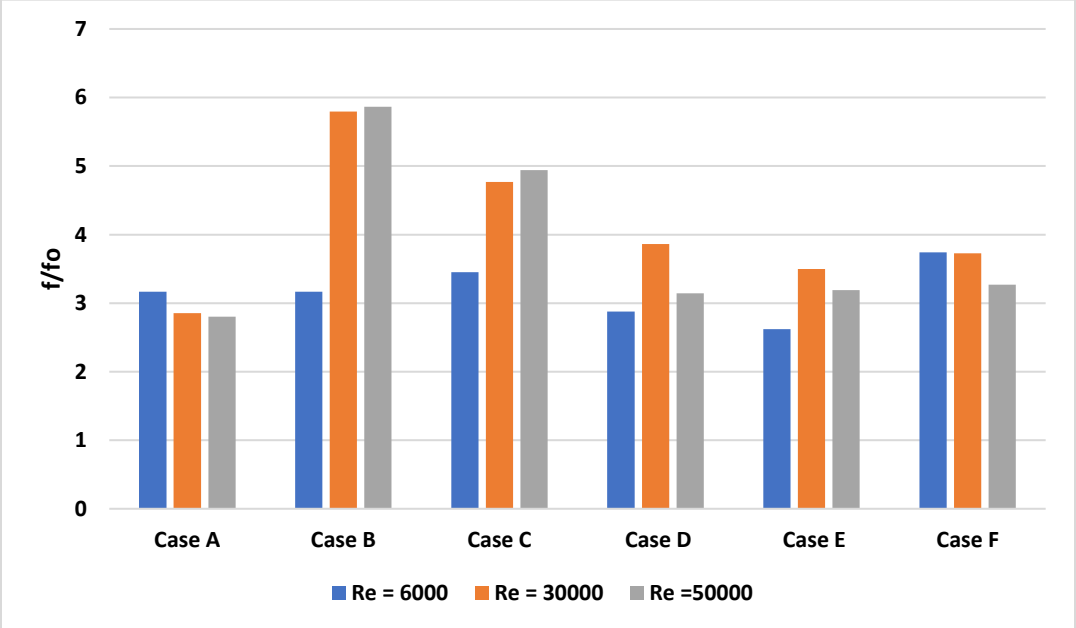


Figure 3-33: Normalized friction factor for all the cases at Ro = 0

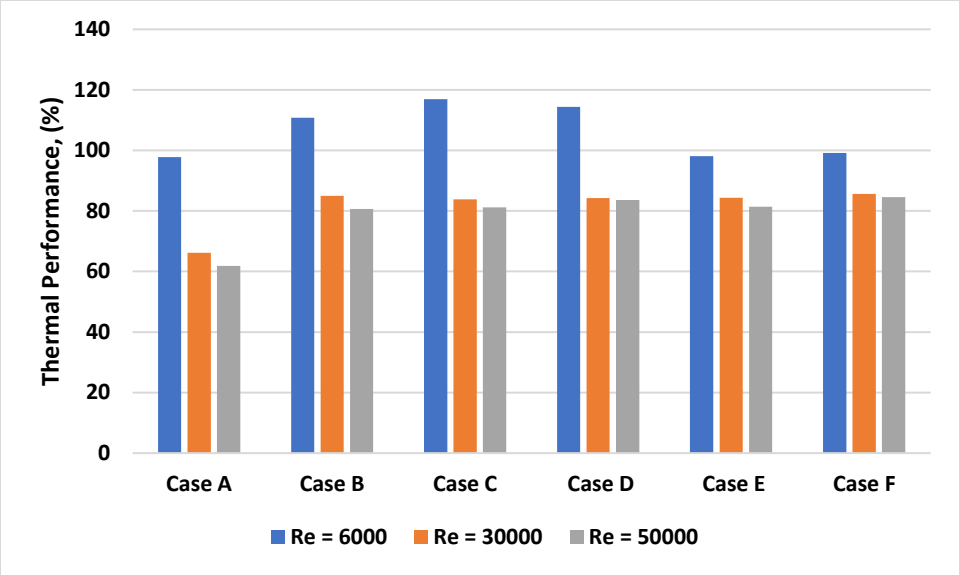


Figure 3-34: Thermal performance for all the cases at Ro = 0

# 4. Study on Gas Turbine Blade Internal Cooling with Ribbed Surface

## 4.1. Introduction

The gas turbine blade tip experiences an elevated temperature difference. It leads to high thermal loads to this section. It is exposed to high gas flow and suffers high local thermal loads. An effective cooling can downgrade the high temperature in this section. Besides, it is able to provide high durability and safe operations. A 180° sharp U-bend passage was implemented in this study to investigate the cooling mechanisms in the mid-portion of the turbine blade. Two different rib geometry i.e., 30°, and 45°. Reynolds numbers were set ranging from 12,000 to 65,000 for stationary and rotational cases to find out flow pattern at different air velocities. The experimental investigations gave us an idea regarding the temperature distributions along the channel. In addition to experimental investigation, numerical investigation was conducted for Re number 25,000, and 65,000 with Large Eddy Simulation (LES) technique to validate the experimental data. The LES technique is useful to design complex flow phenomena. Inside of the gas turbine blades, there is turbulence and vortex rolls were generated which can be predicted from the numerical solutions. Results indicate that the cooling channel with 30° angled ribbed surface cooling channel experiences a peak of heat transfer compared to 45° angled one. However, another important parameter is pressure drop as it lowers the thermal performance of the cooling channel. The 45° angled one encounters a higher friction factor which negatively affects the thermal performance. It is found that the cooling channel with 30° angled rib provides a better heat transfer as well as optimal pressure drop.

## 4.2. Experimental and Numerical Approach

For the rib's experimental study, the same instrumentation was used as in dimpled study. Two different rib geometries i.e., 30°and 45° ribs are showed in Figure 4-1 were investigated. The height of ribs was 5 mm. The rib to rib spacing for both the cases were kept 60 mm. The length for 30° was 64 mm whereas it was kept 80 mm for 45° angled ribs. The channel dimensions are same as in dimpled study except the hydraulic diameter. The hydraulic diameter was considered 50 mm. The ribs were cut from a Plexiglas sheet. They were wrapped with copper foil to ensure uninterrupted heat transfer. 2,000 $W/m^2$ constant heat flux was applied in the bottom wall. Similarly, the numerical approach was followed as dimpled study. However, a new mesh independent study was conducted for this study as it is different geometry compared to dimples. The mesh independent study was conducted for four different number of cells (Figure 4-2) with Case B at Re number 65,000. The surface average Nusselt number was shown a flat value for all the cases. However, the difference between 3.5 and 12.14 million number of cells is 0.12. To save computational time, 3.5 number of cells were considered in the study. The models were made using trimmer mesh and wall Y+ was maintained less than 1.5. Twelve prism layers were set for the rib study. The convergence criterion was set up to $10^{-6}$. The physical time was 1s with 0.0001s time step considered in this study.

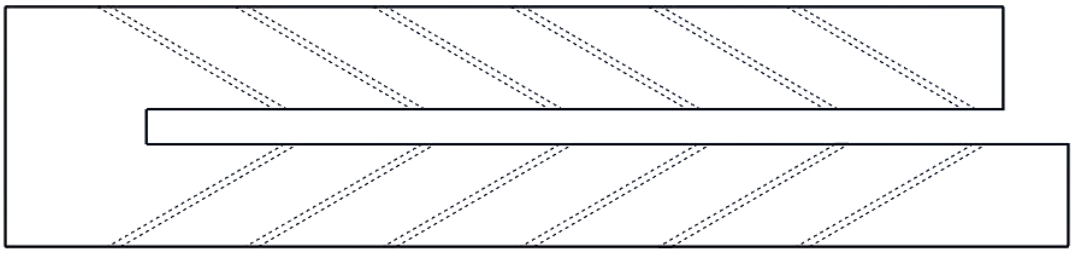

Case A (30° rib geometry)

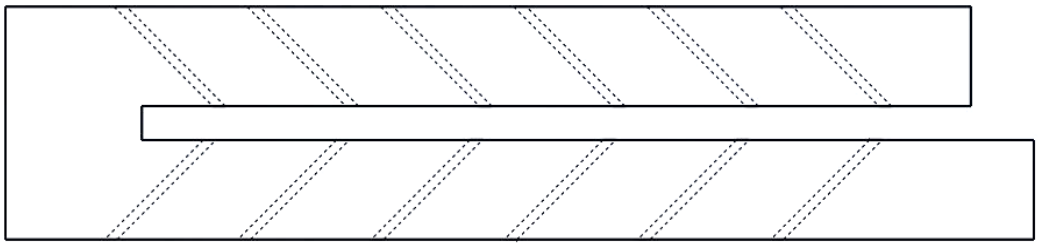

Case B (45° rib geometry)

Figure 4-1: Rib geometry (Case A: 30° rib and Case B: 45° ribs)

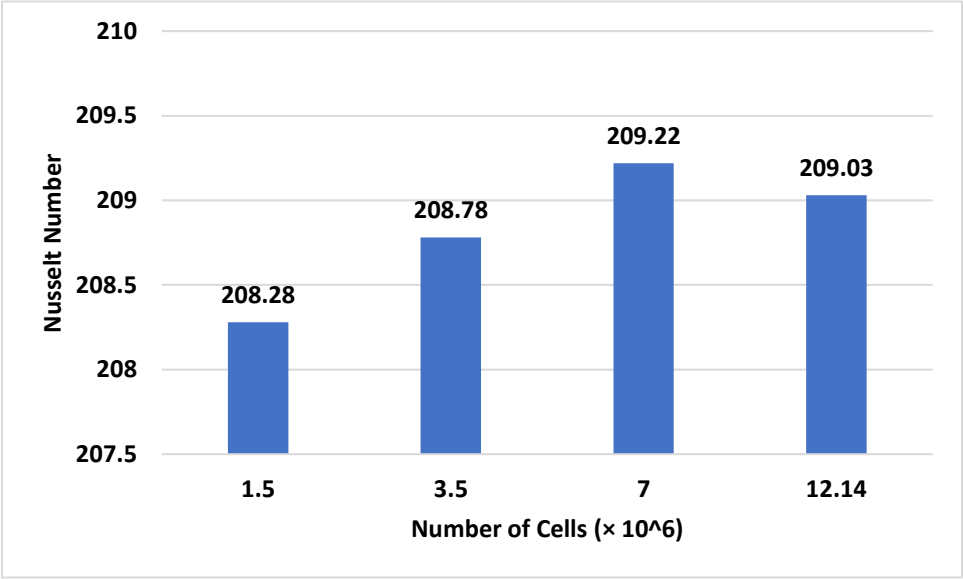


Figure 4-2: Mesh independent study for Case B at Re = 65,000

## 4.3. Results

### 4.3.1. Velocity Distribution Along the Two-bend Channal

Figure 4-3 indicates the velocity distribution along the channel. For Case A and Case B, leg 1 experienced a regular air flow. In the bend section, there are irregularities in the flow. After the bend, the airflow changes its direction of action. After the entrance, it increased and continued right before the bend section. At the bend section, irregularities were found similar to other cases.

Figure 4-4 represents the velocity distribution at rotation number 0.17. Coriolis and buoyancy forces affect the heat transfer in the rotational cases. Also, there is an additional force which is centrifugal force. The rotation effect increases the heat transfer in both the passages. The rotational cooling channels encounter more turbulent flows. The combination of Coriolis and centrifugal force causes much more turbulence in case of rotational motion.

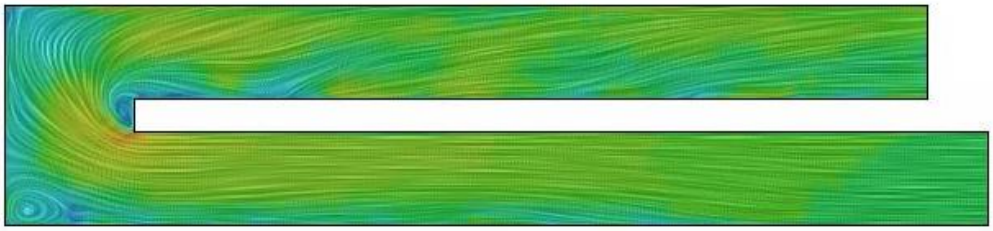

Case A

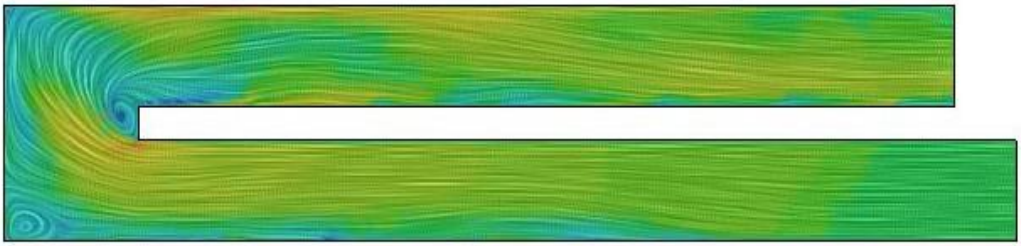

Case B

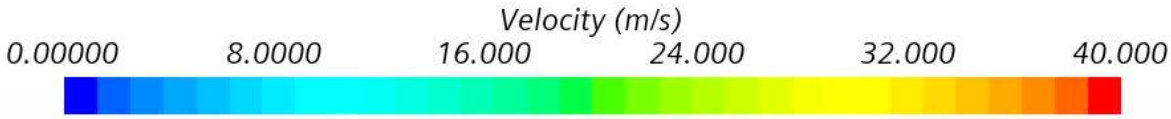


Figure 4-3: Velocity profile along the two-pass channel at Re = 65000 at Ro = 0

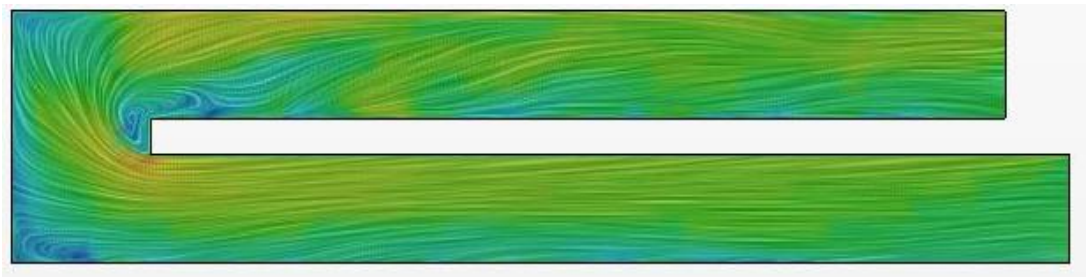

Case A

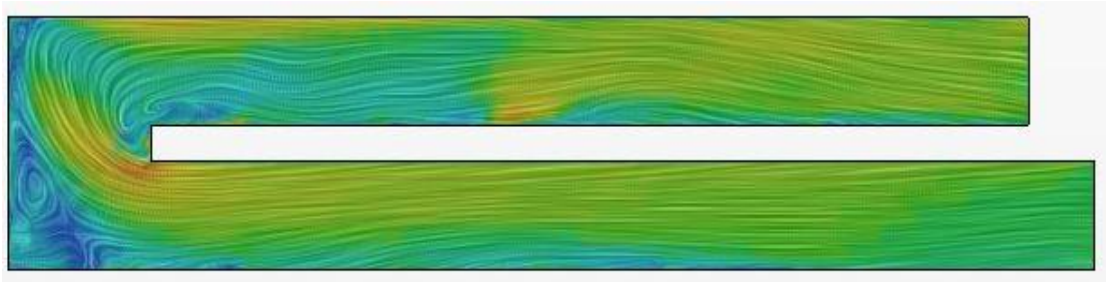

Case B

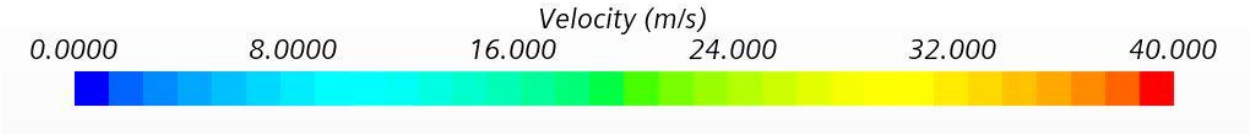


Figure 4-4: Velocity profile along the two-pass channel at Re = 65000 at Ro = 0.17

### 4.3.2. Heat Transfer Augmentation along the Ribbed Surface Channel

Figure 4-5 and Figure 4-6 represented the experimental heat transfer behavior of 30°and 45° ribbed surface cooling channel. For both cases, the heat transfer has increased at the bend section and then it starts to reduce. Air is continously extracting heat from the bottom surface which increases the Nusselt number and it is the highest at the bend section due to the highest recirculation in this section. Figure 4-7 and Figure 4-8 show the heat transfer behavior at 600 RPM. The heat transfer coeeficient is higher for the rotational cases due to Coriolis and centrifugal forces. Figure 4-9 indicates the normalized Nusselt number for Re numbers 25,000 and 65,000 at 600

RPM. The comparision of normalized Nusselt number indicates that the 30° angled ribbed surface is having the higher heat transfer compared to the other one.

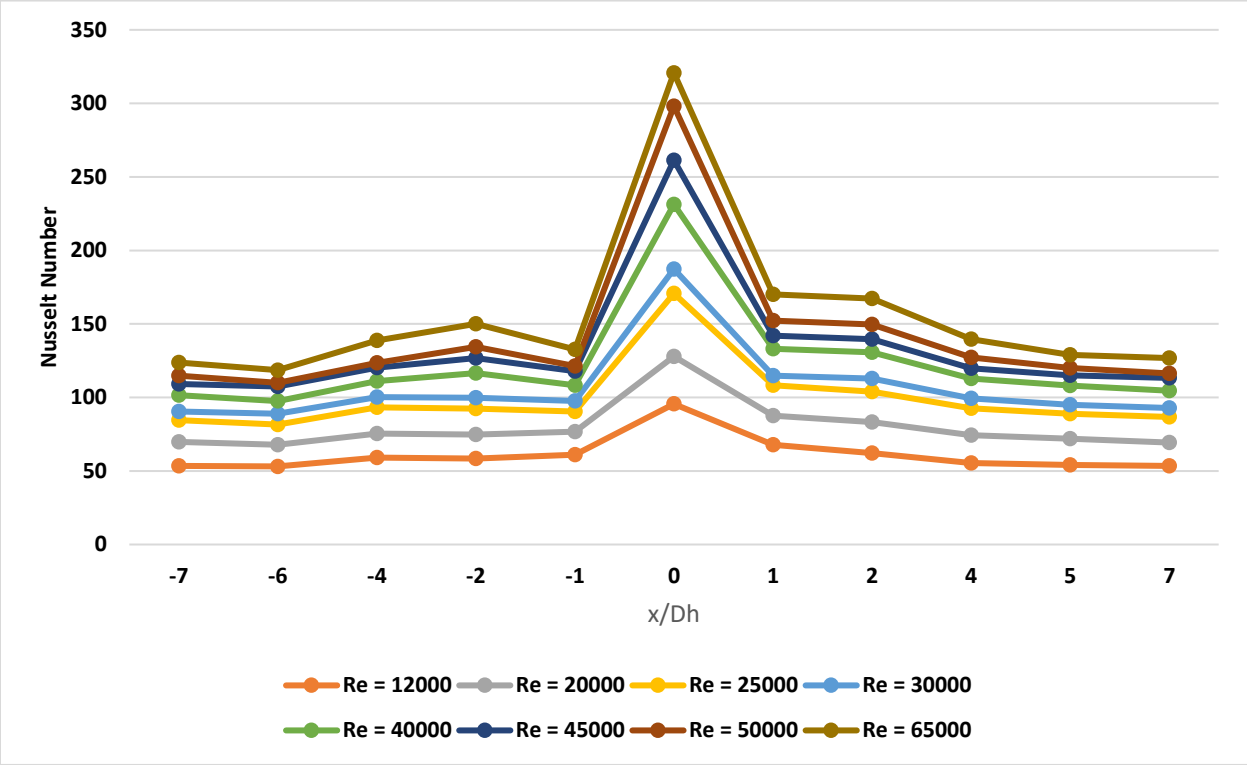


Figure 4-5: Heat transfer augmentation along the channel for 30° ribs at $R_o = 0$ (experimental)

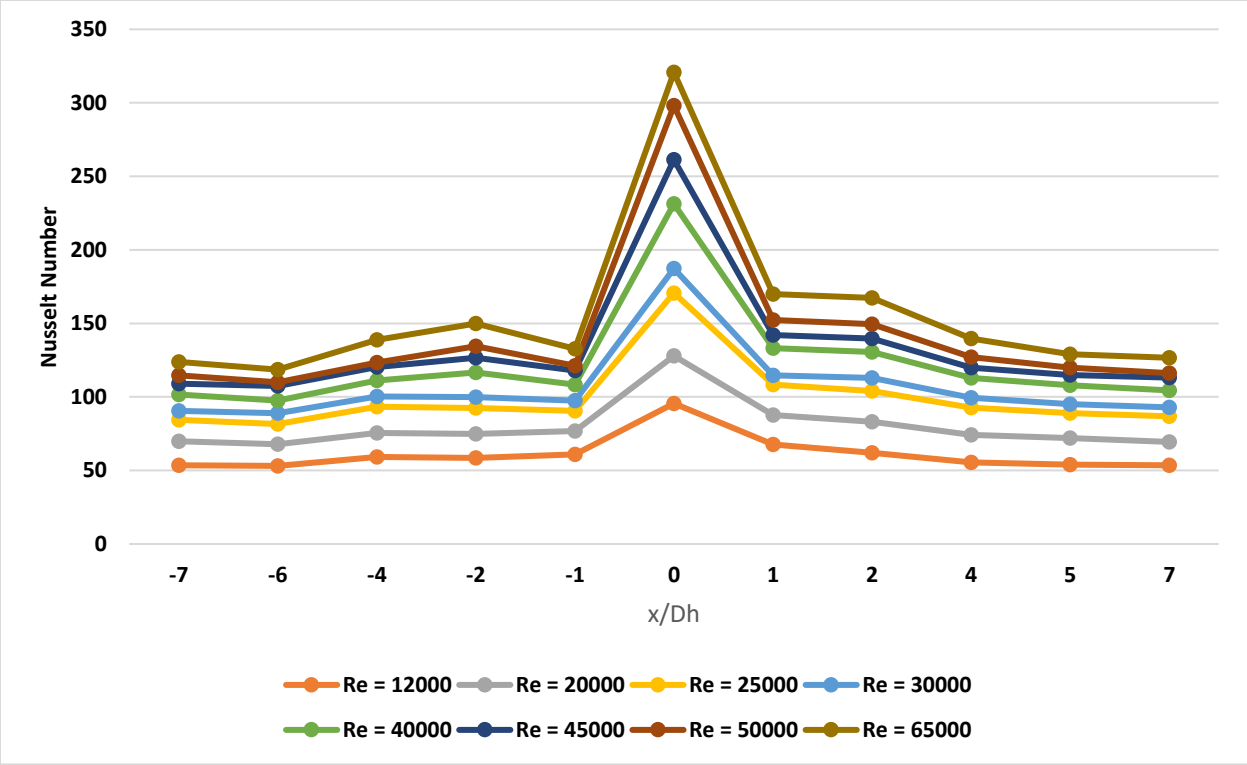


Figure 4-6: Heat transfer augmentation along the channel for 45° ribs at Ro = 0 (experimental)

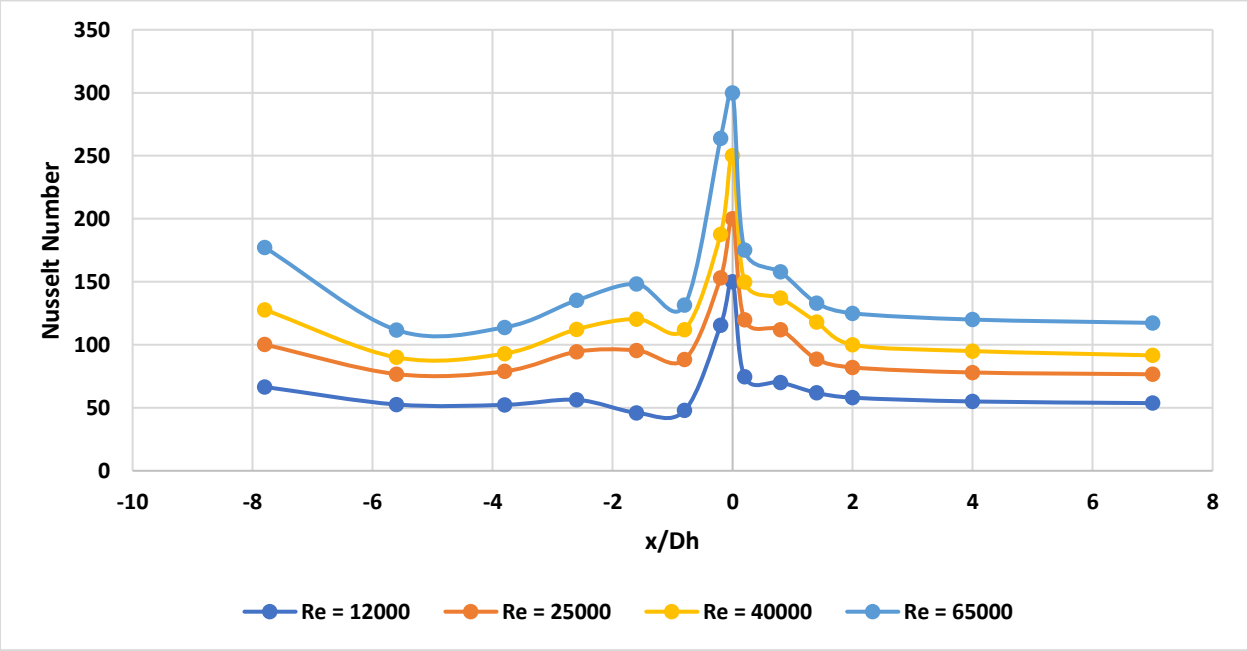


Figure 4-7: Heat transfer augmentation along the channel for 30° ribs at 600 RPM (experimental)

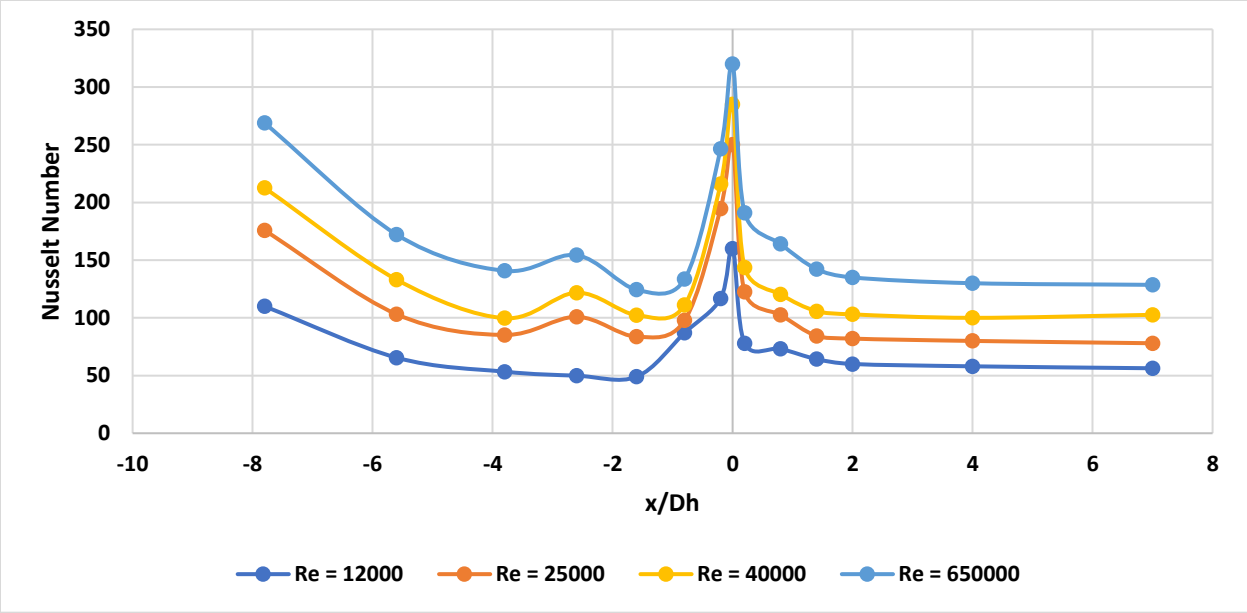


Figure 4-8: Heat transfer augmentation along the channel for 45° ribs at 600 RPM (experimental)

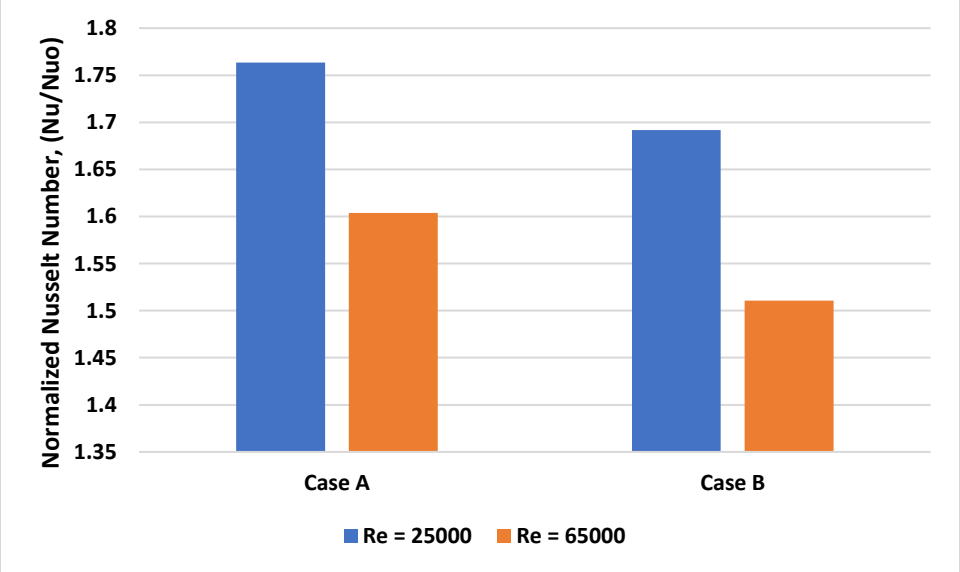


Figure 4-9: Normalized Nusselt number at 600 RPM

### 4.3.3. Thermal Performance

Gas turbine blade internal cooling section always experiences pressure drop which leads to friction to the channel. Excessive friction causes the low durability of the turbine blades. Figure

4-10 represents the friction factor of the ribbed channel. Case A experiences less pressure drop for two air velocities due to 30° angle of the ribs. The 30° angle of the rib directs the air at 30°. As mentioned earlier, the higher friction factor negatively affects the thermal performance of the cooling channel. So, Figure 4-11 shows the same trend of the thermal performance.

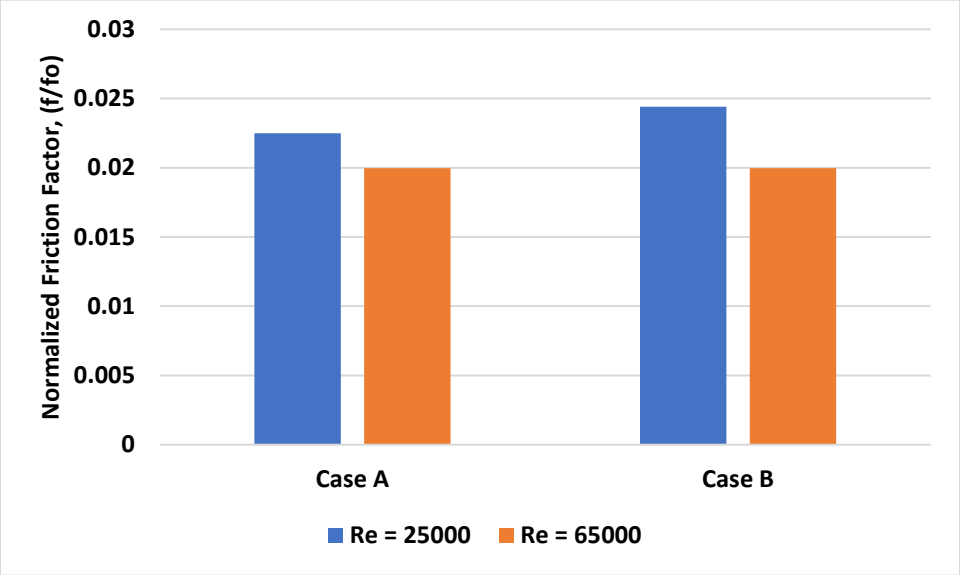


Figure 4-10: Normalized friction factor at 600 RPM

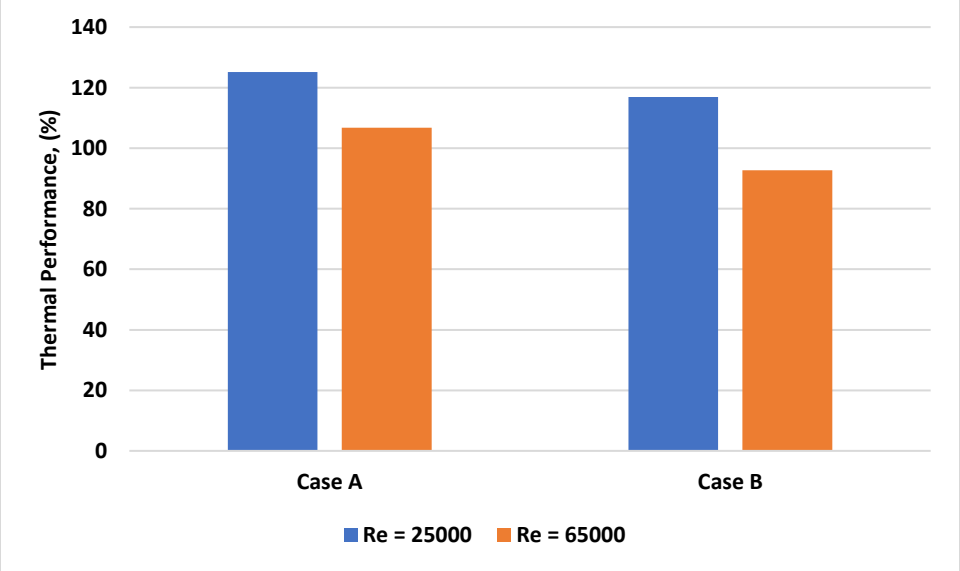


Figure 4-11: Thermal performance at 600 RPM

# 5. Gas Turbine Blade Internal Cooling with Pin-fins

## 5.1. Introduction

Pin-fins are frequently applied in electronic component cooling. Besides, that it is also applied at the trailing edge cooling of the gas turbine blade. The narrow cooling passage of the internal section of the turbine blades is one of the complicated zones of the gas turbine system. It confronts a high temperature. Pin-fins are an excellent structure to insert in this section to ensure an effective cooling. It accomplishes a higher heat transfer co-efficient. Pin-fins are also implemented as a mechanical structure to bridge the thin metallic pressure surface and suction surface. However, pressure drop is significantly higher in case of pin-fin cooling which can lower the thermal performance of the cooling channel. So, the optimization of pin-fin design is important to find out the optimal pressure drop. The heat transfer coefficient and pressure drop depends on the design of the pin-fins, array, and location of the pin-fins. Additionally, a higher rotation number can promote the heat transfer coefficient as well as reduce the pressure drop. The present study considers two different pin-fin designs i.e., partial spherical and dome with different arrays of pin-fins. Experimental and computational investigation was conducted. The experimental study was conducted with the same experimental set-up Reynolds number ranging from 9,000 to 50,000. The computational study was conducted with LES technique. The final judgement was completed based on the heat transfer coefficient, friction factor and thermal performance of the cooling channel. The cooling channel with dome shaped pin-fins with array of 14 × 2 pin-fins showed a better thermal performance compared to the other cooling channels.

## 5.2. Experimental and Numerical Details

Figure 5-1 shows the pin-finned cooling channel considered in this study. For Case A and Case C, 8 rows of pin-fins were inserted with 2 columns both in leg 1 and leg 2. The distance to the X-axis is 55 mm and Y axis is 22 mm. However, the distribution of pin-fins is different for Case B and Case D – 14 rows of pin-fins were inserted with 2 columns for both cooling passages. The distance to the X-axis is 34 mm and Y axis is 22 mm. Pin-fins were also inserted in the bend region for Case B and Case D to find out how the heat transfer and air flow pattern change when the U-bend area is occupied with protrusion. The design details were summarized in Table 5-1. Figure 5-2 illustrates the pin-fins designs considered in the present study.

The experimental setup and procedure were followed same as the earlier chapters. However, the pin-fins were printed using a 3D printer and wrapped with copper foil to ensure the uniform temperature distribution.

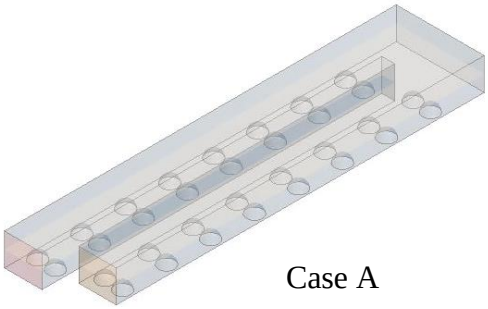

Case A

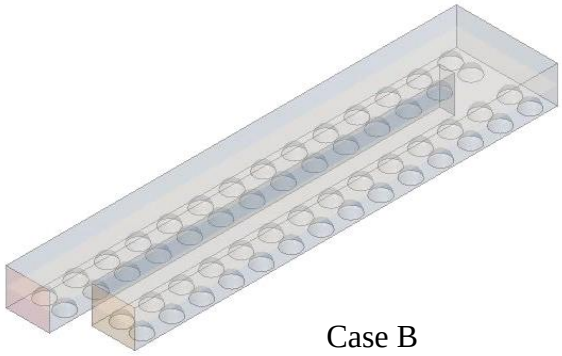

Case B

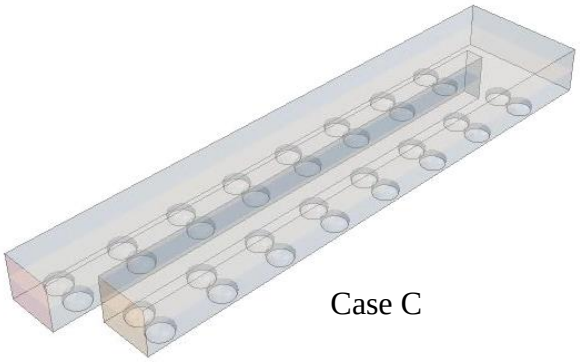

Case C

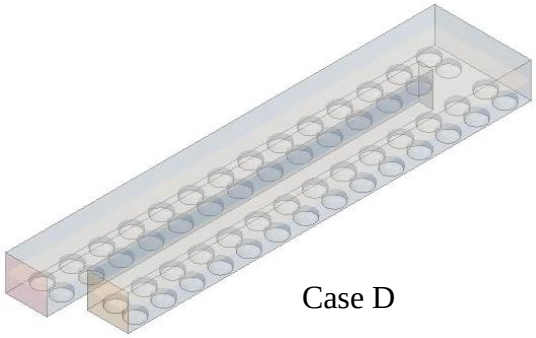

Case D

Figure 5-1: Geometry of pin-finned cooling channel

(a) Partial Spherical Pin-fin

(b) Dome Pin-fin

Figure 5-2: Side view of the pin-fins (a) Partial Spherical Pin-fin and (b) Dome Pin-fin

Table 5-1: Pin-finned cooling channel details

| **Channel Name** | **Pin-fin Type** | **Number of Pin-fins in Leg 1** | **Number of Pin-fins in Leg 2** |
|---|---|---|---|
| Case A | Partial Spherical | 8 × 2 | 8 × 2 |
| Case B | Partial Spherical (Including Bend Region) | 14 × 2 | 14 × 2 |
| Case C | Dome | 8 × 2 | 8 × 2 |
| Case D | Dome (Including Bend Region) | 14 × 2 | 14 × 2 |

## 5.3. Results

### 5.3.1. Velocity Distribution

Figure 5-3 represents the velocity distribution for stationary case and Figure 5-4 represents the velocity distribution for rotation number 0.13. the velocity contours are presented at the horizontal mid-plane for both stationary and rotational cases. Both for stationary and rotational cases, air flow starts with a uniform pattern. Pin-fin creates an obstacle in the path of air flow which creates a secondary flow. For all the cases, near the bend region, it becomes more turbulent, and it continues after the bend. However, for rotational cases, the air flow becomes more turbulent near and after the bend region. The secondary flow and recirculation of air is much higher in the rotational cases.

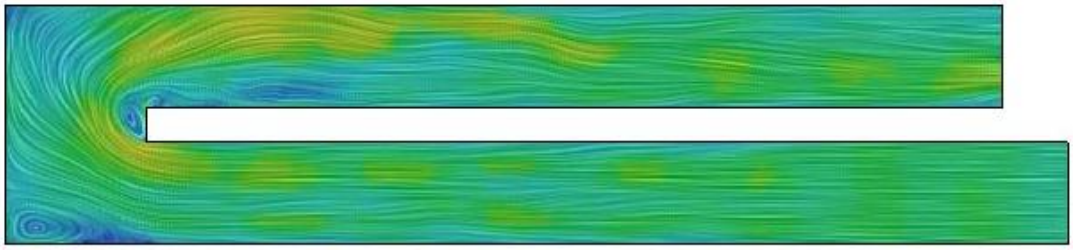

Case A

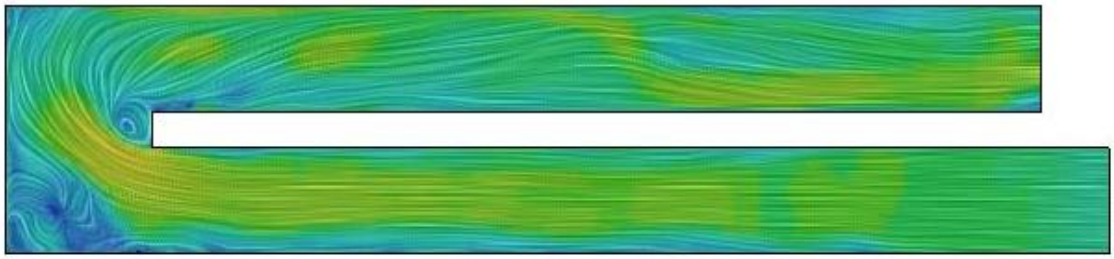

Case B

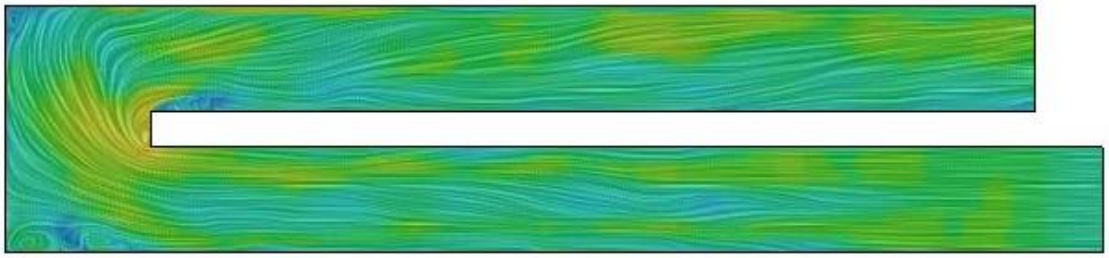

Case C

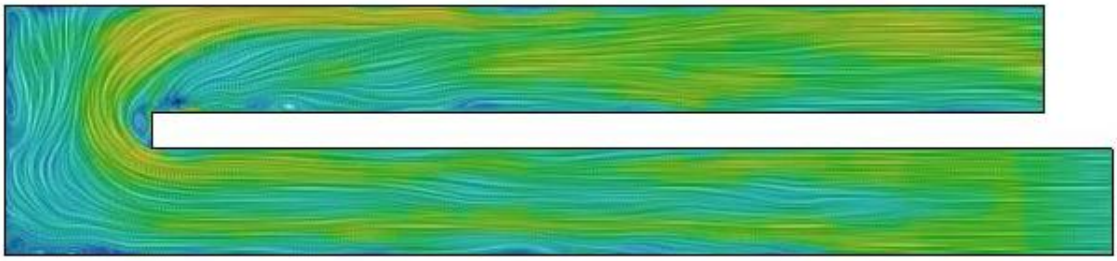

Case D

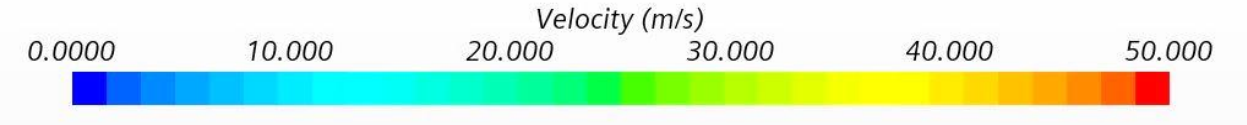


Figure 5-3: Velocity distribution along the cooling channel at Ro = 0

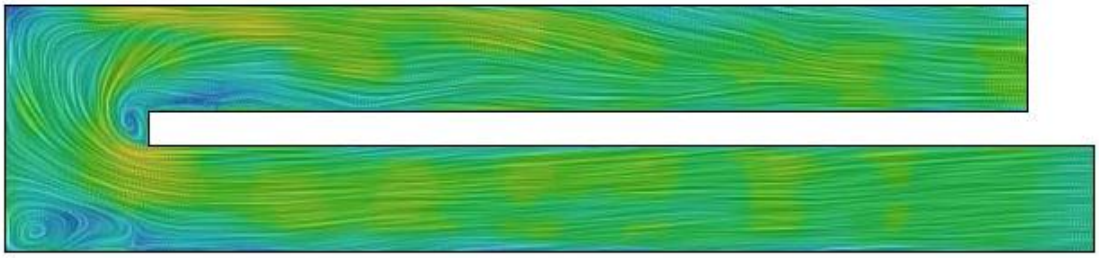

Case A

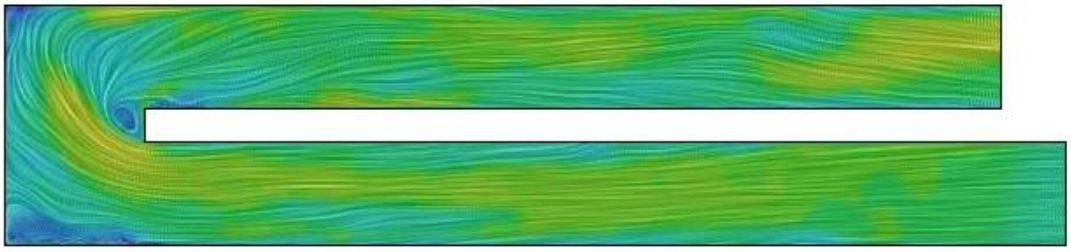

Case B

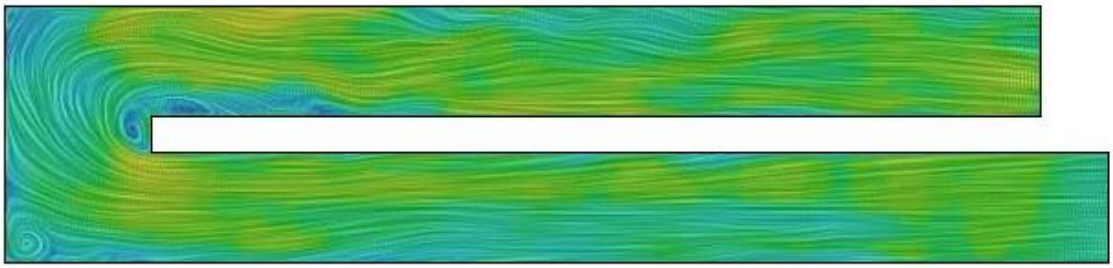

Case C

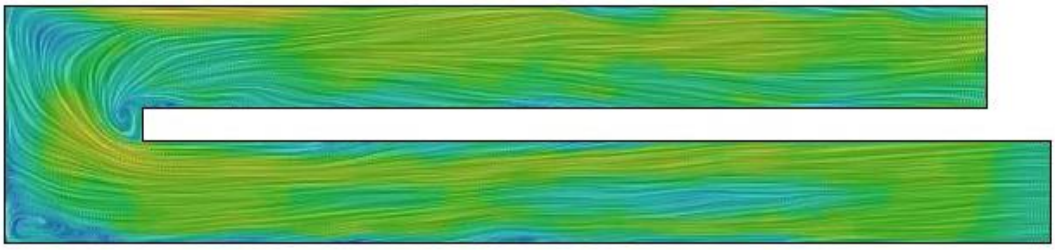

Case D

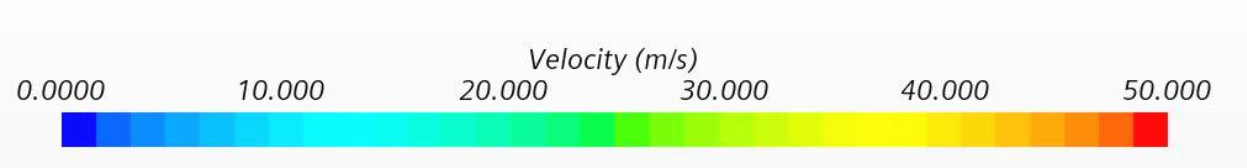


Figure 5-4: Velocity distribution along the cooling channel at $R_o$ = 0.13

### 5.3.2. Temperature Distribution

Figure 5-5 represents the temperature distribution along the cooling channel at Ro = 0 and Figure 5-6 indicates the temperature distribution along the cooling channel at Ro = 0.13. The temperature increases with the distance from the entrance due to the continuous extraction of the

heat from the bottom wall by the working fluid. Temperature decreases at the pin-fin due to direct contact with the air. The dome pin-fin cooling channel encounters low temperature because of its curved shape which increases the heat transfer coefficient.

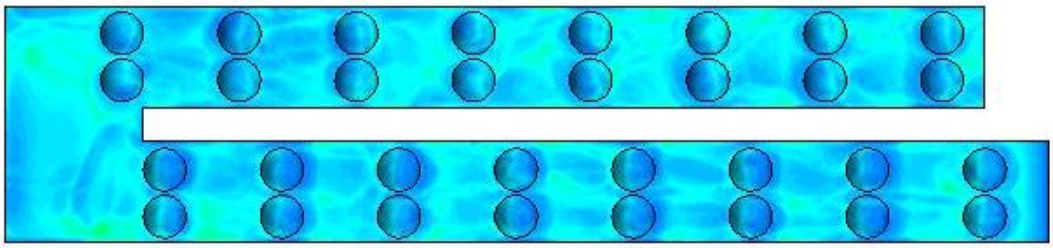

Case A

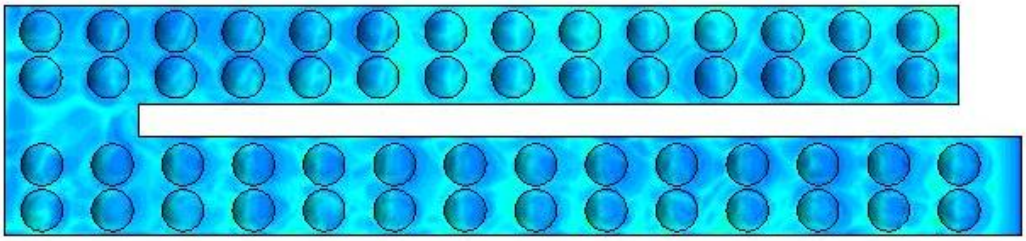

Case B

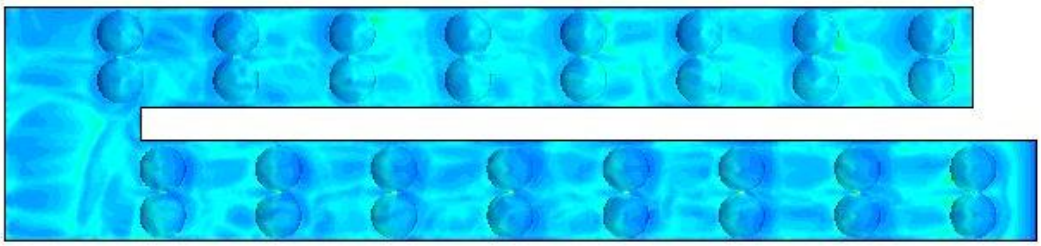

Case C

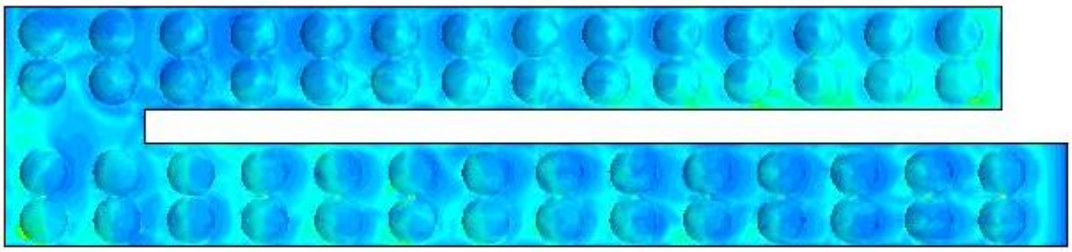

Case D

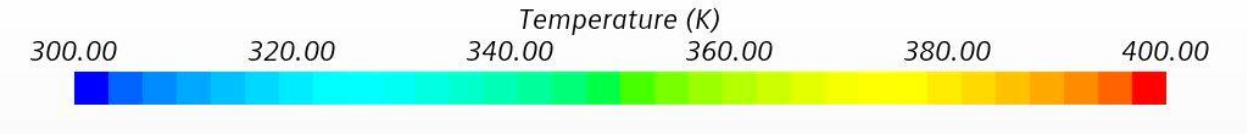


Figure 5-5: Temperature distribution along the cooling channel at Ro = 0

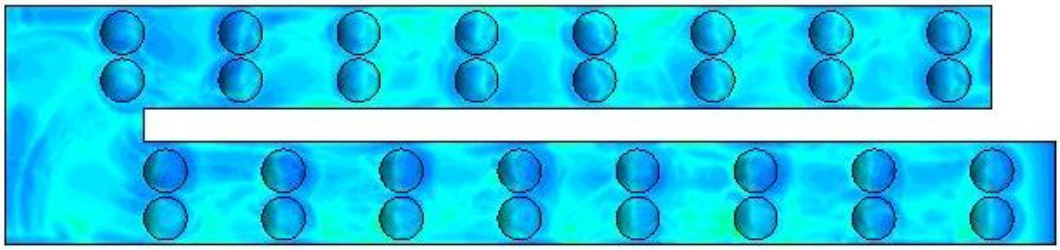

Case A

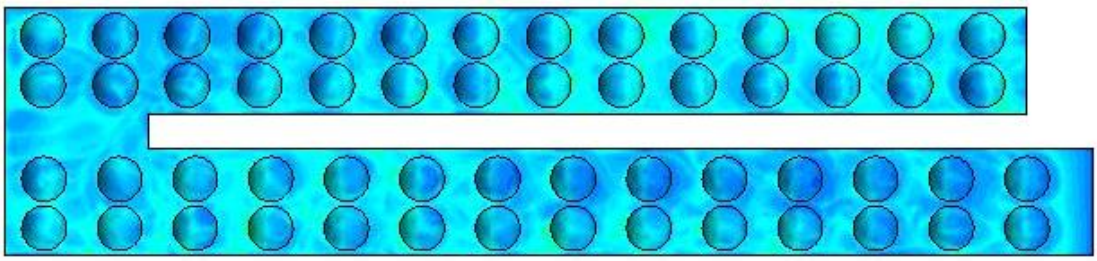

Case B

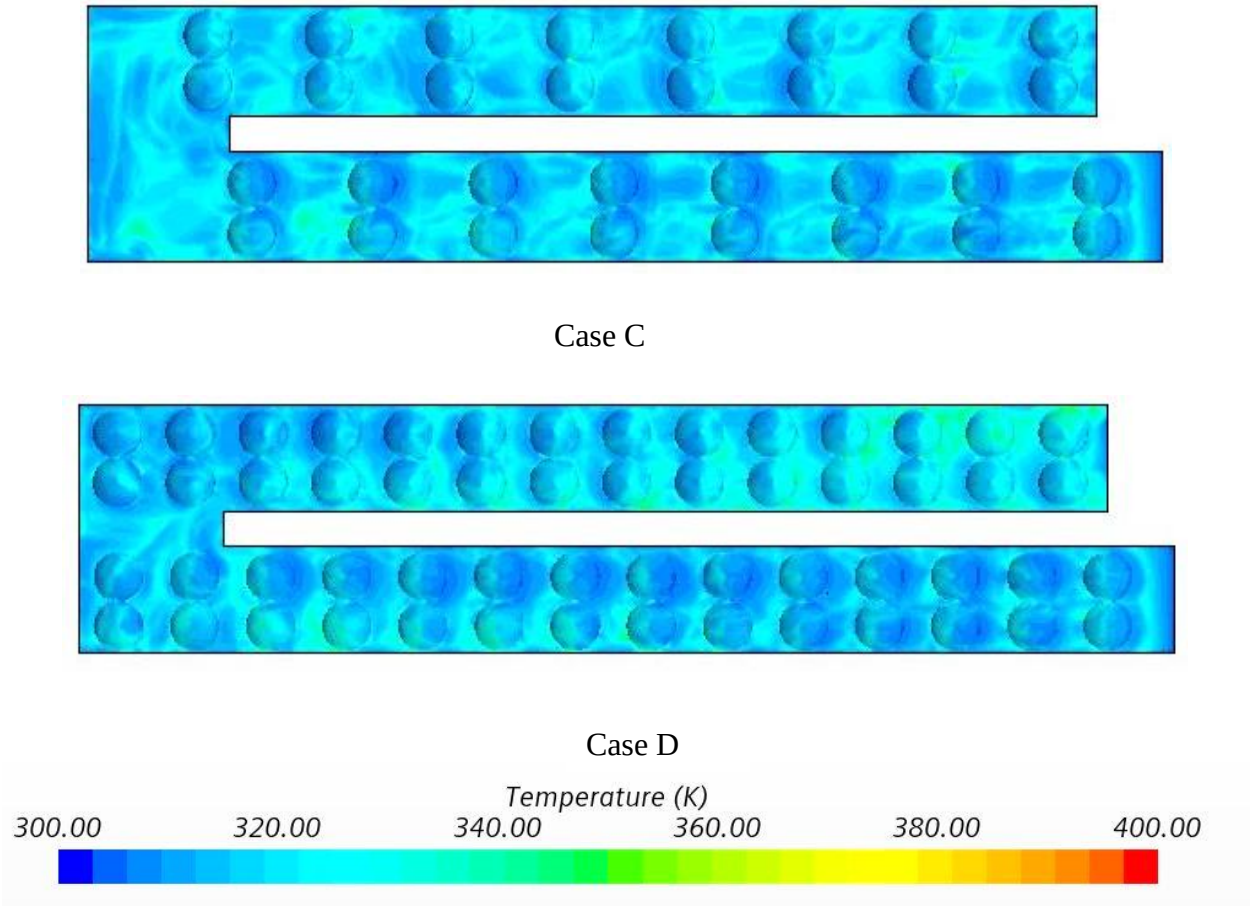


Figure 5-6: Temperature distribution along the cooling channel at Ro = 0.13

### 5.3.3. Heat Transfer Augmentation

The experimental results of heat transfer augmentation along the pin-finned channel are shown in Figure 5-7 and Figure 5-8. At the entrance of the channel, the Nu number reaches the higher values. It decreases in the mid-portion, and at the bend section, it reaches the peak. Before exiting the cooling channel. It reaches its highest peak. The velocity and temperature scenes reveal that at the second leg, the air flow is more turbulent which leads to a higher heat transfer at leg 2. The similar behavior can be found for Case C with $R_o = 0$ and $R_o = 0.13$ (Figure 5-9 and Figure 5-10).

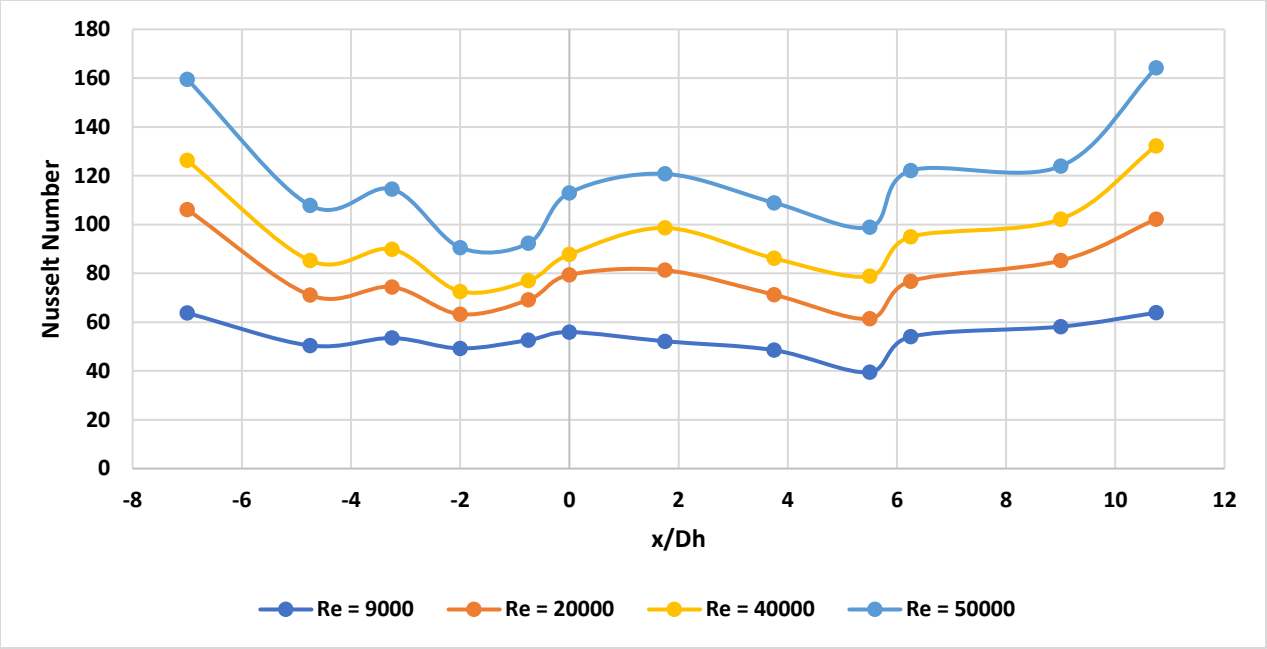


Figure 5-7: Heat transfer distribution along the cooling channel Ro = 0 (Case A)

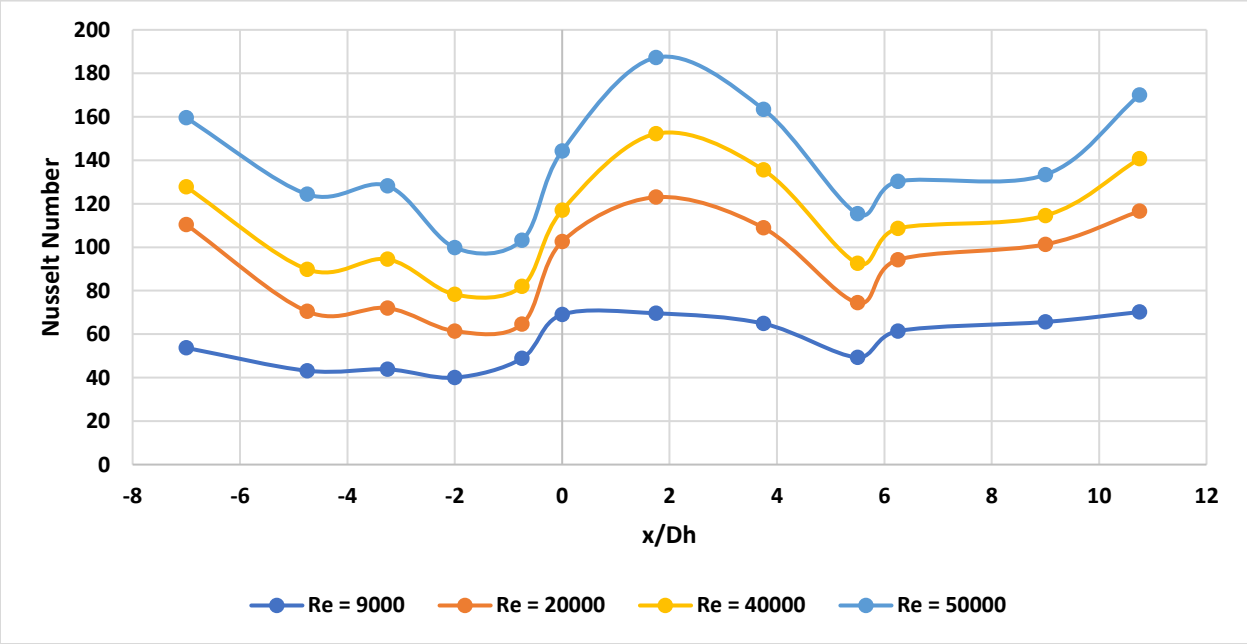


Figure 5-8: Heat transfer distribution along the cooling channel at 600 RPM (Case A)

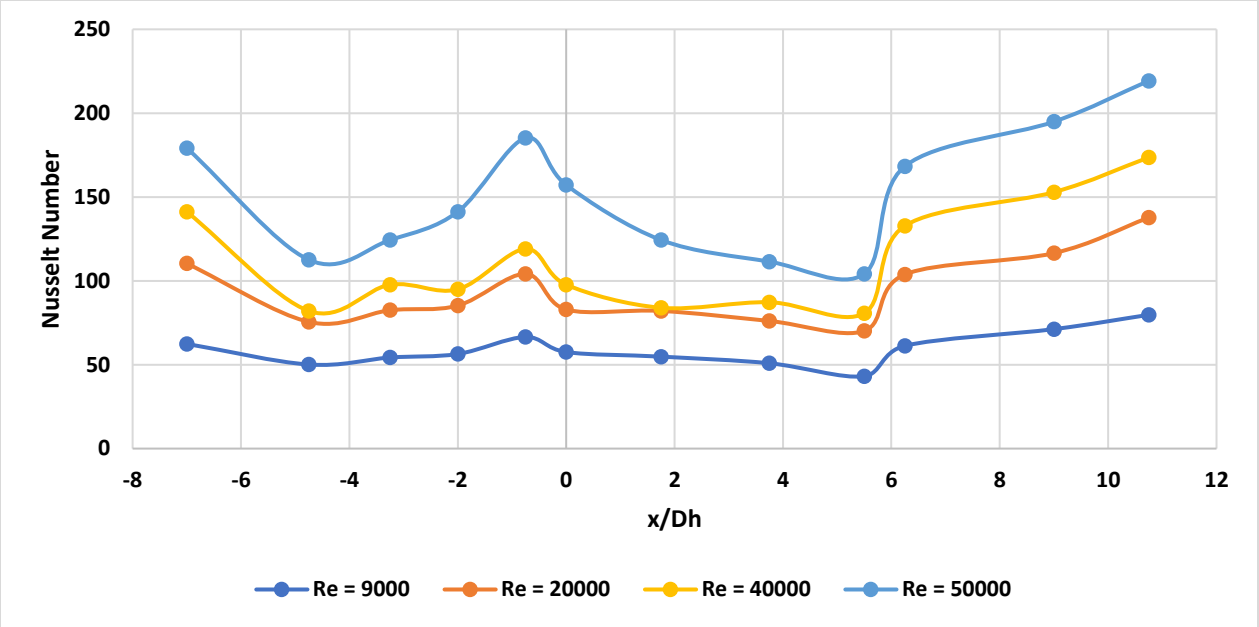


Figure 5-9: Heat transfer distribution along the cooling channel Ro = 0 (Case C)

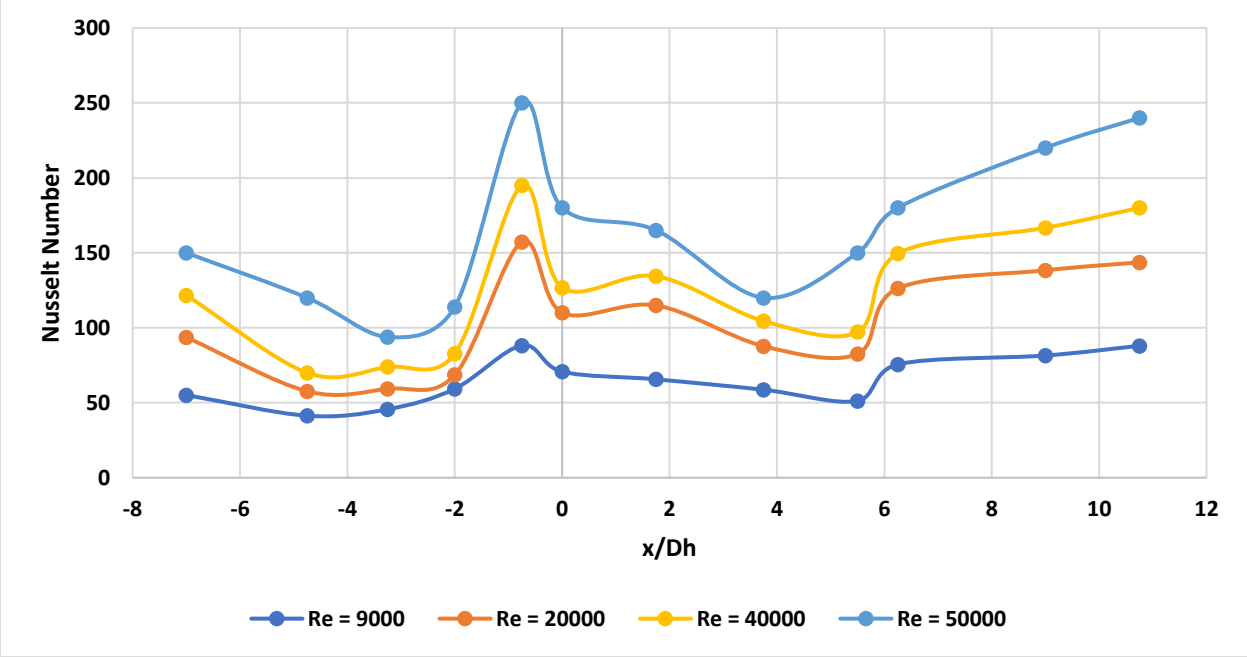


Figure 5-10: Heat transfer distribution along the cooling channel at 600 RPM (Case C)

### 5.3.4. Thermal Performance

Figure 5-11 represents the normalized heat transfer of stationary cases at Re = 50,000. Figure 5-12 represents the the normalized heat transfer for rotatioanl cases at $R_o$ = 0.13. Nusselt number of pin-fin cooling channels were normalized with the smooth surface cooling channel. Case D shows the highest heat transfer enhancement. The normalized friction factor indicates that the Case C is having the higher friction factor (Figure 5-13 and Figure 5-14). Case A expreiences a moderate pressure drop. However, heat transfer coefficient for Case A is significantly low. Thermal performance of Case D shows a higher value (93% for $R_o$ = 0 and 98% for $R_o$ = 0.13) as the heat transfer coefficient is significantly higher in case of Case D (Figure 5-15 and Figure 5-16).

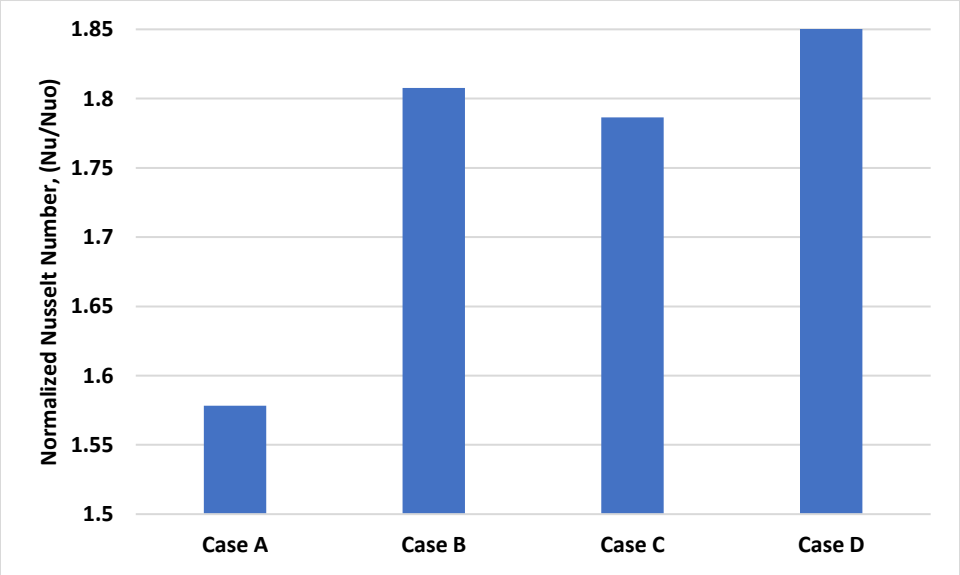


Figure 5-11: Normalized Nusselt number at $R_o$ = 0 at Re = 50,000

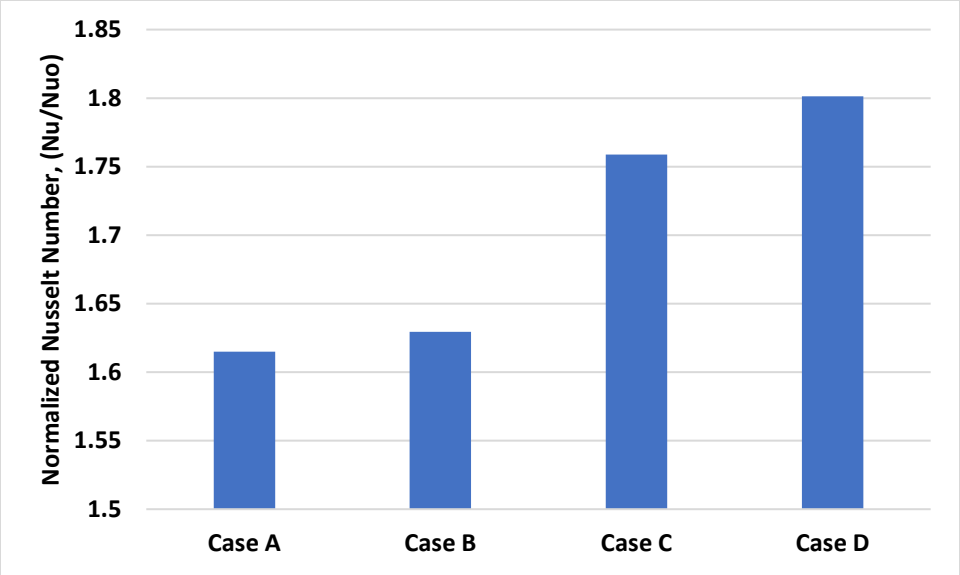


Figure 5-12: Normalized Nusselt number at $R_o = 0.13$

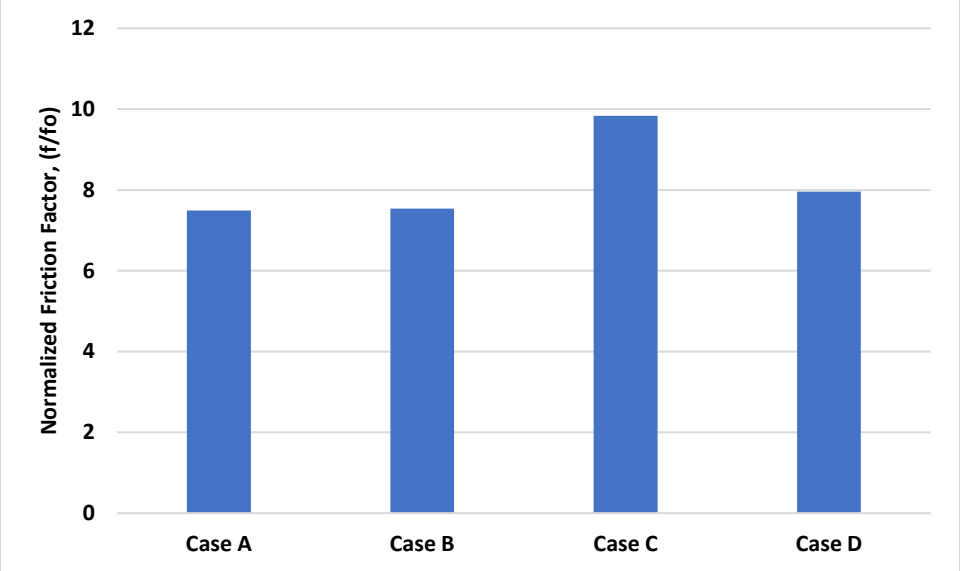


Figure 5-13: Normalized friction factor at Ro = 0 at Re = 50,000

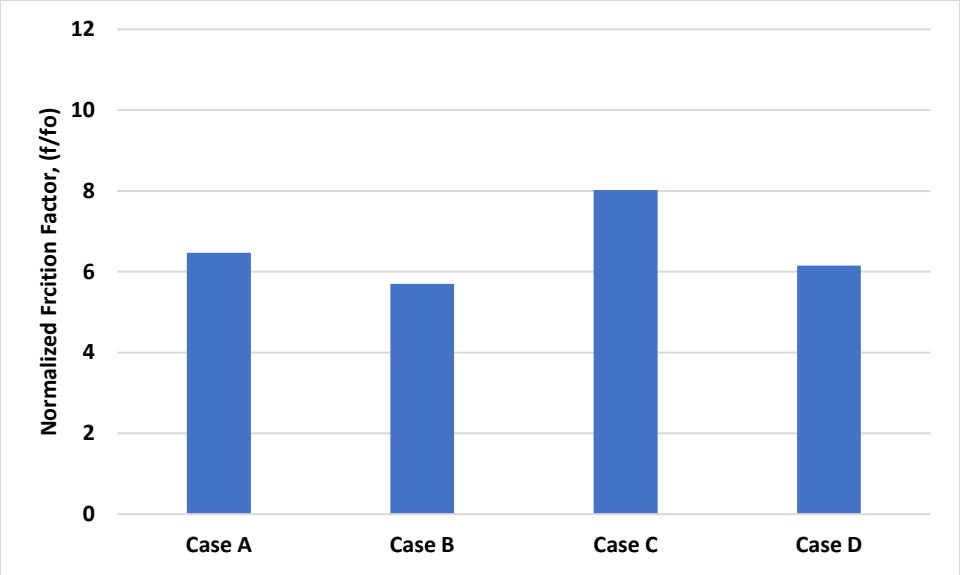


Figure 5-14: Normalized friction factor at Ro = 0.13

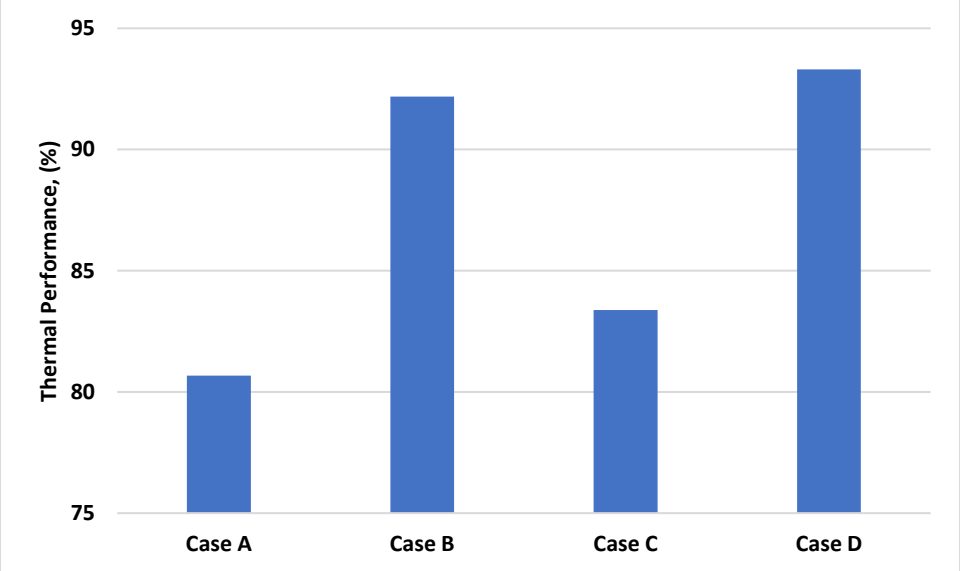


Figure 5-15: Thermal performance at Ro = 0 at Re = 50,000

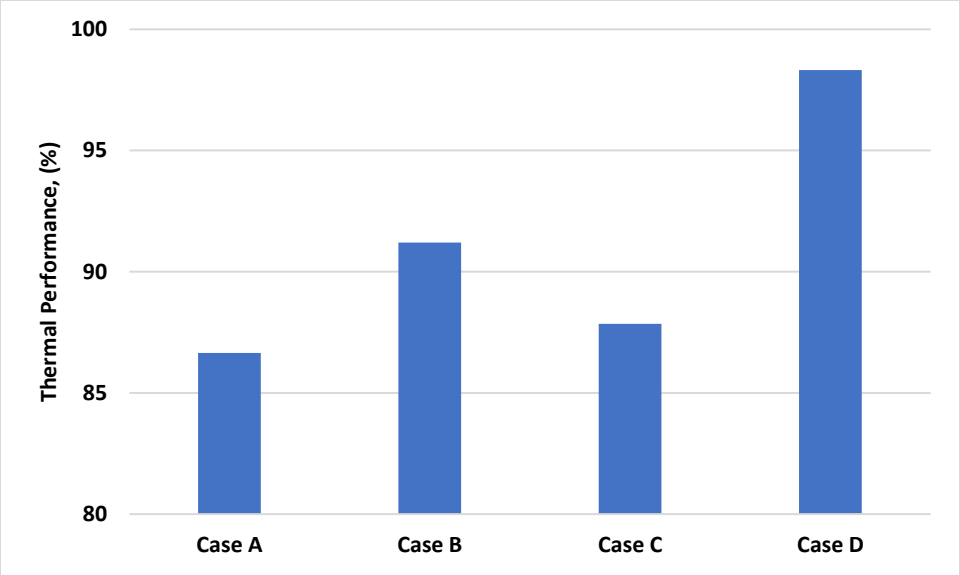


Figure 5-16: Thermal performance at Ro = 0.13

# 6. Effects of Guide Vanes on Dimpled Cooling Channel of Gas Turbine Blade

## 6.1. Introduction

In the earlier chapters, it has been discussed that gas turbine blade internal section can be cooled using dimple cooling, rib-turbulated cooling, jet impingement cooling. However, these cooling mechanisms can be more effective with combination of guide vanes in the bend region. A few researchers introduced guide vanes with smooth and ribbed surface cooling to increase the heat transfer. A 180° sharp turn in the bend region induces a better heat transfer. However, the pressure drop can be as high as 25% of the pressure of the entire channel. An addition of guide vanes in the bend region can optimize the heat transfer and durability of the blade considering thermal efficiency.

Literature indicates that researchers introduced guide vanes with rib turbulated cooling channel. However, no studies show the effect of guide vanes with dimpled surface channels. The purpose of the current study is to investigate the effect of the guide vanes in a dimpled cooling channel. The study has been conducted both experimentally and computationally. While the experimental study represents the real-world temperature distribution along the channel, the computational study represents the air flow behavior in the cooling channel. Previous studies discussed the results of protruded guide vanes with ribbed cooling channel. In this study, two different designs of guide vanes were implemented both as a cavity and protrusion.

## 6.2. Experimental Setup and Numerical Approach

A two-pass dimpled U-bend channel was introduced both for experimental and computational studies. The first passage is 490 mm, and second passage is 460 mm long with a 40

mm hydraulic diameter. 8 – rows of on the first passage and 7 -rows partial spherical dimples on the second passage were imprinted to the bottom surface of the cooling channel. The dimple diameter is 20 mm and depth are 10 mm which leads to dimple depth to diameter ratio as 0.50. The rotational study was conducted with 600 rpm which leads to the rotation number to 0.13. Table 6-1 shows the details of the guide vanes. Figure 6-1 represents the guide vane design and orientation on the cooling surface. Two diverse types such as U and curve shape of guide vanes were inserted in the bend region of the cooling channel both in depression and protrusion. The depth of depression and protrusion is 4 mm. The experimental procedure was the same as mentioned in the earlier chapters.

Table 6-1: Details of cooling channels with guide vanes

| **Cases** | **Guide Vane Type** | **Depression/Protrusion Depth (mm)** |
|---|---|---|
| No GV | N/A | N/A |
| Case A | U-Depression | 4 |
| Case B | Curve-Depression | 4 |
| Case C | U-Protrusion | 4 |
| Case D | Curve-Protrusion | 4 |

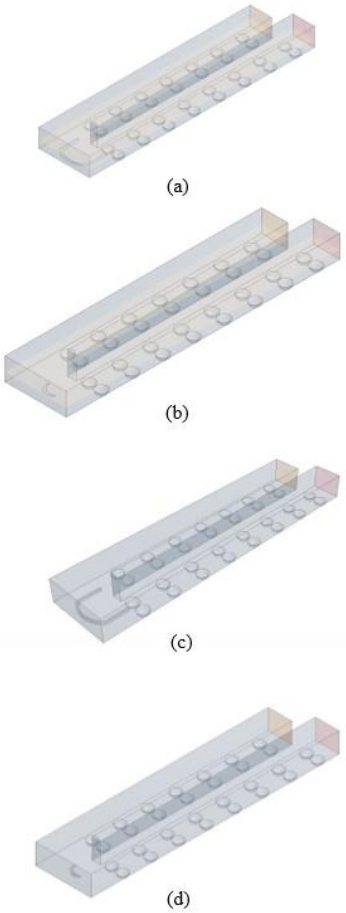


Figure 6-1: Guide vane details (a) U-depression, (b) Curve-depression, (c) U-protrusion, and (d) Curve-depression

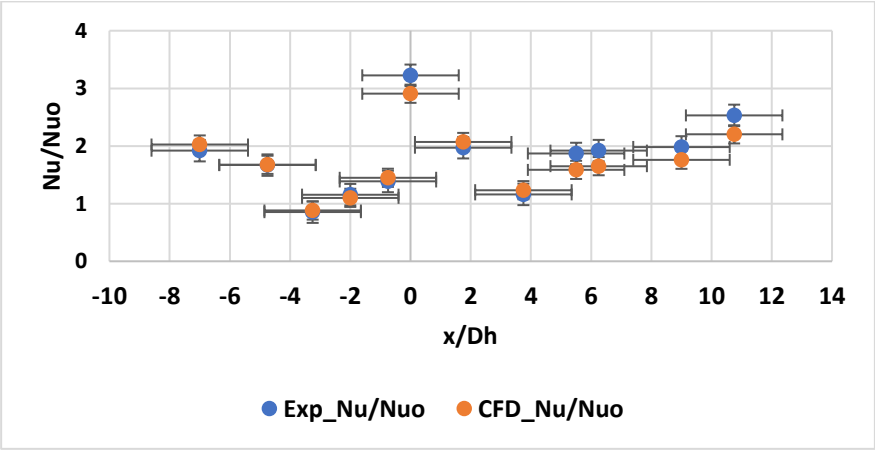


Figure 6-2: Experimental and CFD results comparison u-depression at $R_o$ = 0.13

Figure 6-2 indicates the comparison of experimental and numerical results. Uncertainty analysis was conducted using 95% confidence level. The numerical study was conducted with LES technique. The physics model was implemented the same as the previous studies. However, a new mesh independent study was conducted for the guide vane study. The grid dependence study was conducted at Re = 50,000 at $R_o$ = 0. Four different number of cells were considered for the mesh independent study i.e., 1.8, 2.5, 4.2, and 10 million number of cells (Figure 6-3). Surface average Nusselt number were 135.55, 136.07, 136.97, and 137.75 respectively. The 2.5 and 4.2 million number of cells showed almost the same trend. However, to save computational time 2.5 million cells were considered for the computational study. Figure 6-4 represents the Wall Y+ scenes at $R_o$ = 0.20. For all the cases, the values remain less than 1.

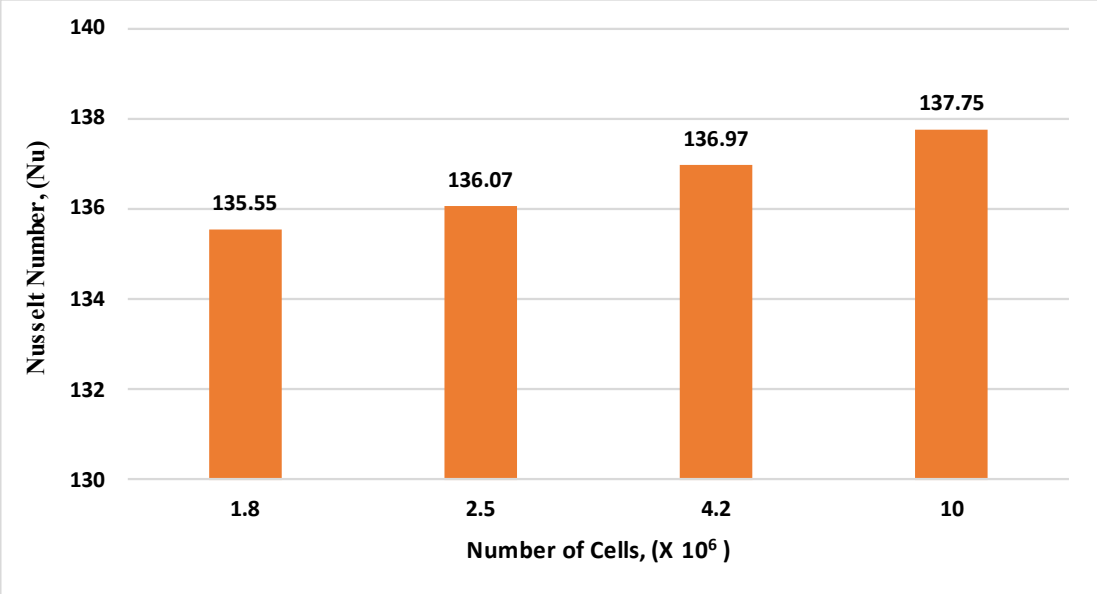


Figure 6-3: Grid independence study with No guide vane channel at $R_o$ = 0 (Re = 50,000)

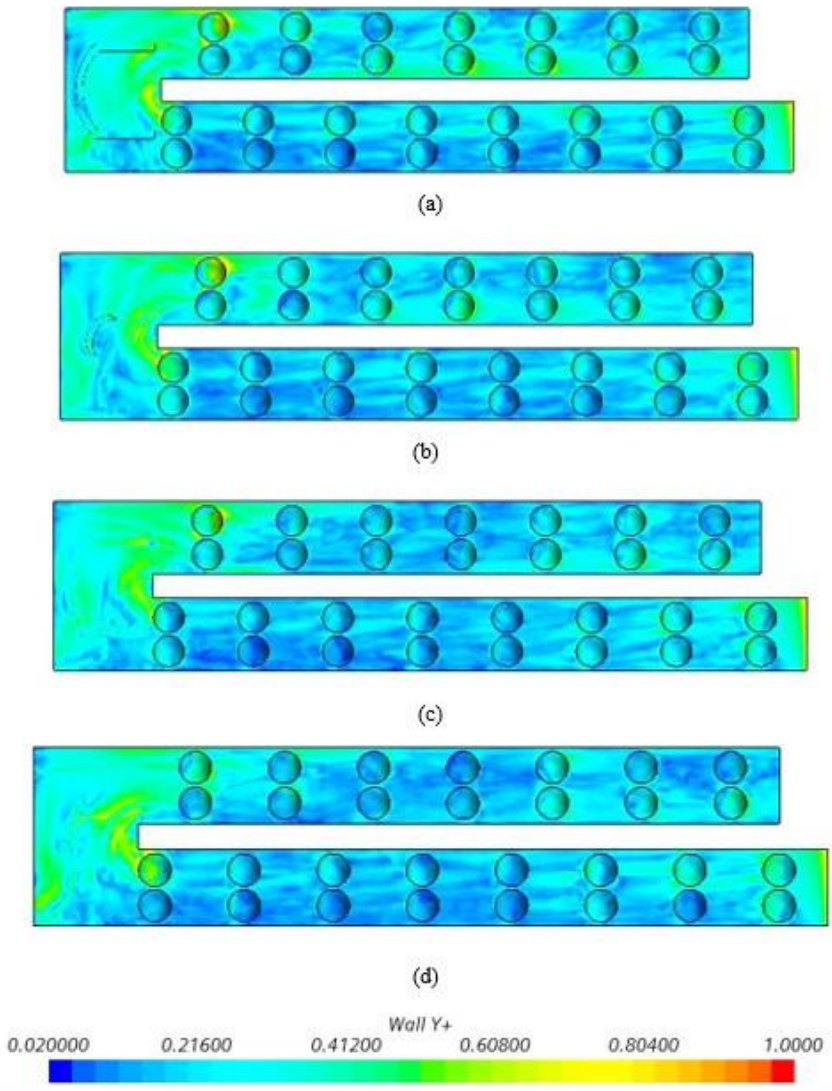


Figure 6-4: Wall Y+ scenes with for $R_o$ = 0.20 (a) Case A, (b) Case B, (c) Case C and (d) Case D

## 6.3. Results

### 6.3.1. Experimental Results

Figure 6-5 and Figure 6-6 show the experimental results for the U-depression guide vane in the dimpled cooling channel both at stationary and 600 RPM. At the entrance of the cooling channel, there is ambient air which makes a higher heat transfer. However, while the air passes through the cooling channel, it extracts heat from the bottom surface. As a result, heat transfer is lower at the mid portion of leg 1. When the air reaches the bend region, it experiences high turbulences and vortex rolls of air and increases the heat transfer. It decreases at the mid portion of the leg 2 and increases while exiting the cooling channel. The rotational cases experience higher heat transfer due to the Coriolis forces.

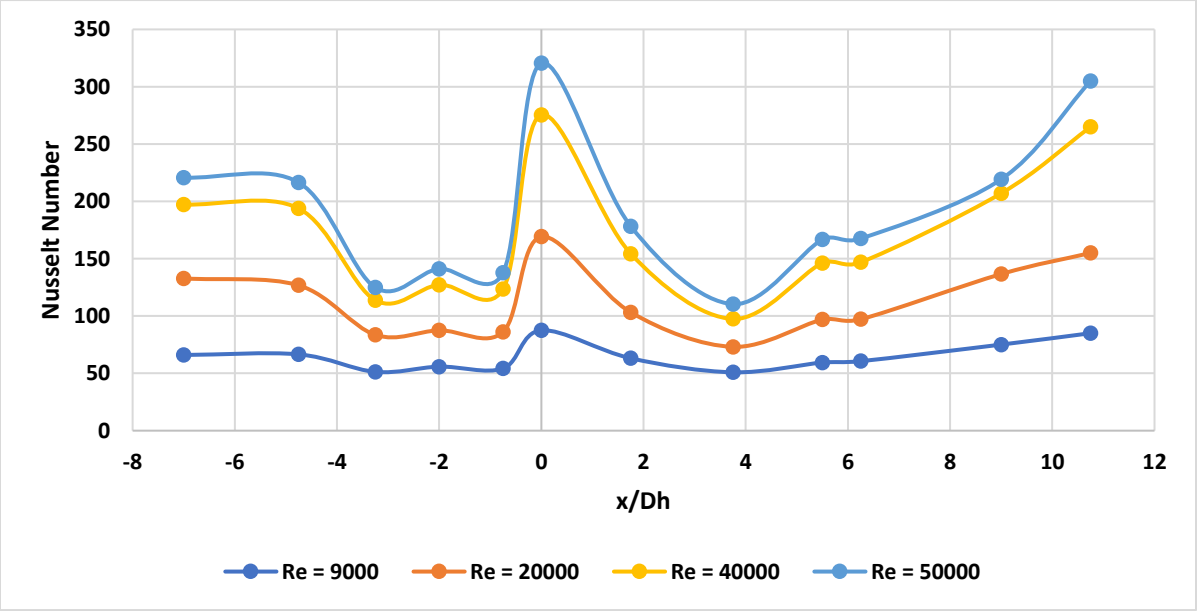


Figure 6-5: Heat transfer distribution along the cooling channel for Case A (Ro = 0)

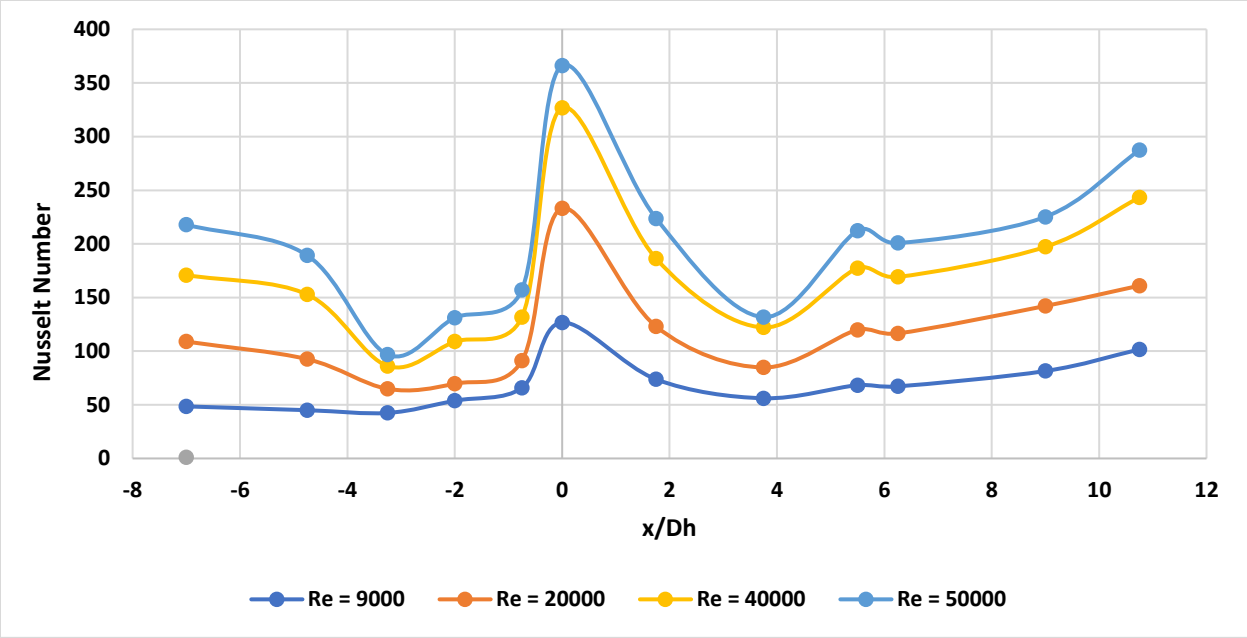


Figure 6-6: Heat transfer distribution along the cooling channel for Case A at 600 RPM

### 6.3.2. Numerical Study

*6.3.2.1. Velocity Distribution along the Channel*

The velocity profile with guide vanes can be found in Figure 6-7 and Figure 6-8. For both stationary and rotational cases, working fluid is at uniform pattern at the leg 1. However, the air becomes more turbulent at the bend region, and it again becomes uniform after the bend section. Figure 6-9 represents the Q-criterion of the cooling channels with guide vanes. The Q-criterion indicates that the magnitude of the vorticity is greater than the magnitude of the strain rate. It can make the flow visualization in a clear flashing to identify vortical structures in the flows, including hairpins and attached eddies. Near the dimples, the vortex shedding is at the higher range. A group of vortices blend inside the dimples and creates a vortex roll.

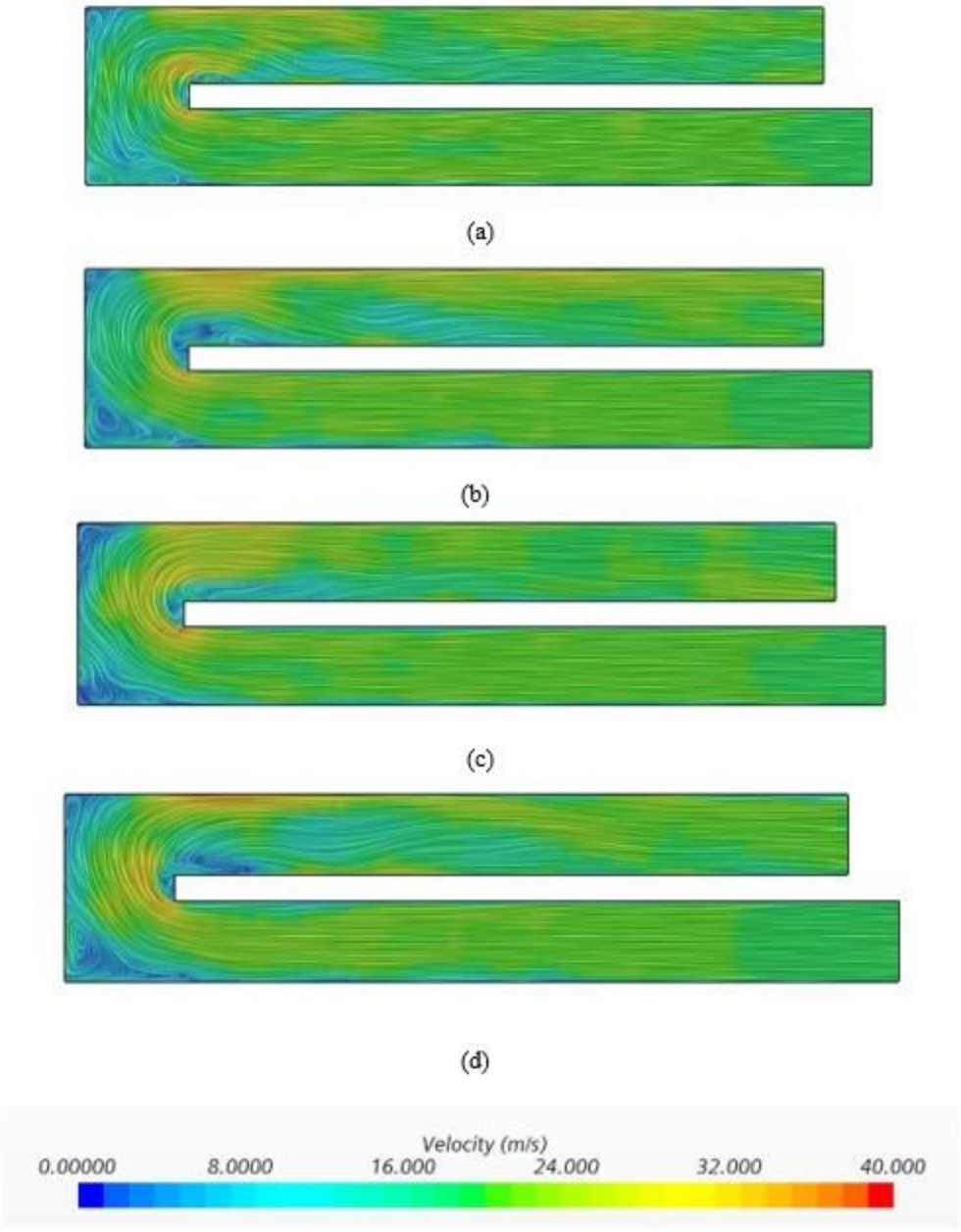


Figure 6-7: Velocity distribution along the cooling channels at Ro = 0 at Re = 50,000 for (a) Case A, (b) Case B, (c) Case C and (d) Case D

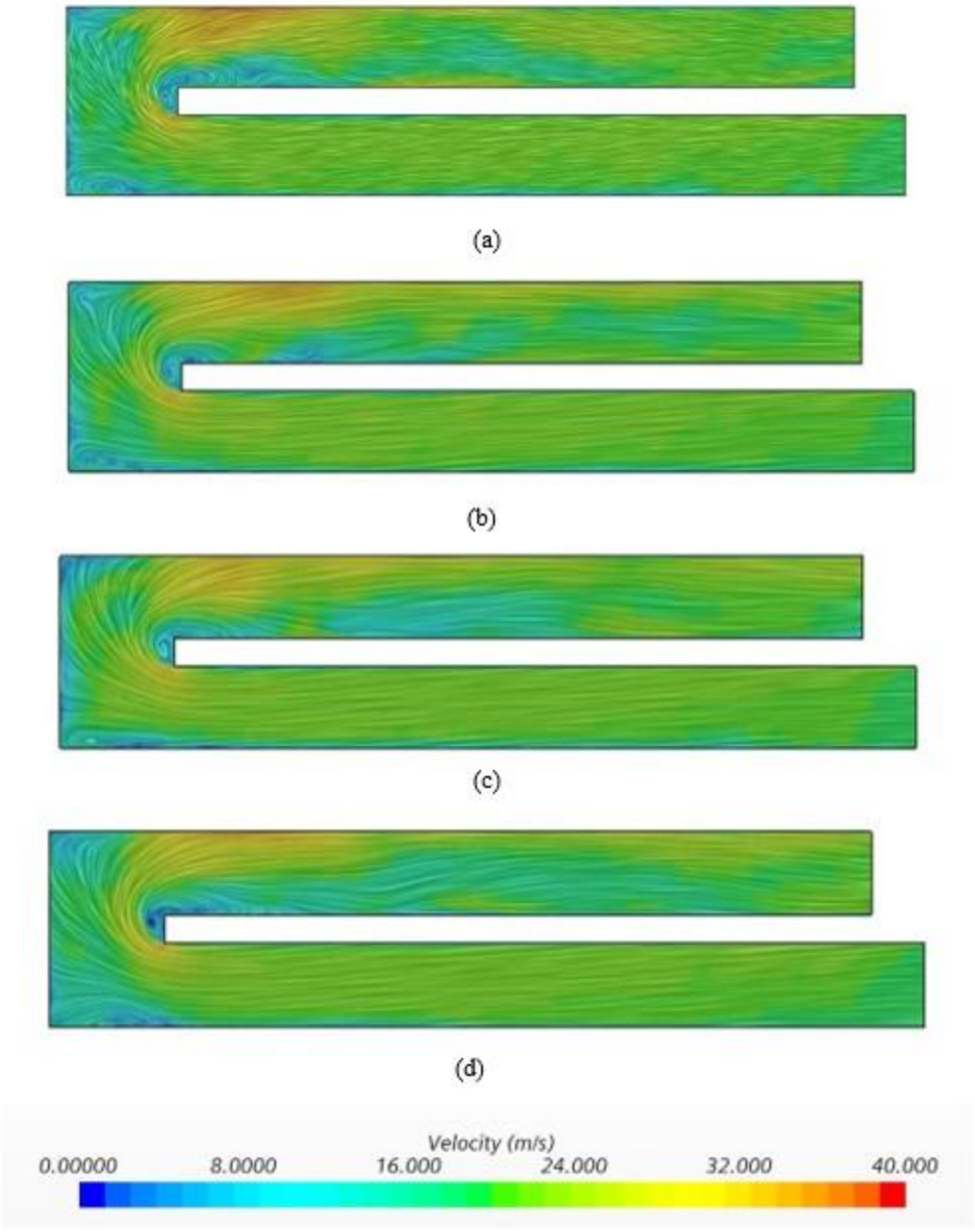


Figure 6-8: Velocity distribution along the cooling channels at $R_o$ = 0.13 for (a) Case A, (b) Case B, (c) Case C and (d) Case D

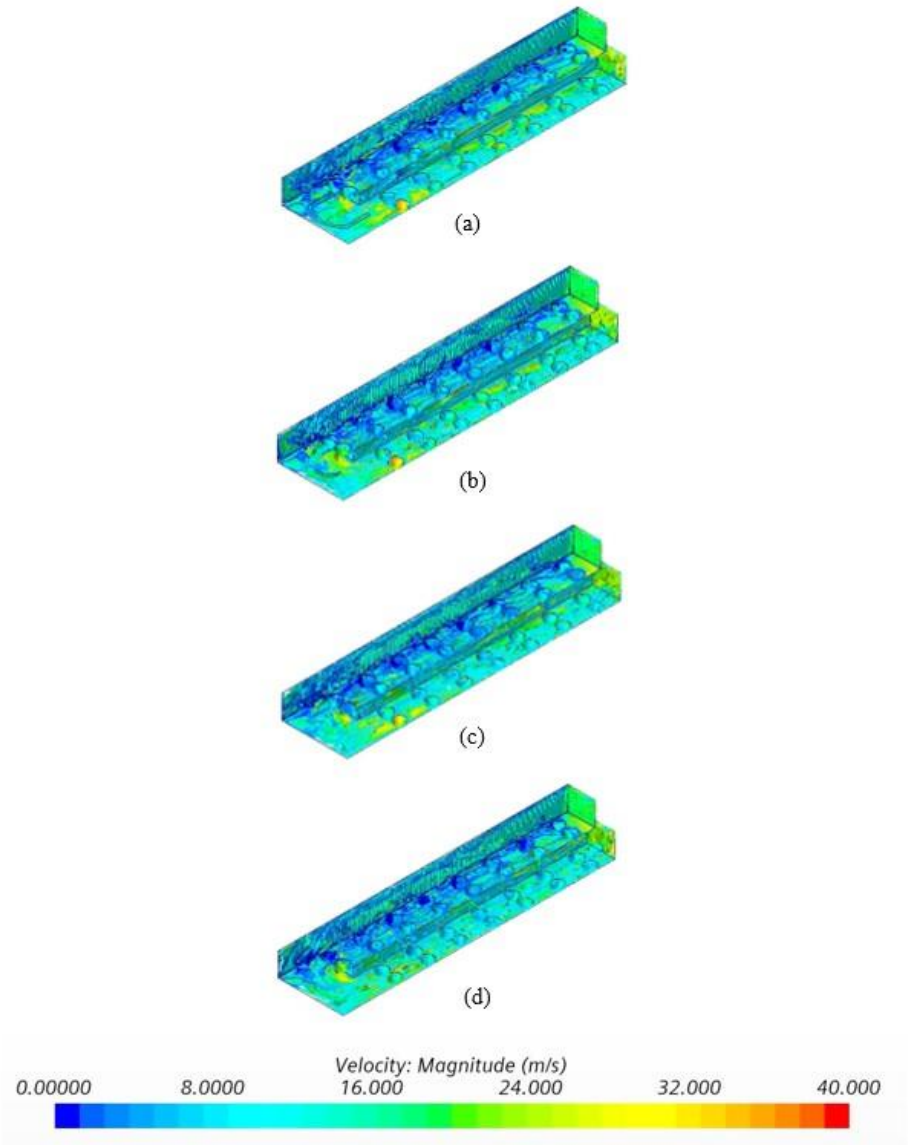


Figure 6-9: Velocity distribution along the cooling channels at Ro = 0.20 for (a) Case A, (b) Case B, (c) Case C and (d) Case D

*6.3.2.2. Heat Transfer Phenomena*

Figure 6-10 and Figure 6-11 reveal the temperature distribution of cooling passage with guide vanes for stationary and rotational cases. The temperature shows a higher value at the leg 1 whereas right before guide vane, guide vane region, and after the guide vane, temperature decreases which indicates a better heat transfer in these regions. The heat transfer enhancement was normalized with the smooth surface cooling passage (Figure 6-12, Figure 6-13, and Figure

6-14). At $R_o = 0$, the ratio of normalized Nusselt number shows that Case A and Case C are having the higher heat transfer compared to the other cases. However, the rotational study indicates that Case A has the best heat transfer enhancement compared to the other designs.

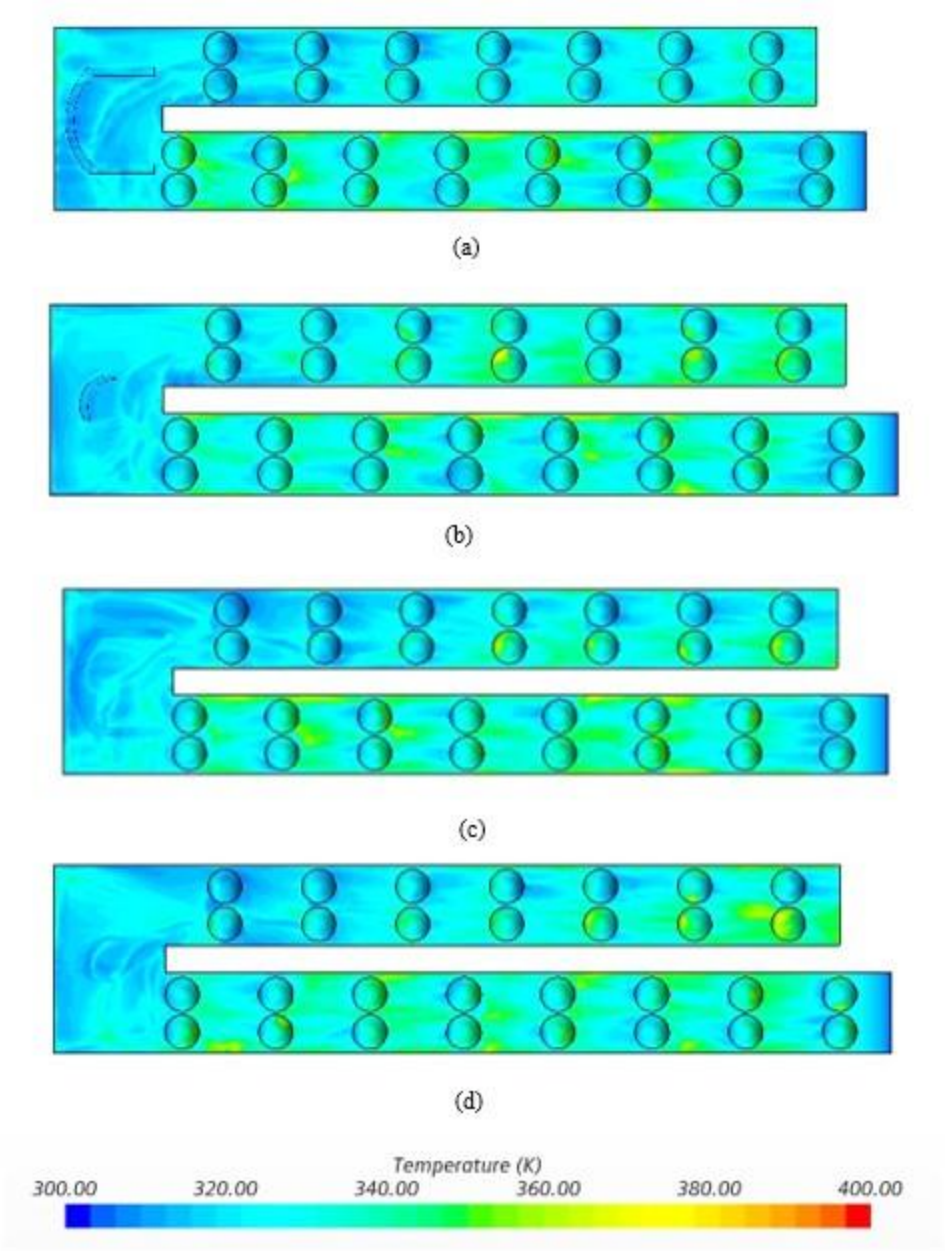


Figure 6-10: Temperature distribution along the cooling channels at Ro = 0 at Re = 50,000 for (a) Case A, (b) Case B, (c) Case C and (d) Case D

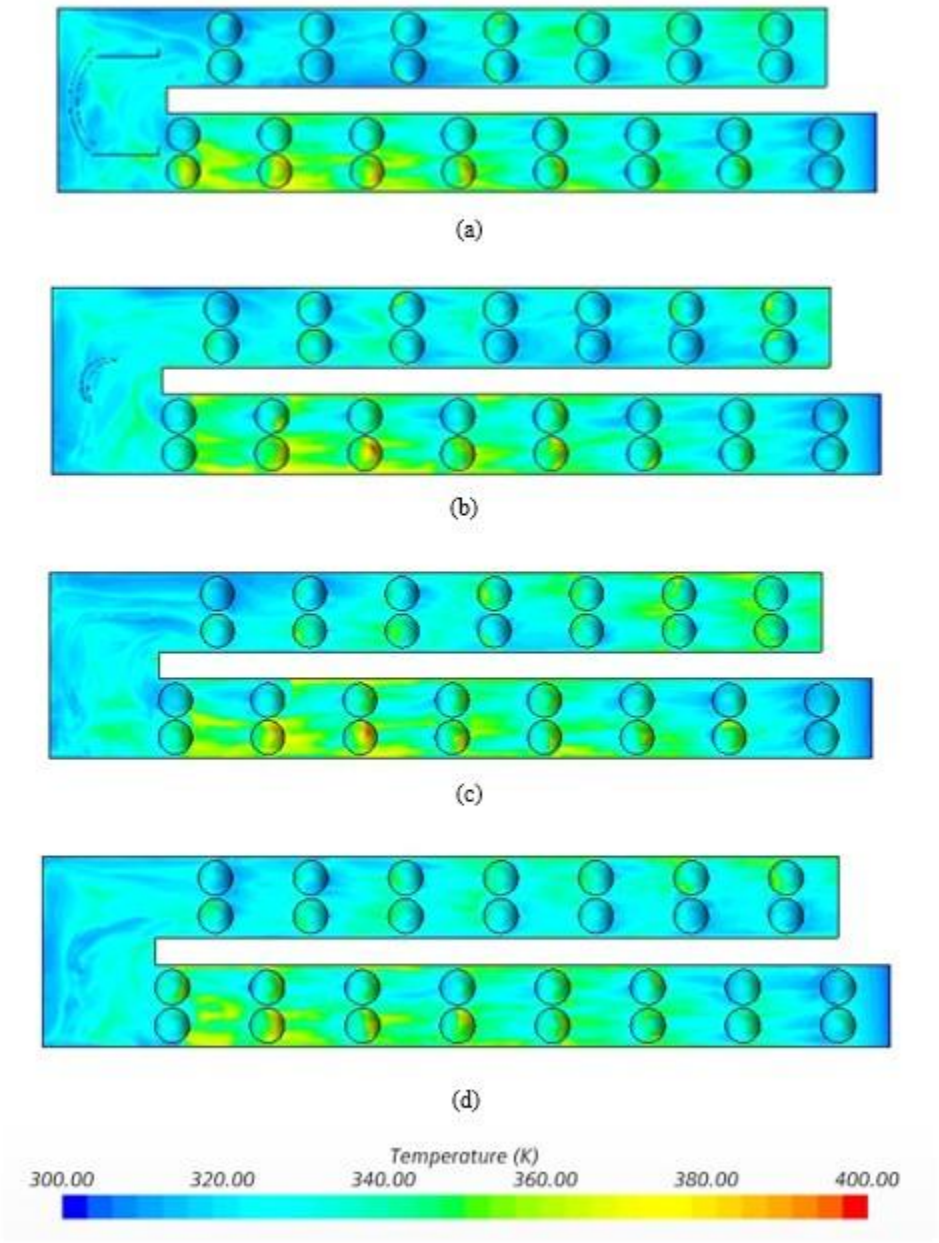


Figure 6-11: Temperature distribution along the cooling channels at Ro = 0.13 for (a) Case A, (b) Case B, (c) Case C and (d) Case D

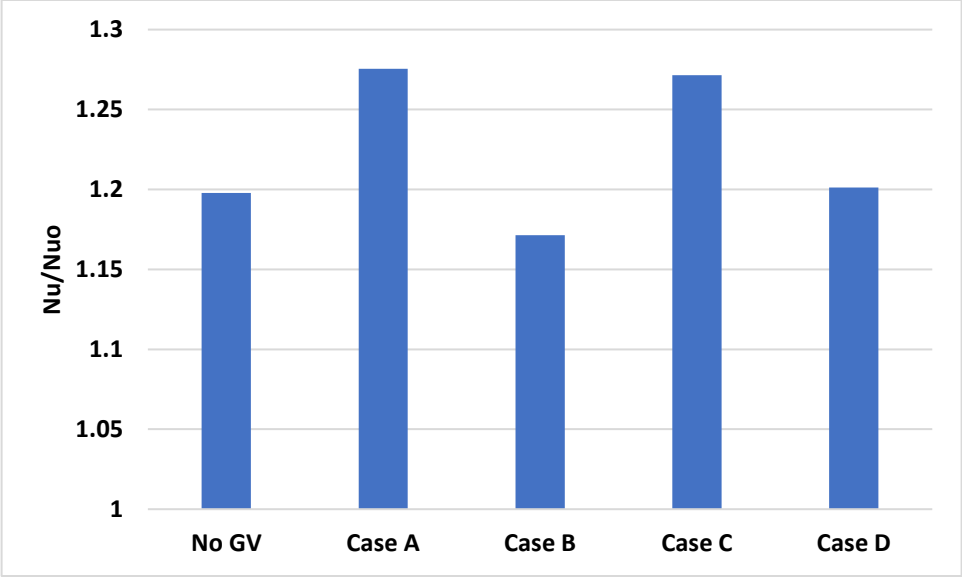


Figure 6-12: Normalized Nusselt number at Ro = 0 and Re = 50,000

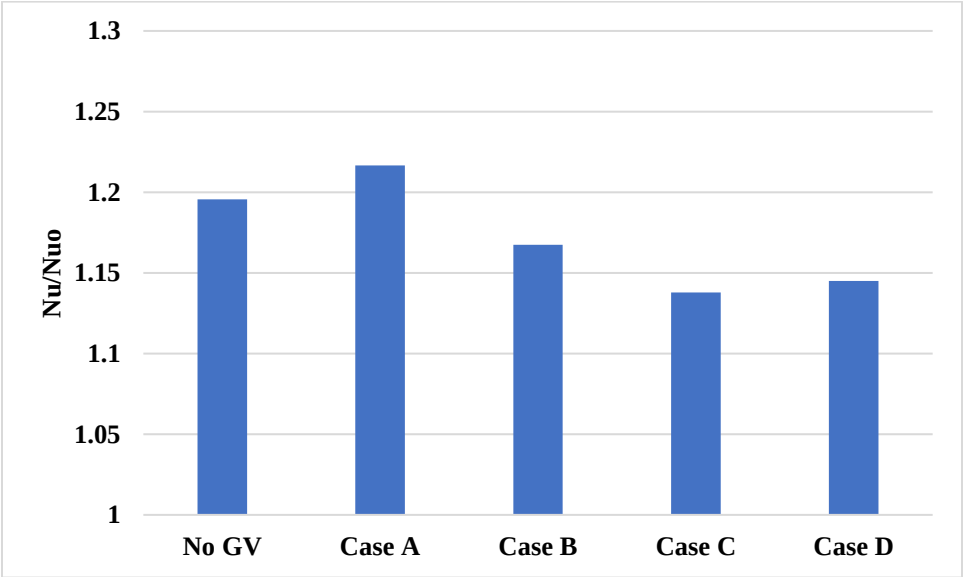


Figure 6-13: Normalized Nusselt number at $R_o$ = 0.13

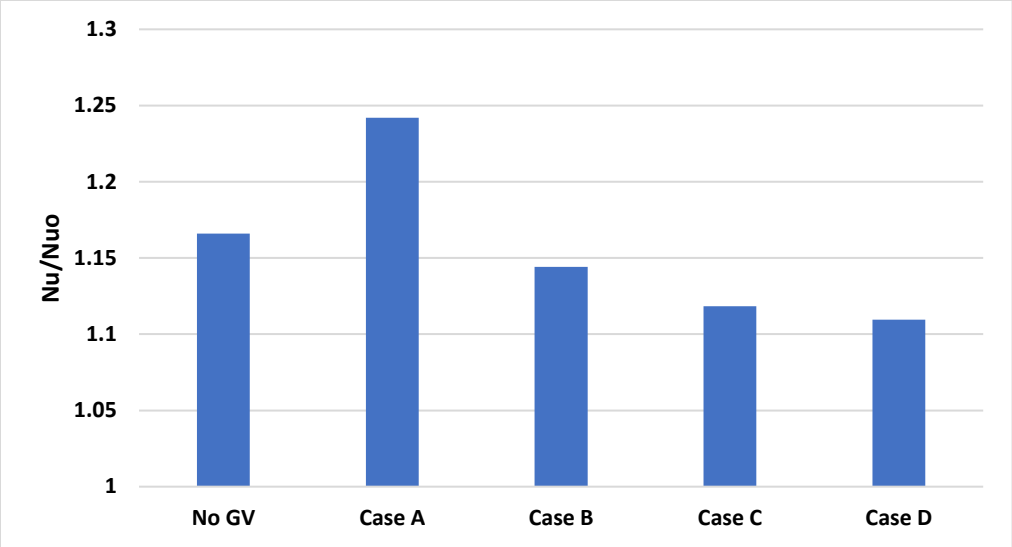


Figure 6-14: Normalized Nusselt number at $R_o$ = 0.20

*6.3.2.3. Thermal Performance*

Pressure drop causes an obstacle to efficient heat transfer. Even though the combination of dimple and guide vane increases the heat transfer coefficient in the cooling channel, there is pressure drop penalty. So, pressure drop should be considered in any dimpled surface design. The pressure drop phenomena are seen in Figure 6-15, Figure 6-16 and Figure 6-17. With the increase of rotation number, the friction factor decreases. It has been observed that Case C showed a higher friction factor. Case A shows a moderate pressure drop. That's why considering the thermal performance, the Case A which is cooling channel with U-depression experiences a higher thermal performance (Figure 6-18, Figure 6-19, and Figure 6-20).

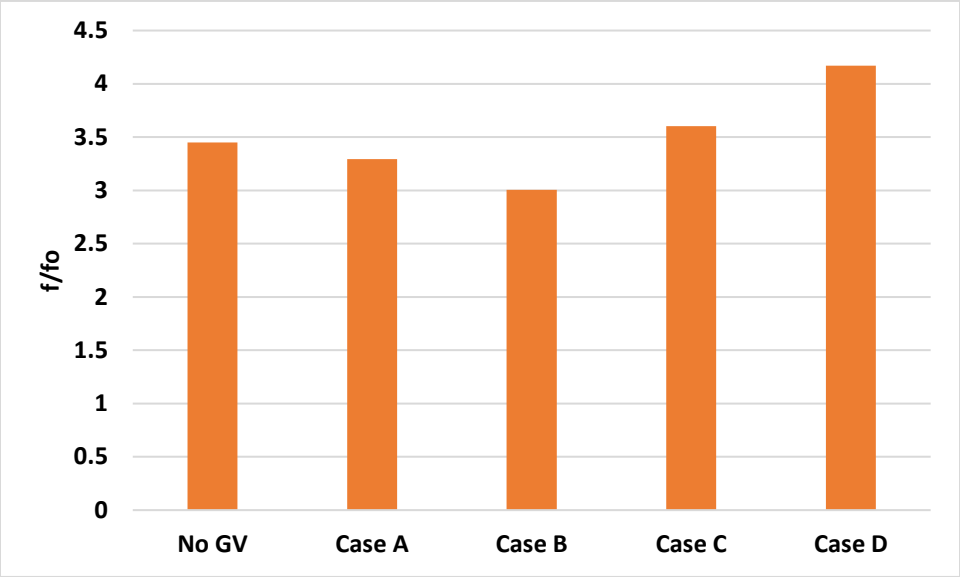


Figure 6-15: Normalized friction factor at Ro = 0 and Re = 50,000

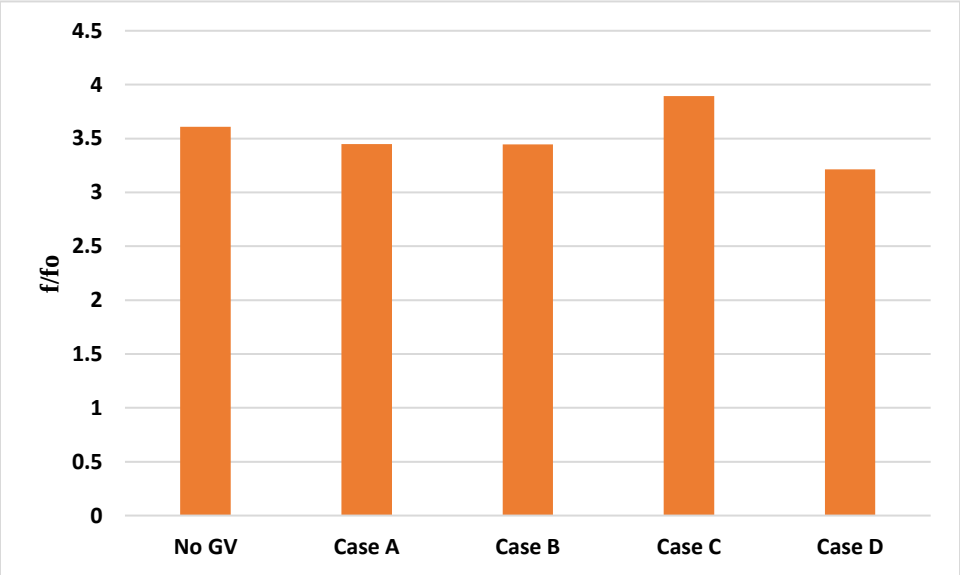


Figure 6-16: Normalized friction factor at $R_o$ = 0.13

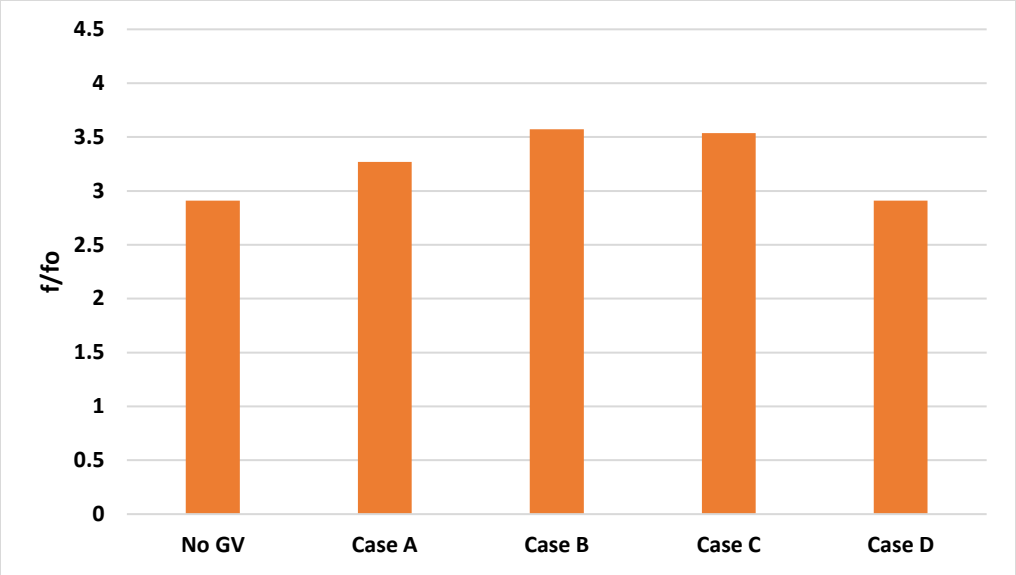


Figure 6-17: Normalized friction factor at $R_o$ = 0.20


Figure 6-18: Thermal performance at Ro = 0 and Re = 50,000

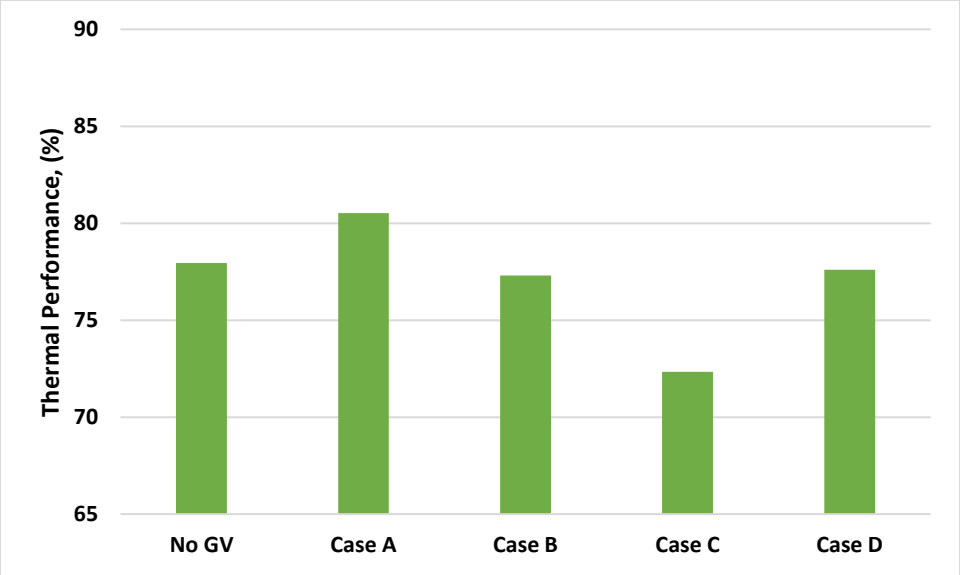


Figure 6-19: Thermal performance at $R_o = 0.13$

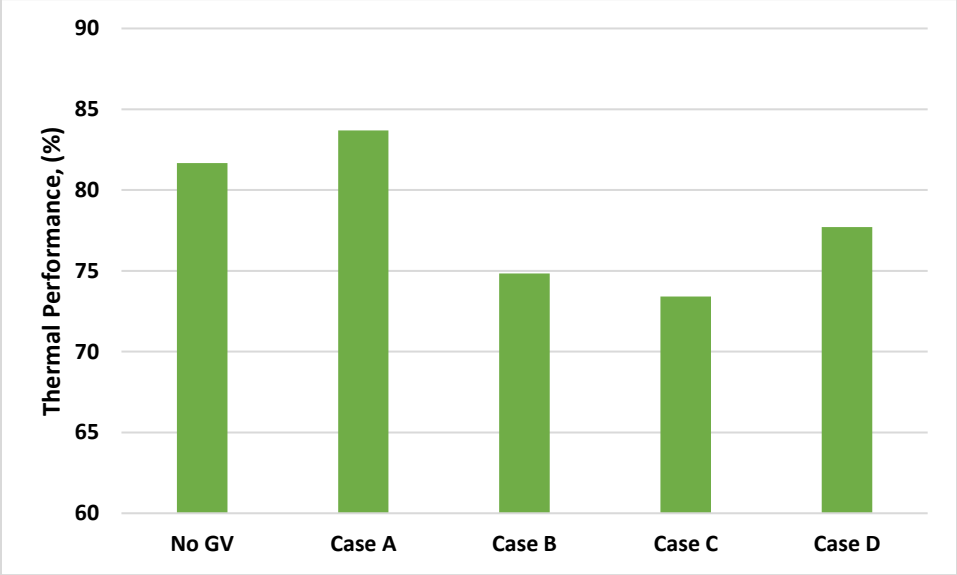


Figure 6-20: Thermal performance at $R_o = 0.20$

# 7. Conclusions and Future Work Recommendations

## 7.1. Research Conclusions

In this research, investigation of heat transfer and flow phenomena of gas turbine blade internal cooling passage has been conducted using smooth, dimple cooling, rib turbulator cooling and pin-fin cooling. Additionally, guide vanes in a dimpled cooling channel were studied. The research conclusions are provided below:

### 7.1.1. Dimple Cooling

The thermal performance of the gas turbine internal channel has been investigated both experimentally and numerically for Re numbers ranging from 6,000 to 50,000 with stationary cases. The experimental and numerical investigation extends by conducting the rotational cases at 300 RPM, 600 RPM, and 900 RPM with Reynolds numbers ranging from 6,000 to 50,000 with smooth surface and dimpled surface cooling channel. The following conclusions emerged:

1. The large eddy simulation predicts the airflow along the channel accurately, which leads to a better comparison of experimental and numerical results.
2. The smooth surface channel showed a low heat transfer rate compared to dimpled surface channels for all the Reynolds numbers. However, the pressure drop was also the lowest in comparison with the dimpled surfaces.
3. The heat transfer increases with the increase of Reynolds number for all cases at all rotational speeds. Combining both increases the centrifugal and buoyancy forces, leading to heat transfer in the cooling channel.

4. The highest heat transfer might not make the cooling channel the most efficient one. For this reason, the effective thermal efficiency that combines both the heat transfer and the friction factor was used and successfully demonstrated the heat transfer effectiveness.

5. The leaf dimpled surface showed the highest thermal performance considering the channel's heat transfer enhancement and friction factor at Re number 50,000.
6. At the lowest Reynolds number flow, the case with the dimple's depth-to-diameter ratio of 0.25 represents the best thermal performance.

### 7.1.2. Rib-turbulated cooling

The thermal performance of the gas turbine internal cooling channel has been investigated with 30° and 45° angled ribs. The investigation was completed experimentally and computationally with Re numbers ranging from 12,000 to 65,000. Large Eddy Simulation (LES) technique was implemented to investigate the air flow pattern in the internal cooling channel. Stationary cases were considered as well as rotational cases with 600 RPM. The following conclusions emerged:

- The large eddy simulation predicts the airflow along the channel accurately, which leads to a better comparison of experimental and numerical results.
- In the first leg, ribs generate vortices. The bend section experiences more turbulence and air creates vortex rolls. In the second leg, again ribs cause vortices. The air vortices increase heat transfer in the cooling channel compared to the smooth surface channel.
- The rotational effects enhance the heat transfer coefficient of the cooling channel due to the Coriolis and centrifugal forces.
- 45° angled ribs encounter more pressure drop and it negatively affects the thermal performance of the 45° angled ribs cooling channel.

### 7.1.3. Pin-fin cooling

The pin-fin cooling investigation was conducted with four different cooling channels with two different pin-fin designs. Both stationary and rotational investigation was completed with Reynolds numbers ranging from 9,000 to 50,000. The rotational study was conducted at 600 RPM. Large Eddy Simulation technique predicts the air flow distribution and heat transfer phenomenon. The major conclusions are -

- When the air flows through the series of pin-fins, it blocks the air flow. This causes horseshoe vortices and strong secondary flows which contributes to the heat transfer enhancement.
- The dome shape pin-fins increase the heat transfer both in stationary and rotational cases because of its tilted curve in the design.
- The highest heat transfer coefficient was found with rotational cases due to Coriolis and buoyancy forces.
- Partial spherical pin-fins extended to the bend region increases the heat transfer. However, due to the excessive pressure drop, thermal performance gets decreased. On the other hand, cooling channel including dome pin-fins at the cooling channel (Both Case B and Case D) has the balance of heat transfer coefficient and pressure drop trend.

### 7.1.4. Guide Vanes

The integration of guide vanes with dimpled cooling channel were investigated in the present study. The turning guide vanes were inserted to the ribbed channel in the open literature. However, the current investigation will give an insight into integration of guide vanes with dimpled cooling channel. The present study considers two different designs of guide vanes in the turn region with

four different orientations. The purpose was to increase the heat transfer of the cooling channel with minimal pressure drop. The following results has been found-

- The U-depression guide vane cooling channel faces the highest heat transfer among the considered channels both in stationary and rotational cases. Also, heat transfer increases with the increase of rotation number.
- For stationary and rotational cases, installing the guide vane does not always increase the heat transfer.
- The curve depression and protrusion encounter more pressure drop compared to the other cooling channels.
- Overall, the U-depression cooling channel obtains the highest thermal performance.

## 7.2. Future Work Recommendations

Based on the findings of the study in hand, future work is recommended as below:

- Further investigation with multi-pass cooling channel is recommended. The investigation can be extended with no-bend cooling channel.
- Combination of dimple, ribs, pin-fins, and guide vanes is recommended for future study.
- Despite the previous contributions on different cross sections of dimples, ribs, pin-fins, it is still not clear which combination would give the best results for a given geometry of the channel. Newer design of dimples, ribs, pin-fins, and guide vanes can be implemented with cooling channel and investigate the heat transfer and pressure drop effect.

- Porous media can be introduced as a cooling surface as it shows a better heat transfer enhancement.
- Application of different working fluid as a coolant can be investigated.
- On last recommended work on how to reduce the friction factor of the cooling channel as high friction factor reduces the turbine life.

# References


[1] Fundamentals of Engineering Thermodynamics 8th Edition by Michael J. Moran (Author), Howard N. Shapiro (Author), Daisie D. Boettner (Author), Margaret B. Bailey (Author)

[2] Han, Je-Chin, Sandip Dutta, and Srinath Ekkad. Gas turbine heat transfer and cooling technology. CRC press, 2012.

[3] Li, Y., Deng, H., Xu, G. and Tian, S., 2015. Heat transfer investigation in rotating smooth square U-duct with different wall-temperature ratios and channel orientations. *International Journal of Heat and Mass Transfer*, *89*, pp.10-23.

[4] Han, J.C., Chandra, P.R. and Lau, S.C., 1988. Local heat/mass transfer distributions around sharp 180 deg turns in two-pass smooth and rib-roughened channels. *ASME Journal of Heat Transfer, 110(1),* pp. 91-98

[5] Li, Y., Xu, G., Deng, H. and Tian, S., 2014. Buoyancy effect on heat transfer in rotating smooth square U-duct at high rotation number. *Propulsion and Power Research*, *3*(3), pp.107-120.

[6] Saravani, M.S., Beyhaghi, S. and Amano, R.S., 2018, June. Effect of Buoyancy and Density Ratio on Heat Transfer in a Smooth Cooling Channel of a Gas Turbine Blade. In *Turbo Expo: Power for Land, Sea, and Air* (Vol. 51081, p. V05AT11A008). American Society of Mechanical Engineers.

[7] Wagner, J.H., Johnson, B.V. and Hajek, T.J., 1991. Heat transfer in rotating passages with smooth walls and radial outward flow. *ASME Journal of Turbomachinery, 113(1),* pp. 42-51

[8] Saravani, M.S., DiPasquale, N.J., Beyhaghi, S. and Amano, R.S., 2019. Heat transfer in internal cooling channels of gas turbine blades: buoyancy and density ratio effects. *Journal of Energy Resources Technology*, *141*(11), pp. 112001-1 – 112001-8

[9] Deng, H., Qiu, L., Tao, Z. and Tian, S., 2013. Heat transfer study in rotating smooth square U-duct at high rotation numbers. *International Journal of Heat and Mass Transfer*, *66*, pp.733-744.

[10] Mayo, I., Arts, T. and Van de Wyer, N., 2017, June. Rotation Effects on the Heat Transfer Distribution in a Two-Pass Rotating Internal Cooling Channel Equipped with Triangular Ribs. In *Turbo Expo: Power for Land, Sea, and Air* (Vol. 50879, p. V05AT16A017). American Society of Mechanical Engineers.

[11] Huh, M., Lei, J. and Han, J.C., 2010, October. Influence of channel orientation on heat transfer in a two-pass smooth and ribbed rectangular channel (AR= 2: 1) under large rotation numbers. In *Turbo Expo: Power for Land, Sea, and Air* (Vol. 43994, pp. 53-65).

[12] Hajek, T.J., Wagner, J.H. and Johnson, B.V., 1986. Coolant passage heat transfer with rotation. Lewis Research Center, Turbine Engine Hot Section Technology, NASA N89-17314

[13] Leontiev, A.I., Kiselev, N.A., Burtsev, S.A., Strongin, M.M. and Vinogradov, Y.A., 2016. Experimental investigation of heat transfer and drag on surfaces with spherical dimples. *Experimental Thermal and Fluid Science*, *79*, pp.74-84.

[14] Burgess, N.K. and Ligrani, P.M., 2004, January. Effects of dimple depth on Nusselt numbers and friction factors for internal cooling in a channel. In *Turbo Expo: Power for Land, Sea, and Air* (Vol. 41685, pp. 989-998).

[15] Turnow, J., Kornev, N., Isaev, S. and Hassel, E., 2011. Vortex mechanism of heat transfer enhancement in a channel with spherical and oval dimples. *Heat and Mass Transfer*, *47*(3), pp.301-313.

[16] Wei, X.J., Joshi, Y.K. and Ligrani, P.M., 2007. Numerical simulation of laminar flow and heat transfer inside a microchannel with one dimpled surface. *ASME Journal of Electronic Packaging*, *129(1)*, pp.63-70

[17] Gupta, G., Little, Z., Reyes, S., Calderon, L., Fernandez, E. and Kapat, J.S., 2017. Experimental and Numerical Study of Flow in a Square Duct with Positive and Negative Spherical Wall Features. In *53rd AIAA/SAE/ASEE Joint Propulsion Conference* (p. 4978).

[18] Xie, G. and Sundén, B., 2010. Numerical predictions of augmented heat transfer of an internal blade tip-wall by hemispherical dimples. *International journal of heat and mass transfer*, *53*(25-26), pp.5639-5650.

[19] Rashidi, S., Hormozi, F., Sundén, B. and Mahian, O., 2019. Energy saving in thermal energy systems using dimpled surface technology–A review on mechanisms and applications. *Applied Energy*, *250*, pp.1491-1547.

[20] Afanasyev, V.N., Chudnovsky, Y.P., Leontiev, A.I. and Roganov, P.S., 1993. Turbulent flow friction and heat transfer characteristics for spherical cavities on a flat plate. *Experimental thermal and fluid science*, *7*(1), pp.1-8.

[21] Chyu, M.K., Yu, Y., Ding, H., Downs, J.P. and Soechting, F.O., 1997, June. Concavity enhanced heat transfer in an internal cooling passage. In *Turbo Expo: Power for Land, Sea, and Air* (Vol. 78705, p. V003T09A080). American Society of Mechanical Engineers.

[22] Moon, H.K., O'connell, T. and Glezer, B., 2000. Channel height effect on heat transfer and friction in a dimpled passage. *J. Eng. Gas Turbines Power*, *122*(2), pp.307-313.

[23] Mahmood, G.I., Hill, M.L., Nelson, D.L., Ligrani, P.M., Moon, H.K. and Glezer, B., 2001. Local heat transfer and flow structure on and above a dimpled surface in a channel. *J. Turbomach.*, *123*(1), pp.115-123.

[24] Xie, G. and Sundén, B., 2010. Numerical predictions of augmented heat transfer of an internal blade tip-wall by hemispherical dimples. *International journal of heat and mass transfer*, *53*(25-26), pp.5639-5650.

[25] Rao, Y., Feng, Y., Li, B. and Weigand, B., 2015. Experimental and numerical study of heat transfer and flow friction in channels with dimples of different shapes. *Journal of Heat Transfer*, *137*(3).

[26] Nishida, S., Murata, A., Saito, H., and Iwamoto, K., 2009. Measurement of heat and fluid flow on surface with teardrop-shaped dimples. In *Proceedings of the Asian Congress on Gas Turbines, 2009-8* (pp. 1-4).

[27] Kim, H.M., Moon, M.A., and Kim, K.Y., 2011. Shape optimization of inclined elliptic dimples in a cooling channel. *Journal of thermophysics and heat transfer*, *25*(3), pp.472-476.

[28] Zhou, F. and Acharya, S., 2001. Mass/Heat Transfer in Dimpled Two-Pass Coolant Passages with Rotation. *Annals of the New York Academy of Sciences*, *934*(1), pp.424-431.

[29] Griffith, T.S., Al-Hadhrami, L. and Han, J.C., 2002, January. Heat transfer in rotating rectangular cooling channels (AR= 4) with dimples. In *Turbo Expo: Power for Land, Sea, and Air* (Vol. 36088, pp. 551-560).

[30] Kim, S., Choi, E.Y. and Kwak, J.S., 2012. Effect of channel orientation on the heat transfer coefficient in the smooth and dimpled rotating rectangular channels. *Journal of heat transfer*, *134*(6).

[31] Kumar, S. and Amano, R.S., 2012, November. Numerical Simulation of Two Pass Gas Turbine Blade Internal Cooling Channels With 90 Degree Varying Height Ribs. In *ASME International Mechanical Engineering Congress and Exposition* (Vol. 45226, pp. 245-253). American Society of Mechanical Engineers.

[32] Amano, R.S., Guntur, K., Martinez Lucci, J. and Ashitaka, Y., 2010, October. Study of flow through a stationary ribbed channel for blade cooling. In *Turbo Expo: Power for Land, Sea, and Air* (Vol. 43994, pp. 471-478).

[33] Kim, K.M., Park, S.H., Jeon, Y.H., Lee, D.H. and Cho, H.H., 2007, January. Heat/mass transfer characteristics in angled ribbed channels with various bleed ratios and rotation numbers. In *Turbo Expo: Power for Land, Sea, and Air* (Vol. 47934, pp. 209-218).

[34] Hahn, T., Deakins, B., Buechler, A., Kumar, S. and Amano, R.S., 2012, August. Experimental Analysis of the Heat Transfer Variations Within an Internal Passage of a Typical Gas Turbine Blade Using Varied Internal Geometries. In *International Design Engineering Technical Conferences and Computers and Information in Engineering Conference* (Vol. 45042, pp. 851-858). American Society of Mechanical Engineers.

[35] Kumar, S., Amano, R.S. and Lucci, J.M., 2013. Numerical simulations of heat transfer distribution of a two-pass square channel with V-rib turbulator and bleed holes. *Heat and Mass Transfer*, *49*(8), pp.1141-1158.'

[36] Taslim, M.E. and Spring, S.D., 1994. Effects of turbulator profile and spacing on heat transfer and friction in a channel. *Journal of Thermophysics and Heat Transfer*, *8*(3), pp.555-562.

[37] Mochizuki, S., Beier, M., Murata, A., Okamura, T. and Hashidate, Y., 1996. Detailed measurement of convective heat transfer in rotating two-pass rib-roughened coolant channels. In *ASME 1996 Turbo Asia Conference*. American Society of Mechanical Engineers Digital Collection.

[38] Han, J.C., and Chen, H.C., 2006. Turbine blade internal cooling passages with rib turbulators. *Journal of Propulsion and Power*, *22*(2), pp.226-248.

[39] Kiml, R., Mochizuki, S. and Murata, A., 2001. Effects of rib arrangements on heat transfer and flow behavior in a rectangular rib-roughened passage: application to cooling of gas turbine blade trailing edge. *J. Heat Transfer*, *123*(4), pp.675-681.

[40] Wang, Z., Ireland, P.T., Kohler, S.T., and Chew, J.W., 1998. Heat transfer measurements to a gas turbine cooling passage with inclined ribs.

[41] Baggetta, L., Satta, F. and Tanda, G., 2019. A possible strategy for the performance enhancement of turbine blade internal cooling with inclined ribs. *Heat Transfer Engineering*, *40*(1-2), pp.184-192.

[42] Ekkad, S.V. and Han, J.C., 2000. A transient liquid crystal thermography technique for gas turbine heat transfer measurements. *Measurement Science and Technology*, *11*(7), p.957.

[43] Metzger, D.E., Berry, R.A. and Bronson, J.P., 1982. Developing heat transfer in rectangular ducts with staggered arrays of short pin fins.

[44] Hwang, J.J. and Lui, C.C., 2002. Measurement of endwall heat transfer and pressure drop in a pin-fin wedge duct. *International Journal of Heat and Mass Transfer*, *45*(4), pp.877-889.

[45] Carcassi, C., Facchini, B. and Innocenti, L., 2003, January. Heat transfer and pressure drop evaluation in thin wedge-shaped trailing edge. In *Turbo Expo: Power for Land, Sea, and Air* (Vol. 36886, pp. 111-122).

[46] Facchini, B., Innocenti, L. and Tarchi, L., 2004, January. Pedestal and endwall contribution in heat transfer in thin wedge-shaped trailing edge. In *Turbo Expo: Power for Land, Sea, and Air* (Vol. 41685, pp. 101-111).

[47] Sahiti, N., Lemouedda, A., Stojkovic, D., Durst, F. and Franz, E., 2006. Performance comparison of pin fin in-duct flow arrays with various pin cross-sections. *Applied Thermal Engineering*, *26*(11-12), pp.1176-1192.

[48] Siw, S.C., Chyu, M.K. and Alvin, M.A., 2012, June. Heat transfer enhancement of internal cooling passage with triangular and semi-circular shaped pin-fin arrays. In *Turbo Expo: Power for Land, Sea, and Air* (Vol. 44700, pp. 493-503). American Society of Mechanical Engineers.

[49] Jin, W., Jia, N., Wu, J., Lei, J. and Liu, L., 2019. Numerical Study on Flow and Heat Transfer Characteristics of Pin-Fins With Different Shapes. In *ASME Turbo Expo 2019: Turbomachinery Technical Conference and Exposition*. American Society of Mechanical Engineers Digital Collection.

[50] Effendy, M., Yao, Y., Yao, J. and Marchant, D.R., 2019, June. Pin-fin shape and orientation effects on wall heat transfer predictions of gas turbine blade. In *AIP Conference Proceedings* (Vol. 2114, No. 1, p. 020008). AIP Publishing LLC.

[51] Ricklick, M.A. and Carpenter, C., 2014. Comparison of Heat Transfer Prediction for Various Turbulence Models in a Pin Fin Channel. In *50th AIAA/ASME/SAE/ASEE Joint Propulsion Conference* (p. 3838).

[52] Delibra, G., Borello, D., Hanjalić, K. and Rispoli, F., 2009. URANS of flow and endwall heat transfer in a pinned passage relevant to gas-turbine blade cooling. *International Journal of Heat and Fluid Flow*, *30*(3), pp.549-560.

[53] Liang, C. and Rao, Y., 2020. Computational Analysis of Rotating Effects on Heat Transfer and Pressure Loss of Turbulent Flow in Detached Pin Fin Arrays With Various Clearances. *Journal of Heat Transfer*, *142*(12).

[54] Wheeler, A. J., and Ganji, A.R., 2010, *Introduction to Engineering Experimentation*, 3rd Edition, Pearson Higher Education, New Jersey

[55] Kim, H.M., Moon, M.A., and Kim, K.Y., 2011. Shape optimization of inclined elliptic dimples in a cooling channel. *Journal of Thermophysics and Heat Transfer*, *25*(3), pp.472-476.

# Curriculum Vitae

## Summary

- 5+ years of professional engineering experience (internships, energy assessment, and factory visit)
- 5+ years of research experience with CFD, 3D CAD, engineering calculations and experimental work (1 year in undergraduate level, 4+ years in Ph.D. level)
- 4+ years of teaching experience (Fluid Mechanics, Design and Experimentation with LabView in Mechanical Engineering Department-University of Wisconsin-Milwaukee)
- 3+ years of professional energy auditing experience (Industrial Assessment Center-U.S. Department of Energy)

## Experience

**Engineer – Metal Processing and Paint,** *Kohler Co.* **July 2022 - Present**

- Support day to day metal processing and paint operations
- Support productivity improvement projects that involve process and/or design changes
- Support and drive projects to improve safety and quality
- Identify and implement process improvements and cost reductions
- Analyze and coordinate engineering changes and new product releases to production
- Manage engineering changes to our existing product for manufacturability and/or cost reduction
- Support capital projects as required to improve safety, quality, productivity, and capacity
- Develop operator work instructions to certify components and operations are consistent and high quality

**Manufacturing Engineer (Co-Op),** *Kohler Co.* **January 2022 - July 2022**

- Checking regular plant activity
- Worked on metal fabrication
- Worked preventive, corrective, and administrative maintenance work order
- Daily plant inspection and prepare work order based on the inspection report
- Safety measures checking according to OSHA
- Maintain and practice 5S and Kaizen
- Maintain and prepare Bill of Materials (BOM)

- Documentation of new work order and update SAP
- Follow up with the technicians and shift supervisors regarding work order

**Research Assistant,** *University of Wisconsin-Milwaukee* **August 2017 – August 2022**

- Working on gas turbine internal cooling with a dimpled surface to perform efficient cooling in gas turbine blades
- Design optimization of dimples using 3D CAD and CFD analysis
- Developed a new dimple design which is 10% more efficient than the existing ones
- Working on gas turbine internal cooling with jet impingement cooling process
- Thermal and fluid behavior analysis was done using Star CCM+ software
- Running simulation using high performance computing cluster and Linux server system.
- Developed correlation between CFD data and experimental data
- Used mesh independence study to find out the optimum number of cells for the solution
- Performed various simulations to optimize the design using RANS and LES model
- Used different steady-state, multiple reference frames, and transient models
- Evaluated object design performance based on temperature, the velocity of air, Nusselt number, Reynolds number, and Convective Courant Number
- Train several undergraduate students

**Teaching Assistant,** *University of Wisconsin-Milwaukee* **August 2017 – January 2022**

- Teach mechanical design and experimentation
- Teach fluid mechanics theory and conduct laboratory sessions
- Teach basic computational fluid dynamics

**Lead Energy Auditor**, *WM Industrial Assessment Center–U.S.DOE* **February 2019–August 2022**

- Conduct ASHRAE level 2 energy audits on industrial facilities in Wisconsin and northern parts of Illinois
- Conduct 25+ energy assessments, perform as lead student in 2 energy audits
- Evaluate utility bills and summarize energy savings opportunities
- Analyze equipment and control systems to offer energy savings and production improvement
- Delivered complete energy assessment report in terms of energy savings opportunities, cost-saving, carbon reduction, implementation cost, and payback period

- Saved annually 41 million kWh electricity, 98,000 kW demand, and 3.5 million therms natural gas which is about $150,000 in terms of cost savings
- Conduct training sessions, contact with clients, and personnel of facilities.
- Worked on different proposal writing for DOE funds

**Engineering Intern,** *Gas Technology Institute* **May 2021 - August 2021**

- Worked at emerging technology. Assisted in the preparation of test plan, worked at the ResCom Lab on experimental set-up building and experiments, contributed to the final project report writing
- Prepared the test plan for Time and Motion Study
- Worked at Illinois National Guard Project
- Hands-on experience in handling HVAC units and mechanical tools
- Designed Pipe and Instrumentation Diagram
- Job safety preparation

**Engineering Trainee**, *Rural Power Company Limited* **November 2016 – February 2017**

- Inspected gas turbine, steam turbine, HRSGs, etc.
- Acquainted with the major inspection of the steam turbine system
- Worked in sub-station, distribution zone of electricity, and submitted reports on equipment conditions

**Intern Engineer**, *Dhaka Water Supply & Sewerage Authority* **December2014–January 2015**

- Inspected water pumps, motors, generators, and other equipment.
- Visited sub-stations, worked in office management, and submitted daily reports.

**Education**

**Doctor of Philosophy** – Mechanical Engineering, University of Wisconsin-Milwaukee, Wisconsin August 2022

**Bachelor of Science**- Mechanical Engineering, Military Institute of Science and Technology, Bangladesh January 2016

**List of Publications**

The detailed list of publications can be found at Farah Nazifa Nourin - Google Scholar

**Awards and Achievement**

1. National Award: 2020 Industrial Assessment Center Outstanding Student Award from U.S. Department of Energy (rb.gy/4ljub9)
2. UWM Chancellor Award 2018, 2020, and 2021
3. Lead Energy Auditor Certificate from U.S. Department of Energy
4. Merit Scholarship from the People's Republic of Bangladesh in 2010 and 2012